NAVAL POSTGRADUATE SCHOOL
Monterey, California

THESIS

ADAPTIVE MULTI-LAYER LMS CONTROLLER DESIGN AND ITS APPLICATION TO ACTIVE VIBRATION SUPPRESSION ON A SPACE TRUSS

by

Timothy A. Barney

June 2001

Thesis Advisor: Young S. Shin
Co-Advisor: Brij N. Agrawal

Approved for public release; distribution is unlimited

20010806 088

REPORT DOCUMENTATION PAGE		Form Approved OMB No. 0704-0188

Public reporting burden for this collection of information is estimated to average 1 hour per response, including the time for reviewing instruction, searching existing data sources, gathering and maintaining the data needed, and completing and reviewing the collection of information. Send comments regarding this burden estimate or any other aspect of this collection of information, including suggestions for reducing this burden, to Washington headquarters Services, Directorate for Information Operations and Reports, 1215 Jefferson Davis Highway, Suite 1204, Arlington, VA 22202-4302, and to the Office of Management and Budget, Paperwork Reduction Project (0704-0188) Washington DC 20503.

1. AGENCY USE ONLY *(Leave blank)*	2. REPORT DATE June 2001	3. REPORT TYPE AND DATES COVERED Master's Thesis

4. TITLE AND SUBTITLE ADAPTIVE MULTI-LAYER LMS CONTROLLER DESIGN AND ITS APPLICATION TO ACTIVE VIBRATION SUPPRESSION ON A SPACE TRUSS	5. FUNDING NUMBERS
6. AUTHOR(S) Barney, Timothy A.	

7. PERFORMING ORGANIZATION NAME(S) AND ADDRESS(ES) Naval Postgraduate School Monterey, CA 93943-5000	8. PERFORMING ORGANIZATION REPORT NUMBER

9. SPONSORING / MONITORING AGENCY NAME(S) AND ADDRESS(ES)	10. SPONSORING / MONITORING AGENCY REPORT NUMBER

11. SUPPLEMENTARY NOTES
The views expressed in this thesis are those of the author and do not reflect the official policy or position of the Department of Defense or the U.S. Government.

12a. DISTRIBUTION / AVAILABILITY STATEMENT Approved for public release; distribution is unlimited.	12b. DISTRIBUTION CODE

13. ABSTRACT *(maximum 200 words)*

This thesis develops an adaptive controller that actively suppresses a single frequency disturbance source at a remote position and tests the system on the NPS Space Truss. The experimental results are then compared to those predicted by an ANSYS finite element model. The NPS space truss is a 3.7-meter long truss that simulates a space-borne appendage with sensitive equipment mounted at its extremities. One of two installed piezoelectric actuators and an Adaptive Multi-Layer LMS control law were used to effectively eliminate an axial component of the vibrations induced by a linear proof mass actuator mounted at one end of the truss. Experimental and analytical results both demonstrate reductions to the level of system noise. Vibration reductions in excess of 50dB were obtained through experimentation and over 100dB using ANSYS, demonstrating the ability to model this system with a finite element model. This thesis also proposes a method to use distributed quartz accelerometers to evaluate the location, direction, and energy of impacts on the NPS space truss using the dSPACE data acquisition and processing system to capture the structural response and compare it to known reference signals.

14. SUBJECT TERMS Active Vibration Suppression, Piezoceramic Actuators, Impact Analysis, Adaptive Controller, LMS	15. NUMBER OF PAGES 214
	16. PRICE CODE

17. SECURITY CLASSIFICATION OF REPORT Unclassified	18. SECURITY CLASSIFICATION OF THIS PAGE Unclassified	19. SECURITY CLASSIFICATION OF ABSTRACT Unclassified	20. LIMITATION OF ABSTRACT UL

NSN 7540-01-280-5500

Standard Form 298 (Rev. 2-89)
Prescribed by ANSI Std. 239-18

THIS PAGE INTENTIONALLY LEFT BLANK

ADAPTIVE MULTI-LAYER LMS CONTROLLER DESIGN AND ITS APPLICATION TO ACTIVE VIBRATION SUPPRESSION ON A SPACE TRUSS

Timothy A. Barney
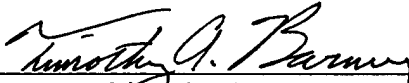Lieutenant, United States Navy
B.S., Eastern Michigan University, 1993

Submitted in partial fulfillment of the
requirements for the degree of

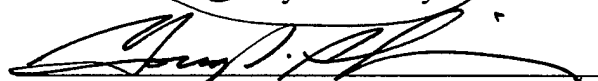## MASTER OF SCIENCE IN MECHANICAL ENGINEERING

from the

NAVAL POSTGRADUATE SCHOOL
June 2001

Author: _____
Timothy A. Barney

Approved by: _____
Young S. Shin, Thesis Advisor

_____
Brij N. Agrawal, Co-Advisor

_____
Terry R. McNelley, Chairman
Department of Mechanical Engineering

iii

THIS PAGE INTENTIONALLY LEFT BLANK

ABSTRACT

This thesis develops an adaptive controller that actively suppresses a single frequency disturbance source at a remote position and tests the system on the NPS Space Truss. The experimental results are then compared to those predicted by an ANSYS finite element model. The NPS space truss is a 3.7-meter long truss that simulates a space-borne appendage with sensitive equipment mounted at its extremities. One of two installed piezoelectric actuators and an Adaptive Multi-Layer LMS control law were used to effectively eliminate an axial component of the vibrations induced by a linear proof mass actuator mounted at one end of the truss. Experimental and analytical results both demonstrate reductions to the level of system noise. Vibration reductions in excess of 50dB were obtained through experimentation and over 100dB using ANSYS, demonstrating the ability to model this system with a finite element model. This thesis also proposes a method to use distributed quartz accelerometers to evaluate the location, direction, and energy of impacts on the NPS space truss using the dSPACE data acquisition and processing system to capture the structural response and compare it to known reference signals.

THIS PAGE INTENTIONALLY LEFT BLANK

TABLE OF CONTENTS

THIS PAGE INTENTIONALLY LEFT BLANK

LIST OF FIGURES

THIS PAGE INTENTIONALLY LEFT BLANK

LIST OF TABLES

THIS PAGE INTENTIONALLY LEFT BLANK

LIST OF ABBREVIATIONS AND ACRONYMS

ADC	Analog to Digital Conversion
ADCH	Analog to Digital Channel
APDL	ANSYS Parametric Design Language
CPU	Central Processing Unit
DAC	Digital to Analog Conversion
DACH	Digital to Analog Channel
DC	Direct Current
DCM	Direction Cosine Matrix
DOF	Degree of Freedom
DSA	Dynamic Signal Analyzer
D&D	Drag and Drop
EVA	Extra-Vehicular Activity
FBG	Fiber-optic Bragg Grating
FEM	Finite Element Method
	Finite Element Model
FIR	Finite Impulse Response
GUI	Graphic User Interface
I/O	Input / Output
IDIFF	Integral Plus Double Integral Force Feedback
LMS	Least Mean Square
NASA	National Air and Space Administration
NPS	Naval Postgraduate School
NRL	Naval Research Laboratory
PPF	Positive Position Feedback
PZT	Lead Zirconate Titanate
RTI	Real Time Integration
RTILIB	RTI Library
SG	System Gain
S/N	Serial Number
SRDC	Spacecraft Research and Design Center
SSL	Smart Structures Laboratory

THIS PAGE INTENTIONALLY LEFT BLANK

LIST OF SYMBOLS

A	Area	[M]	Mass Matrix
[AP]	Application Vector	$\vec{P}$	Poling Axis
[c]	Elasticity Matrix	[s]	Compliance Matrix
C	Control Signal	[S]	Strain Tensor (Vector)
[C]	Damping Matrix	[T]	Stress Tensor (Vector)
[d]	Piezoelectric Matrix (strain)	U	Potential Energy
[e]	Piezoelectric Matrix (stress)	V	Voltage
E	Elastic Modulus	x	Displacement (generic)
$\vec{D}$	Electric Flux Vector	X	Typical Input
$\vec{E}$	External Electric Field Vector	Y	Typical Output
G	Modulus of Rigidity	z	Digital Sequence Term
G_1	Feedback Gain	α	Rayleigh Damping Constant
[H]	Shaping Matrix	β	Rayleigh Damping Constant
H	Transfer Function	δ	Displacement (small)
I	Moment of Inertia	$\in$	Strain, Axial
[ISO]	Isolation Vector	$[\varepsilon^\in]$	Dielectric Matrix, Constant $\in$
J	Polar Moment of Inertia	$[\varepsilon^\sigma]$	Dielectric Matrix, Constant σ
k	Elemental Stiffness	ρ	Density
[K]	Stiffness Matrix	σ	Stress
K	Generic Constant	ζ	Damping Ratio
L	Length		

THIS PAGE INTENTIONALLY LEFT BLANK

ACKNOWLEDGMENTS

THIS PAGE INTENTIONALLY LEFT BLANK

I.   INTRODUCTION

A.   BACKGROUND

As the use of space and satellites continues to grow in the 21st Century, technology will yield smaller devices with reduced power requirements. These advancements are countered by our growing demand for faster and higher-bandwidth communications and will predictably lead to larger satellites. As satellites have become larger and more complex, historically the launch booster capability has not been appreciably increased. This trend continues to motivate engineers to design satellites that are lighter, more densely configured, and capable of deploying large antennas and reflectors when on orbit.

Another result of our continued introduction of space vehicles and the degradation of existing satellites is the drastic increase in the population of orbital micrometeorites. This increase, coupled with the cross-section provided by larger satellites implies that orbital impacts will become much more frequent. Currently most damage assessment is provided via performance degradation analysis. This can led to wasted manpower trying to troubleshoot a device that was literally vaporized at impact and no longer exists. More significantly, the introduction of large, manned space stations will require a method of damage assessment other than "go look and see what has been hit." Rapid and accurate response to an impact could mean the difference between life and death for the astronauts onboard. This thesis will propose a method of rapid impact assessment using a distributed sensor system.

These larger, lightweight satellites are also more prone to low frequency

1

vibrations than ever before. When on orbit, the operating frequencies of equipment installed on the same structure may induce performance degradation or premature failure of other satellite components. In order to protect sensitive equipment from these vibrations, there are two possible approaches. These options are to dampen the vibration or actively suppress the effect at a specific location. This thesis will discuss vibration suppression.

Inherent in all structures is a degree of natural passive damping. This may be enhanced with installed devices, such as visco-elastic dampers. These devices may be large, and thus not worth the additional lift capacity required to bring them to orbit. Active damping is another option available for vibration reduction. Implementing an active damping system can be difficult due to the difficulties in modeling the dynamic characteristics of the structure. However, if the control law does not depend on the structure, then active suppression techniques may be chosen.

The Naval Postgraduate School (NPS) Space Truss is a small-scale flexible structure that has two piezoceramic actuators installed. The piezoceramic actuators were selected because of their high bandwidth, lightweight, and low power consumption. Previous experiments have shown that a computer-modeling program can predict reductions in vibration amplitude using a detailed dynamic model of the NPS Space Truss with the active damping simulated on the model. The simulated results of the controller developed by this thesis were also evaluated with this model and verified by experiments on the NPS Space Truss.

The NPS Space Truss is now a test platform for further experiments on active vibration reduction and impact analysis. The techniques learned using the NPS Space Truss could be applied to larger structures, such as the International Space Station.

B.   OBJECTIVES

The objective of this thesis were as follows:

- Develop an active vibration control system that is capable of reducing single frequency vibrations at a remote location and is independent of structural characteristics.

- Evaluate the controller using an active FEM and compare the results with the experimental response.

- Develop a method to determine the location, force, and orientation of an impact using a minimal distributed sensor grid.

C.   SCOPE OF THESIS

The scope of this thesis includes:

- Creation of a control algorithm to actively suppress an axial component of a constant frequency disturbance at a random point from a remote location.

- The integration of the dSPACE digital signal processing system [Ref. 1] as the heart of both the signal analysis used for impact analysis and the active control system on the NPS space truss.

- Evaluation of the active controller using an ANSYS [Ref. 2] finite element model of the NPS space truss.

- Comparison of the FEM results with the actual truss by experimentation.

- Proposal of a method to determine impact characteristics using a system of distributed sensors.

The use of ANSYS, MATLAB [Ref. 3], and dSPACE were instrumental to the work contained herein. This thesis is not intended to replace the use of tutorials available in MATLAB, ANSYS or dSPACE. On-line and printed guides and tutorials are available to give the layman an opportunity to learn the system in order to use the information presented. A basic outline of how to get the programs and systems operating is included, and has sufficient detail to allow a user with some experience to run the desired programs. Where specific program instructions are given, menu commands will be used with a ">" to indicate a sub-menu selection, or the commands as typed.

D.   METHODOLOGY

The research for this thesis followed several different paths that involved signal processing, active control systems, FEM, and the implementation of the various software packages used. The first goal was to reduce the vibration of various nodal points on the NPS Space Truss, with the ultimate objective of total stabilization. Due to the inherent limitations of vibration damping in a structure with multiple transmission paths, the idea of active suppression became the primary focus. A single axis approach was chosen as the first iteration on the system for the sake of testing and simplicity.

The Adaptive Multi-Layer LMS Controller was developed one piece at a time. After initial experimental testing proved that the *Adaptive Notch Canceller* [Ref. 4] could be applied to the NPS Space Truss, it was decided to include a frequency identification

4

routine that would make the controller more versatile. After the identification algorithm was applied, it was discovered that the nodal signal could not be used for identification due to the ability of the controller to suppress the signal to the noise level. The identification input was then shifted to the disturbance generator, vice the nodal signal.

Further testing quickly revealed that the LMS gain was a variable based on the frequency of the disturbance. The next modification added the ability of the controller to adjust the magnitude of the gain based on system response. This was only partially successful due to the phase shifts experienced over the frequency range of interest. The ability of the controller to change the sign of the gain was then added to the system. The logic for the adaptive gain adjustment, translated into mathematical a format, came from literally dozens of experimental runs attempting to determine a pattern to the optimal gain values. The controller was essentially complete at this point.

After initial testing, a second active element was installed in the NPS Space Truss in order to evaluate the new controllers ability to adapt regardless of actuator position and orientation. This testing was completely successful and no additional adjustments were required based on which element was chosen. The remaining experimentation, evaluation, and tuning was dedicated to documenting the abilities of the system and adjusting the various adaptation rates for maximum stability.

The next phase in the research dealt with the modification of a FEM created for previous research [Ref. 5] to determine the ability of a software model to predict the new controllers effectiveness. With the assistance of Mr. Sheldon Imaoka, a Collaborative Solutions, Inc., Engineering Consultant, the original ANSYS structural model was modified to include the new active element and the program to implement the controller

was written. It was determined that limiting the analytical controller implemented in the FEM to include only the phase adjustment portion of the controller would significantly simplify the programming requirements and allow for a valid comparison of the steady state operations. That decision also dictated multiple runs of each experiment to determine the optimal gain values required. This experience, coupled with the dozens of experimental experiments run with the same goal, was valuable in determining qualitatively the ability of the model to duplicate actual structural responses to the control system. The video files that were created by ANSYS also allowed for amplification of the displacements and resulted in a greater understanding of the entire structures response to suppressing a single nodes axial vibration.

The finial phase of the research was dedicated to developing a method of determining impact characteristics based only on sensory input. The idea of a neural network was explored and discarded as overly complex. The concept that was eventually decided on was based on the idea that the some level of accuracy on impact location, force and energy could be obtained by comparing impact signals with known impact responses. Signal cross correlations were used to compare signals and initial testing was done. The testing produced results that were generally encouraging, but were not extensive enough for documentation purposes. This phase of the research was discontinued due to time limitations and is thus referred to in the Future Research section.

E.   THESIS ORGANIZATION

Chapter II contains background information, theory and a summary of the work that preceded the tasks performed by the author. Chapter III contains the details on the

development and implementation of an active controller for the NPS space truss, using MATLAB / Simulink, and dSPACE. Chapter IV describes the finite element model created in ANSYS. Chapter V describes the experimental methodology used to verify the controller using the finite element model. Chapter VI is a description of the proposed method of signal processing required for impact analysis and recommendations for further study regarding the Adaptive Multi-Layer LMS controller. Finally, Chapter VII provides conclusions in the areas researched.

THIS PAGE INTENTIONALLY LEFT BLANK

II.   THE NPS SPACE TRUSS

A.   TRUSS DESCRIPTION

1. Background

The NPS space truss obtained by the Spacecraft Research and Design Center (SRDC) at NPS from the Naval Research Laboratory (NRL) and is as exact replica of the NRL space truss. The engineers at NRL obtained approximately a 100-fold reduction in power amplitude due to the active control system using the controller [Ref. 6].

To date, the NPS space truss has had modal testing performed, and two active control piezoelectric struts have been installed and tested. Planned research using the NPS space truss includes the integration of fiber-optic strain gages.

2. Elements and Construction

The NPS space truss is 3.67 meters long, 0.67 meters tall, and is composed of 52 aluminum nodes joined by 161 elements in a cubic 12-bay structure. It is attached at the center to a fixed base plate and mounted on a Newport Vibration Control System Table. The layout of the unmodified truss is shown in Figure 1.
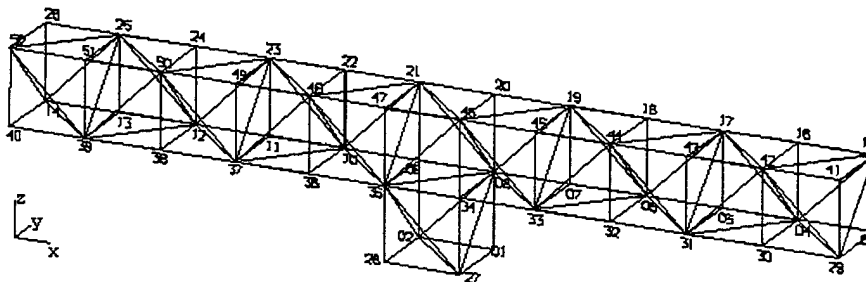
Figure 1. The NPS Space Truss [From Ref. 5]

The node balls are precision milled from 7075-T6 Aluminum and a standoff is used to provide an interface between the elements and the node ball. The elements are 5/16-inch aluminum alloy tubing with 0.035-inch wall thickness and have two lengths, a shorter length for the battens and longerons (100 total), and a larger length for the diagonal elements (61). An exploded view of the element to node assembly is shown in Figure 2. A more detailed description of the truss can be found in Reference 5 and the assembly procedure used is Reference 7.
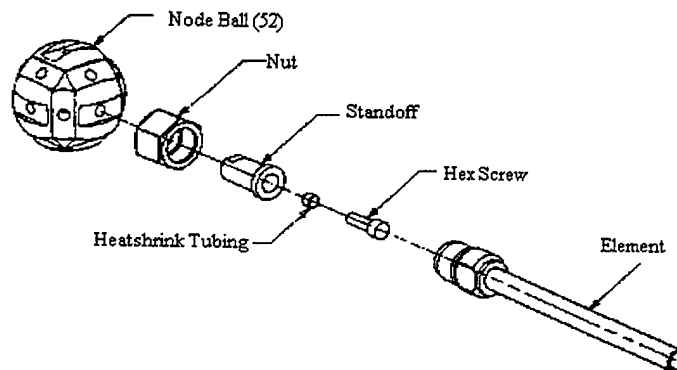
Figure 2. Node Assembly Details [From Ref. 8]

The isolation table uses a compressed Nitrogen cushion to provide for high frequency vibration attenuation (greater than 99% above 12 Hz) [Ref. 9]. Detailed data on the NPS space truss are contained in Appendix A.

B.   ACTIVE CONTROL ELEMENT

1. Overview

The active elements installed in the NPS space truss consist of piezoelectric actuators and co-located force transducers. These components are mounted to steel rods in a manner that is compatible with the truss elements. Together with the nodal 3-axis

10

accelerometers and the computer data processing system, these components comprise the adaptive suppression system.

2. Piezoelectric Theory

Piezoelectric (also called piezoceramic) materials elongate when a voltage is applied in a pre-determined direction. Conversely, when a deformation is applied to a piezoelectric material with either an external force or strain, an internal electric potential will be developed that can be measured. In this manner, piezoelectric material is used for both a sensor and as an actuator.

Piezoelectric materials are anisotropic in nature with orthogonal directions related to the poling axis mechanically by Poisson's ratio. While not truly linear, and containing some hysteresis, the piezoelectric effect can be modeled as such, with minimal error. The piezoelectric electroelastic relations can be described with the following equation [Ref. 10], shown in stiffness method form:

$$\begin{Bmatrix} T \\ \bar{D} \end{Bmatrix} = \begin{bmatrix} [c] & [e] \\ [e]^T & -[\varepsilon^\epsilon] \end{bmatrix} \begin{Bmatrix} S \\ -\bar{E} \end{Bmatrix} \tag{2.1}$$

The stress and strain vectors represent the three axial and three shear stresses and strains.

Rewriting equation (2.1) in the applied force method, given by [Ref. 11]:

$$\begin{Bmatrix} S \\ \bar{D} \end{Bmatrix} = \begin{bmatrix} [s] & [d] \\ [d]^T & [\varepsilon^\sigma] \end{bmatrix} \begin{Bmatrix} T \\ \bar{E} \end{Bmatrix} \tag{2.2}$$

These equations, when the [d] and [e] matrices are zero, reduce to Hooke's Law and the dielectric equation [Ref. 10, p. 4]. The relationship between the [d] and [e] matrices is given by:

$$[e] = [c]^\epsilon [d] \qquad (2.3)$$

Where [c] is a symmetric, (6 x 6) matrix that contains all of the linear elastic and flexural terms. The [e] and [d] matrices are (6 x 3) and contain the piezoelectric coupling terms. The [ε] matrix is a diagonal matrix with the dielectric permitivities. The individual constants in the matrices are usually indexed by their coordinate axes (1, 2 and 3); the 3-axis is the poling axis.

3. Application and Operating Characteristics

Piezoelectric actuators are attractive due to their high bandwidth, compact size, and low power requirements. Special care must be used while working with them because even though the power required by a piezoelectric actuator is low, the voltages required are high.

The basic schematics for a piezoelectric actuator are presented in Figure 3. The actuators are mounted such that the desired applied force is in the direction of the poling axis. In the following figure, the poling axis, applied electric field, and the resulting displacement are shown in the piezoelectric crystal.
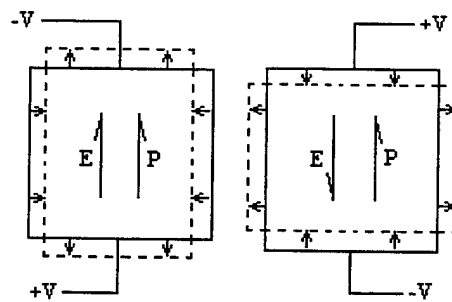
Figure 3. Piezoelectric Actuator Configuration

Piezoelectric materials are limited to an applied electric field of 2kV/mm [Ref. 12]. To functionally eliminate this problem, piezoelectric material are stacked commonly

12

in the direction of the poling axis, with interleaving foil electrodes to provide a greater cumulative strain and thereby greater force to the structure. The polarity of the piezoelectric wafers is inverted at each step to simplify the electrode placement and maintain uniform global effect. This configuration for a stacked linear actuator is shown in Figure 4.

Defines polarization direction in wafer
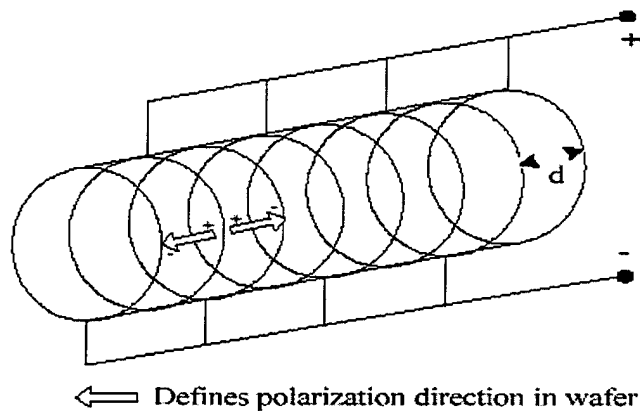
Figure 4. Stacked Piezoelectric Actuator [From Ref. 13]

The active piezoelectric element is mounted in the structure such that the poling axis is directly in line with the element that it is replacing to allow for the maximum piezoelectric effect to be felt by the structure. The piezoelectric active control element selected was the Piezoelectric Translation Model P-848-30, built by Polytek Physik Instrumente of Hamburg, Germany [Ref. 5] and shown in Figure 5. The P-843.30 has a maximum operating voltage of 100V and is cylindrical in shape, with a 14-mm diameter and 73-mm length. Other characteristics are listed in Appendix A.
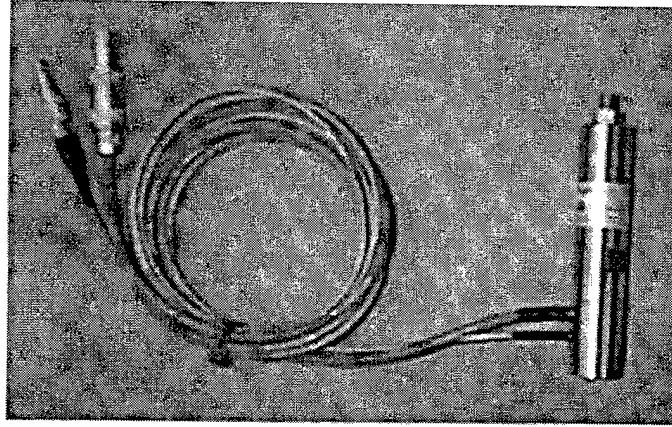
Figure 5. Physik Instrumente P-843.30 [From Ref. 5]

The second connector shown in Figure 5 is for an integrated metal foil strain gage that was not used for this research. The P-843.30 has a rated open loop travel characteristic of 45 μm/100V +/- 20-percent. Verification of this was performed prior to installation [Ref. 14, pp. 25-28]. The results from this measurement are presented in Figure 6.
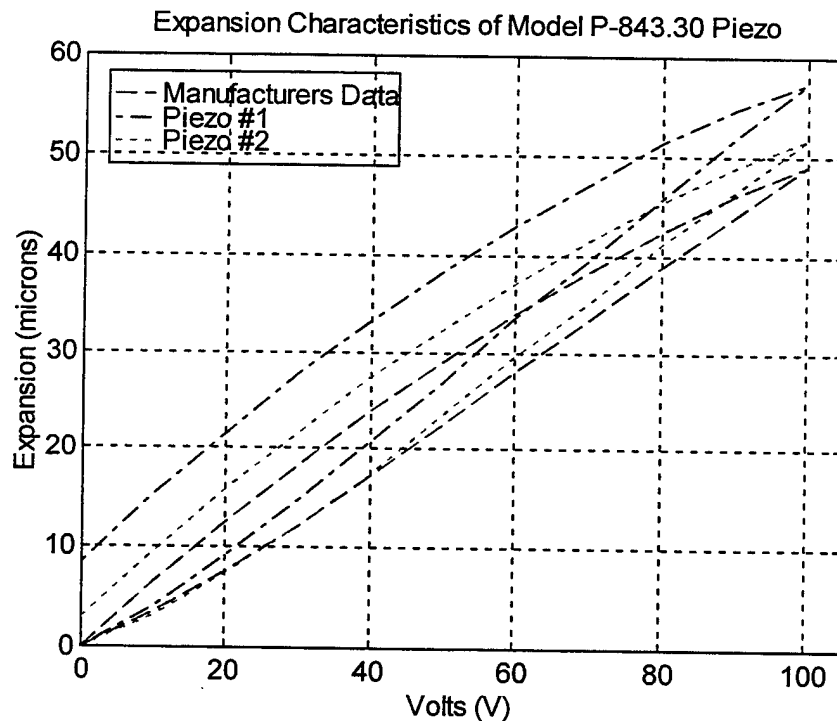
Figure 6. Piezo Model P-843.30 Expansion Characteristics [From Ref. 14]

14

An average of 50 μm/100V was assumed for further calculations.

4. Locating The Active Element

The optimal active strut location was based on the element that experienced the maximum strain energy in the first mode. A finite element model of the NPS space truss constructed in MATLAB and the strain energy was calculated based on the deformation of the truss [Ref. 5]. As noted in the analysis, there is an odd symmetry to the locations of the maximum strain energy due to the diagonal elements in the truss.

Based on the results of this analysis, Element 101 was replaced by the first active truss. The second active element was placed base on the symmetry of the analysis and replaced Element 107. Operational experience with the current controller suggests that this may not have been the best choice. The ability of the user to select the control node is limited by the physical nature of the structure. If the active elements were placed in geometrically unrelated positions, the likelihood of both of them being ineffective at a give frequency, relative to the same control node location, is greatly reduced. The control element location was not altered after initial placement due to the cost of the piezoelectric elements and their susceptibility to failure due to applied torque during the instillation process.

The program used to determine the mode shapes [Ref. 5] was verified and slightly altered and is included in Appendix B. The first ten natural frequencies computed by the MATLAB model are shown in Table 1, along with the experimental results from modal testing [Ref. 14].

Mode #	Analytical	Actual	Mode #	Analytical	Actual
1	14.13	14.64	6	72.24	74.54
2	15.44	16.26	7	79.71	80.66
3	28.72	30.41	8	97.41	101.01
4	32.04	33.97	9	120.21	126.23
5	60.23	62.93	10	129.68	135.97

Table 1. NPS Space Truss Modal Frequencies [Ref. 14]

The first four mode shapes for the NPS Space Truss were obtained by taking the eigenvector displacements and adding them to their respective nodal coordinates. The mode shapes generated by this model are included in Appendix C. It should be noted that these analysis were conducted on a bare truss model (without the additional mass and stiffness of the LPACT and the active elements). The ANSYS analysis was done on a modified truss model that includes all the systems installed in the truss as used in the experimental system. The mode shapes from this analysis are also included in Appendix C and are noticeably different from the bare truss model. It is recommended that a modified model be used if further verification of the optimal active element location is desired.

5. Force Transducer

Previous research using the NPS Space Truss used an installed force transducer that was collocated with the active elements. The original PCB Piezotronics Model 208B02 General Purpose ICP Force Sensor is a still present in the experimental setup and a second was installed with the additional active element [Ref. 15]. Their physical properties were included in the ANSYS FEM, but neither output was used in this research. The model 208B02's operating characteristics are included in Appendix A.

6. Installation of the Active Element

The second active element was constructed with identical components and procedures as the first element [Ref. 14]. The assembled active element is shown in Figure 7.
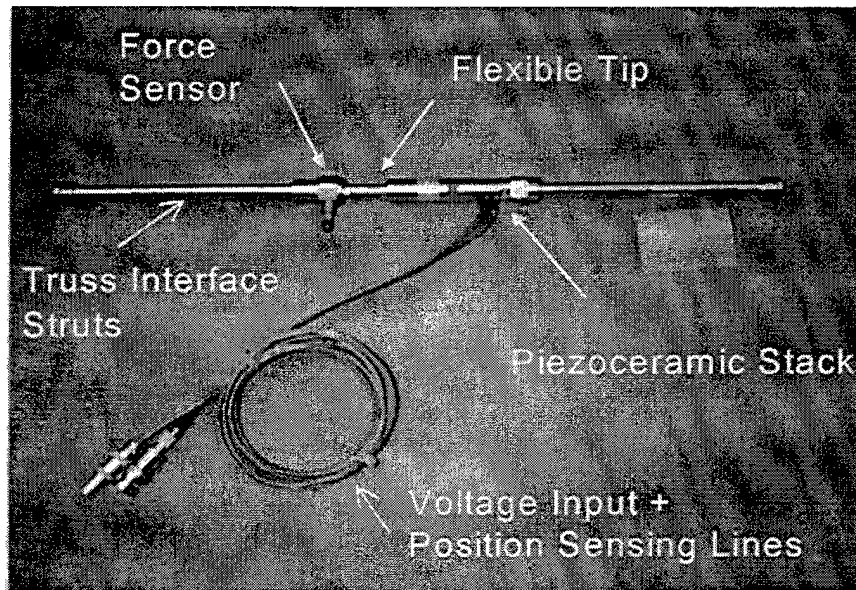
Figure 7. Assembled Active Control Element [From Ref. 14]

C. LINEAR PROOF MASS ACTUATOR (LPACT)

The disturbance force is provided by a Linear Proof Mass Actuator (LPACT) installed at the end of the NPS space truss. The LPACT is a model CML-030-020-1 manufactured by Planning Systems, Incorporated, from Melbourne, FL and is powered by a separate amplifier and controller assembly with embedded feedback electronics. The LPACT has mounted accelerometers for use in monitoring or driving the feedback loops that were not used in this research, but could be used as a disturbance reference signal for frequency identification. The LPACT is shown in Figure 8 and further details are included in Appendix A.

17
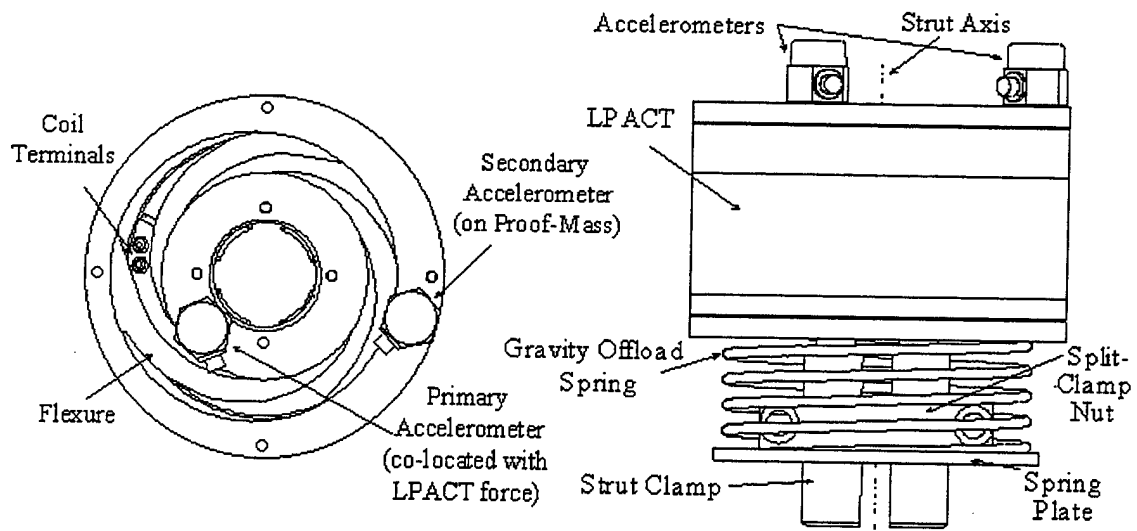
Figure 8. LPACT [From Ref. 16]

A picture of the installed LPACT is provided as Figure 9.
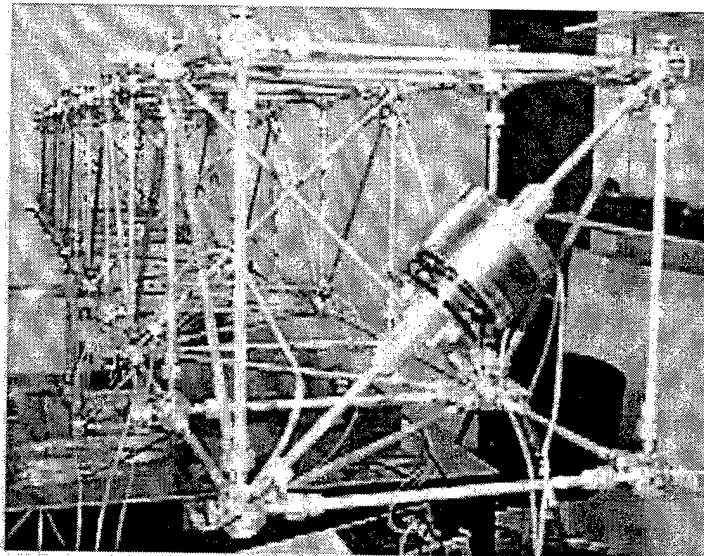
Figure 9. LPACT Mounted on NPS Space Truss [From Ref. 14]

The LPACT has its own frequency characteristics shown in Figure 10. The natural frequency at about 8.5-Hz is below the range of 10 to 30 Hz tested in these experiments. The mass of the LPACT does contribute to a shift in natural frequencies of the truss and is modeled in ANSYS. The addition of a new natural frequency in the 8-10 Hz range, that is the product of the LPACT spring, is not included in either FEM.

18
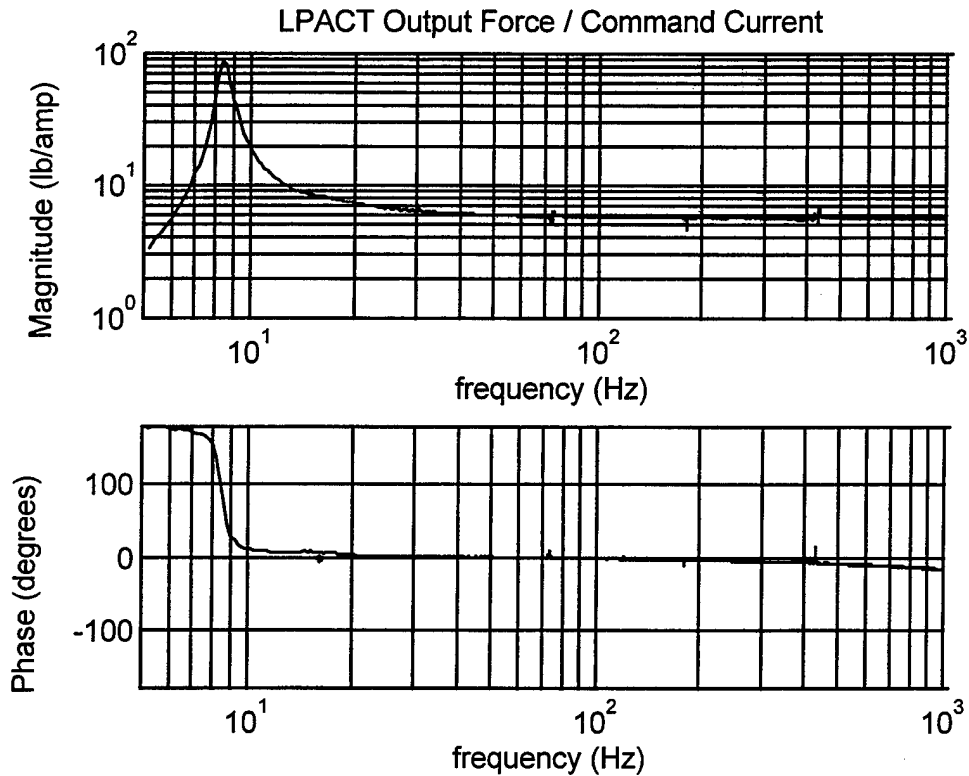
Figure 10. LPACT Transfer Function (feedback loops off) [From Ref. 16]

D.   LASER DIODE ASSEMBLY

The laser diode attached to the truss [Ref. 14] was relocated to node 26 of the truss.   The laser was directed to the far wall.   The only use of this assembly was to effectively amplify the truss vibrational motion and thus serve as a visual demonstration of the controller in action.   The mounting consisted of a thin aluminum rod, with a mass at the end, housing the laser.   The laser diode selected is a 1-mW, 635-nm Model PLC6351FW from Lasermate Corporation of Walnut, CA powered by a Hewlett Packard E3615A DC Power Supply, operating at 2-4 Volts nominal.   A picture of the laser diode assembly is included as Figure 11 and further details are can be found in Reference 14.
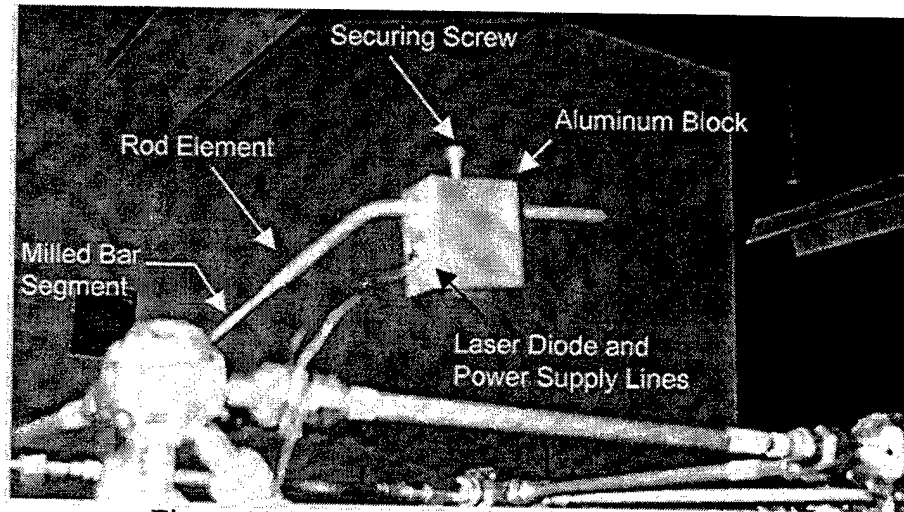
Figure 11. Laser Diode Assembly [From Ref. 5]

E.   PREVIOUS EXPERIMENTS

Three previous theses have been completed on the NPS space truss: One by CAPT Brent K. Andberg, USMC, an other jointly by LT Scott Johnson and LT John Vlattas, USN, and the third by LT Carey M. Pantling, USN.

1. Andberg [Ref. 17]

In his thesis, CAPT Andberg developed an FEM of the NPS space truss using an NRL code entitled NRLFEMI. He then performed modal testing on the truss to confirm the model. The experimental data was lacking in that it failed to observe the first mode. Finally, CAPT Andberg performed a technology demonstration of the use of Fiber-optic Bragg Gratings (FBG), used in this example to detect the motion of a simple cantilever beam. In the future, FBGs will be installed on the NPS space truss for shape determination.

2. Vlattas and Johnson [Ref. 14]

This Master's Thesis focused on two areas, the re-performance of modal testing with the HP 35665A two-channel spectrum analyzer and integration and testing of an active control device. They recommended that modal testing be again done, to overcome some of the limitations of the dSPACE system that was installed at the time. As will be discussed in the next chapter, a new dSPACE system was installed on the NPS space truss, and would be available for this purpose, if desired.

The active controls integration produced good results, with a maximum reported reduction of 14.817 dB at 16.85 Hz. They reported using a disturbance amplitude of 100 mV for the LPACT source. It was determine early on through the current course of this research that this did not even provide a sensor signal sufficient to overcome system noise. Therefore, the 14.817-dB reduction in amplitude is held in question.

3. Pantling [Ref. 5]

This Master's Thesis concentrated on the analytical modeling of the NPS Space Truss while active control methods were being applied. Models were created using both MATLAB/Simulink and ANSYS software packages. An IDIFF control law was used to realize a 15-20 dB reduction in vibration at the force transducer as observed using the dSPACE data acquisition and processing system. This was compared to 18-22 dB reductions as predicted by an ANSYS actively controlled finite element model. This was used to demonstrate the validity of predicting the effectiveness of a control authority using a FEM.

The use of the IDIFF controller did reduce the magnitude of the examined degree of freedom, but could result in large increases in other DOF's that were not used in the control law. He recommended the development of other control laws and the implementation of additional active elements.

III. CONTROLLER DESCRIPTION AND INTEGRATION

A. OVERVIEW

The active vibration control research done using the NPS Space Truss has primarily focused on minimizing the effect of equipment induced vibration on other components installed on the truss. Attempts have been made to reduce the vibration transmitted via a single truss element with the intent of reducing the total energy of the structure. The effectiveness of that approach is limited by the percent of vibrational energy that is transmitted by the control element. The control authority of the actuator becomes the limiting factor if energy is introduced into the structure that cancels out the disturbance effect at a specific node. As stated in the OBJECTIVES of this research, the control system developed in this thesis reduces single frequency vibrations at a remote location and is independent of structural characteristics. The control law is also flexible enough to allow the user to choose the node on the truss that they want to control, the active element they want to use, and the axis of concern. This allows for a specific focus for the purpose of the active element and significantly improved results.

The last active vibration control research on this structure was done using an integral plus double integral force feedback (IDIFF) control system that was incorporated by Vlattas and Johnson [Ref. 14] and evaluated by Pantling [Ref. 5]. The effect of this controller was a reduction of 15-20 dB in the vibration force as measured directly adjacent to the active control element. This method was replaced with a newly developed, adaptive multi-layer LMS controller that utilizes the same hardware configuration as previous work, but is able to reduce the vibration acceleration at a

23

remote sensor location. This system consistently reduces single frequency vibrations to the level of system noise at any one of several key nodes, using either of two installed active control elements. Results documented in this research show reductions in excess of 50 dB.

Figure 12 is an overview of the entire system, showing the positions of the disturbance source, nodal sensors, and active elements. It also includes the generalized flow path of the control signal and the processing elements, but is not intended to be an all-inclusive description. Detailed descriptions of the mathematics and experimental application are outline in the rest of this section.

The adaptive multi-layer LMS controller was developed using MATLAB/SIMULINK software and implemented using dSPACE RTI on a dSPACE DS1103 PPC Controller Board. The DS1103 has a Motorola PowerPC 604e microprocessor for a central processing unit (CPU), and resides in a triple-wide ISA slot in a host PC [Ref. 1, p. 12]. The DS 1103 board uses connectors for an external input/output (I/O) box that contains BNC fittings and standard computer cable connections for analog to digital (ADC), digital to analog (DAC) and support for other cabling formats (e.g. RS-232). Control of the dSPACE CPU and access to its memory (128MB) is done with the use of the dSPACE Control Desk. Specifics of each software component are discussed in grater detail in the following sections.
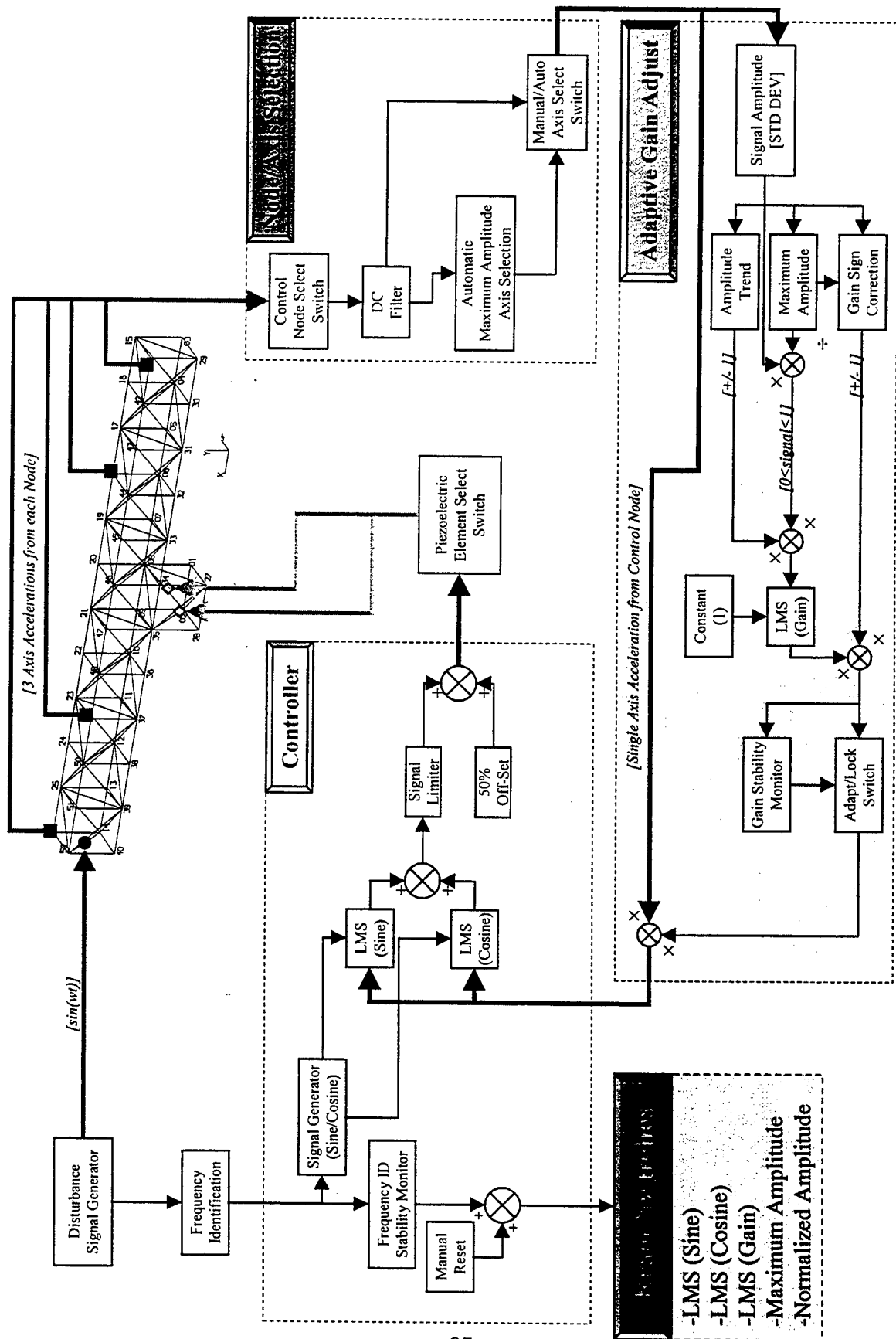
Figure 12. Control System Overview

B.   ADAPTIVE MULTI-LAYER LMS CONTROLLER

1. Adaptive Phase Adjustment

In 1998, Bertran and Montoro proposed an *Adaptive Notch Canceller* [Ref. 4]. Their work originated from the need to suppress vibrations induced by rotating machinery. This controller needed only mild structural assumptions (stable, linear, single input, single output plant, with tonal disturbances), which are consistent with the NPS Space Truss. This control algorithm was used as the foundation of the adaptive controller developed in this thesis. The advantages of this algorithm include its computational simplicity, neutral response to uncontrolled frequencies, and the possibility to operate multiple controllers in parallel at different frequencies. A diagram block describing this controller is shown in Figure 13.
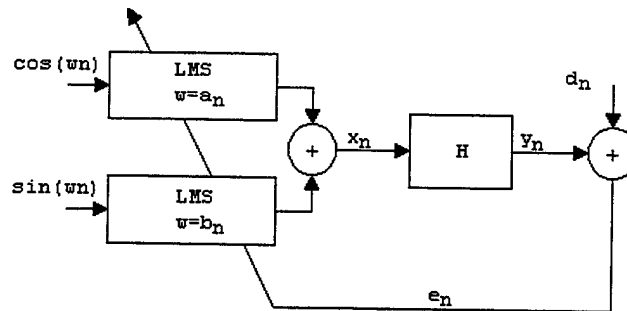
Figure 13. Adaptive Notch Canceller [Ref. 4]

Each of the LMS blocks implement an adaptive finite impulse response (FIR) filter of length one, using the stochastic gradient algorithm known as the Least Mean-Square (LMS) algorithm. The mathematical relationships of the signals shown in Figure 13 are:

$$H(j\omega) = \alpha e^{j\beta}$$
$$\omega \equiv \text{ Digital Frequency } [0, 2\pi]$$

(3.1)

$$x_n = a_n \cos(\omega n) + b_n \sin(\omega n)$$
$$n \equiv \text{ Time Index}$$
$$n \in \mathbb{N}$$

(3.2)

$$y_n = a_n \alpha \cos(\omega n + \beta) + b_n \alpha \sin(\omega n + \beta)$$

(3.3)

$$e_n = y_n + d_n$$

(3.4)

$$a_{n+1} = a_n + \mu e_n \cos(\omega n)$$

(3.5)

$$b_{n+1} = b_n + \mu e_n \sin(\omega n)$$

(3.6)

Assuming that the disturbance is a constant sinusoidal signal in the form:

$$d_n = D e^{j(\omega n + \gamma)}$$

(3.7)

For a convergence analysis, assuming the control signal rewritten as:

$$x_n = A_n e^{j\omega n}$$
$$\text{where,}$$
$$A_n = a_n + j b_n$$

(3.8)

The corresponding system output is then:

$$y_n = A_n \alpha e^{j(\omega n + \beta)}$$

(3.9)

Substituting equation (3.9) into the error equation (3.4), you get:

$$e_n = A_n \alpha e^{j(\omega n + \beta)} + d_n$$

(3.10)

Equations (3.5) and (3.6) can be converted into complex form and combined:

$$A_{n+1} = A_n + \mu e_n e^{-j\omega n}$$

(3.11)

27

By combining equations (3.10) and (3.11), the iterative equation for the exponential gain term is obtained:

$$A_{n+1} = A_n + \mu\left(A_n \alpha e^{j(\omega n + \beta)} + d_n\right)e^{-j\omega n}$$

$$A_{n+1} = \left(1 + \mu\alpha e^{j\beta}\right)A_n + d_n \mu e^{-j\omega n} \tag{3.12}$$

Now, substituting equation (3.7) into the above equation yields:

$$A_{n+1} = \left(1 + \mu\alpha e^{j\beta}\right)A_n + \mu D e^{j\gamma} \tag{3.13}$$

Because the disturbance and the plant variables (α and β) are assumed constant at a given frequency, the equation converges if:

$$\left|1 + \mu\alpha e^{j\beta}\right| < 1 \tag{3.14}$$

If the proper value of μ is chosen, the value of A_n will approach a constant as the time index (n) approaches infinity. Therefore equation (3.11) can be written as:

$$A_{n+1} = A_n + \mu e_n e^{-j\omega n}$$

$$\mu e_n e^{-j\omega n} = A_n - A_{n+1}$$

$$\mu e_n e^{-j\omega n} = 0 \text{ (as } n \to \infty)$$

$$\Downarrow$$

$$\lim_{n \to \infty} e_n = 0 \tag{3.15}$$

One of the main advantages of this algorithm is computational efficiency. It requires only seven floating-point operations per iteration (two addition, five products, and two trigonometric evaluations).

28

2. Adaptive Gain Adjustment

The convergence analysis of the adaptive phase adjustment algorithm requires that the correct value of the unit-less adaptation constant (μ) be determined. In order to make the controller more versatile, a method of determining this value automatically was developed and implemented as a gain factor applied to the error signal.
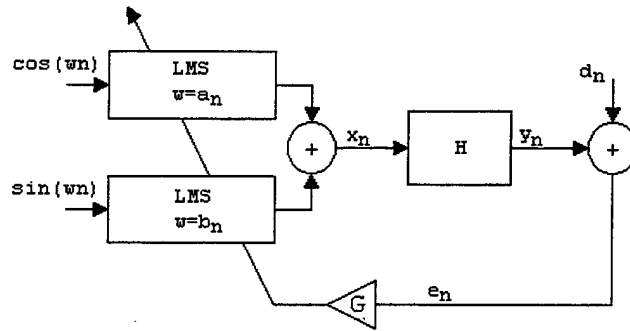
Figure 14. External Gain applied to LMS Controller

By introducing the variable gain (G) to the error signal, the system is modified as shown in Figure 14. By defining an adaptation constant internal to the LMS algorithm as μ', then equations (3.5) and (3.6) become:

$$a_{n+1} = a_n + \mu' G e_n \cos(\omega n) \qquad (3.16)$$

$$b_{n+1} = b_n + \mu' G e_n \sin(\omega n) \qquad (3.17)$$

If we redefine the effective adaptation constant (μ) as the product of an internal adaptation constant (μ') and an external gain (G), then the original LMS equations and convergence criterion are unchanged. This configuration allows the stability and rate of convergence of the phase adjustment algorithm to be controlled independently of μ'.

$$\mu = \mu' G \qquad (3.18)$$

29

The initial attempts to initiate a third LMS to control the gain directly were not successful due to complex and varying relationships between adaptation rates, structural phase effects, and the effects of various error and gain magnitudes. It was decided to split the adaptive gain adjustment into two distinctive parts. The first part deals specifically with the required sign of the gain to be applied to the phase adjust error signal. The second algorithm adjusts the magnitude of the gain to improve convergence rate, thus provide a faster response.

The sign correction factor is verified every second, based on a comparison of an instantaneous error amplitude compared to the largest amplitude recorded. If the current amplitude is larger than the previous maximum, the sign of G is reversed and the maximum is updated. The signal used to represent the error amplitude is the raw error signals standard deviation, which is directly proportional to the maximum amplitude of a constant frequency signal. The implementation of this logic statement is shown in detail in section [III.C. 1.e].

A third LMS algorithm was used to adjust the magnitude of the gain (G) as shown in Figure 15. As previously noted, the adaptation rates of the various sections of the controller are critical. The initial magnitude of G must be large enough to allow for the correct sign to be determined prior to significant variation in the magnitude. If the gain LMS adjustments the magnitude of the gain through zero (from positive to negative), the effect of the magnitude adjustment counters the sign adjustment. The two algorithms would then become competitive as the gain magnitude oscillates around a zero mean. The phase adjustment error signal would not necessarily have a zero mean due to frequency variations, but the magnitude of the error signal would be reduced to typical

30

experimental system noise levels, thus effectively stopping controller adaptation regardless of the of the actual error. With the proper adaptation rates applied to the system, the controller will therefore converge regardless of the value of μ. That does not assure controller effectiveness, only convergence, because the gain corrected error (Ge_n) is artificially being forced to zero as the gain LMS removes the system input. The net effect of this condition would be to transform the controller into another disturbance source that may, or may not suppress the original disturbance.
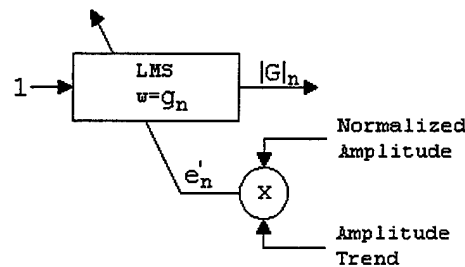
Figure 15. Gain Amplitude Adjust LMS

In Figure 21, the "Normalized Amplitude" is used to establish an error magnitude and is the instantaneous amplitude used for to determine the gain sign, divided by the maximum value. As the name suggests, this bounds the error magnitude to 1. The "Amplitude Trend" is set to either +/- 1 based on the approximate derivative of the error amplitude. This combination results in a range of errors of $-1 \le e'_n \le 1$. This results in the following system of equations:

$$-1 \le e'_n \le 1 \tag{3.19}$$

$$|G|_n = g_n(1) = g_n \tag{3.20}$$

$$g_{n+1} = g_n + \mu_{Gain} e'_n \tag{3.21}$$

This results in a maximum step size per iteration of the gain to be applied to the controller phase adjustment error signal of:

$$\left| |G|_{n+1} - |G|_n \right| \leq \mu_{Gain} \tag{3.22}$$

This provides a predictable foundation upon which to base the response time of the other LMS algorithms as described in section [III.B. 4].

3. Frequency Identification

In order to make this controller as robust as possible, it is necessary to identify the disturbance frequency and generate the appropriate sine and cosine functions. This also supports the assumption in the convergence analysis that the inputs to the phase adjusting LMS algorithms are sine and cosine functions of the actual disturbance frequency. Only the accuracy of the method of frequency identification is relevant to the operation of the controller, not the method. For a proof of concept, the identification process used here assumes that there is a single frequency disturbance source and updates the calculated frequency every 1.5 seconds. It is assumed that a signal would be available from the disturbance source that could be used for identification purposes. In this case, the disturbance frequency identification is done using the signal generator output to the LPACT.

The disturbance is assumed to satisfy equation (3.23).

$$d_n = A\cos(\omega n + \alpha) \tag{3.23}$$

It follows that d_n also satisfies the linear difference equation (3.24).

$$d_n + a_1 d_{n-1} + a_2 d_{n-2} = 0$$

with,

$$a_1 = -2\cos(\omega)$$

$$a_2 = 1$$

(3.24)

Rewriting equation (3.24) as a set of linear equations,

$$d_n = -\begin{bmatrix} d_{n-1} & d_{n-2} \end{bmatrix} \begin{bmatrix} a_1 \\ a_2 \end{bmatrix}$$

(3.25)

The solution requires only two samples, but in order to account for system noise, N samples are taken and the system is written as,

$$\begin{bmatrix} d_2 \\ \vdots \\ d_N \end{bmatrix} = -\begin{bmatrix} d_1 & d_0 \\ \vdots & \vdots \\ d_{N-1} & d_{N-2} \end{bmatrix} \begin{bmatrix} a_1 \\ a_2 \end{bmatrix}$$

or

$$[d] = [D][a]$$

(3.26)

Using the least mean squared method to solve this system yields the best fit for the values of $[a]$,

$$[a] = \left([D]^T[D]\right)^{-1}[D]^T[d]$$

(3.27)

Defining the following function:

$$A(z) = 1 + a_1'z^{-1} + a_2'z^{-2} = \frac{z^2 + a_1'z + a_2'}{z^2}$$

(3.28)

It can be shown that an equivalent form of the numerator is,

$$z^2 + a_1'z + a_2' = (z - e^{j\omega})(z - e^{-j\omega}) = z^2 - \left(e^{j\omega} + e^{-j\omega}\right)z + \left(e^{j\omega}\, e^{-j\omega}\right)$$

$$a_1' = -\left(e^{j\omega} + e^{-j\omega}\right)$$

$$a_2' = \left(e^{j\omega}\, e^{-j\omega}\right) = 1 \tag{3.29}$$

Using trigonometric equalities, it is shown that equation (3.29) also satisfies equation (3.24).

$$a_1' = \left(e^{j\omega} + e^{-j\omega}\right) = -2\cos(\omega) = a_1$$

$$a_2' = \left(e^{j\omega}\, e^{-j\omega}\right) = 1 = a_2 \tag{3.30}$$

Substituting the original values of a_1 and a_2 into the numerator of equation (3.28),

$$z^2 + a_1 z + a_2 = 0 \tag{3.31}$$

Solving for the roots of the numerator,

$$z^2 + a_1 z + a_2 = 0$$

$$z = \frac{-a_1 \pm \sqrt{a_1^2 - 4a_2}}{2}$$

$$z_1 = \frac{-a_1}{2} + \frac{\sqrt{-a_1^2 + 4a_2}}{2} \tag{3.32}$$

$$z_2 = \frac{-a_1}{2} + \frac{\sqrt{a_1^2 - 4a_2}}{2}$$

Using the first root to solve for the frequency,

$$\frac{-a_1}{2} + j\frac{\sqrt{-a_1^2 + 4a_2}}{2} = A_{Re} + jA_{Im}$$

therfore,

$$\omega = \left| tan^{-1}\left(\frac{A_{Im}}{A_{Re}}\right) \right| \qquad \text{[Digital Frequency (Rad)]} \tag{3.33}$$

$$f = \frac{\omega}{2\pi}(Sample\ Frequency) \qquad \text{[Frequency (Hz)]}$$

The implantation of this calculation is shown in section [III.C. 1.a].

34

4. Component Integration

The interactions between the various parts of an adaptive multi-layer LMS controller are dictated by their individual adaptation rates. For the LMS algorithm, the update rate is established by the system sample frequency ($^1/_{\Delta t}$) and the step size as determined by the following equation,

$$w_n = w_{n-1} + \mu u_n e_n$$
$$\Delta w = w_n - w_{n-1} \equiv \text{Step Size}$$
where,
$$\mu \equiv \text{LMS Adaptation Constant}$$
$$u_n \equiv \text{LMS Input Signal}$$
$$e_n \equiv \text{LMS Error Signal}$$

(3.34)

This makes the each LMS algorithm have an adaptation rate of,

$$R_{LMS} = \frac{\mu u_n e_n}{\Delta t}$$

(3.35)

The exact value of each step size is a function of the LMS error signal. As the controller minimizes the error, the step size is reduced and the reaction rate slows down to reach equilibrium at zero error.

For the gain sign correction algorithm, the correction is applied at predetermined intervals (ΔT). The size of the correction is determined by the magnitude of the initial gain (G_n). This makes an effective adaptation rate,

$$R_{Sign} = \frac{2G_n}{\Delta T}$$

(3.36)

The initial adaptation rates are estimated based on the observed orders of magnitude of the error signals. The orders of magnitude used in for this research are

35

listed below. The units on the error (e) and input (u) signals are irrelevant as long as the cancel out.

$$\mu'_{Phase} = 1x10^{-5}$$

$$\mu_{Gain} = 1x10^{-3}$$

$$u_{Phase} = 1$$

$$G = 1x10^2 \qquad u_{Gain} = 1$$

$$e_{Phase} = 1x10^{-3}$$

$$\Delta T = 1.5 \text{ sec} \qquad e_{Gain} = 1$$

$$\Delta t_{LMS} = 1x10^{-3} \text{ sec}$$

$$\Delta t_{LMS} = 1x10^{-3} \text{ sec}$$

The initial adaptation rates are estimated as follows,

$$R_{Sign} = \frac{2G}{\Delta T} = \frac{2(1x10^2)}{1.5} \simeq O(100) \text{ sec}^{-1} \tag{3.37}$$

$$R_{Phase} = \left(\frac{\mu' Gue}{\Delta t}\right)_{Phase} = \frac{(1x10^{-5})(1x10^2)(1)(1x10^{-3})}{1x10^{-3}} \simeq O(0.001) \text{ sec}^{-1} \tag{3.38}$$

$$R_{Gain} = \left(\frac{\mu ue}{\Delta t}\right)_{Gain} = \frac{(1x10^{-3})(1)(1)}{1x10^{-3}} \simeq O(1) \text{ sec}^{-1} \tag{3.39}$$

Both the sine and cosine LMS algorithms have the same adaptation rates, labeled here as the "Phase" rate. One of the key relationships is the relative dominance of the gain LMS algorithm compared to the phase LMS with respect to reaction time. This is required because the magnitude of G controls the convergence rate of the phase algorithm. If the convergence rates were on the same order of magnitude, the effect of one could conceivable cancel out the other. If the phase algorithm is made dominant, then the benefit of the gain LMS would be significantly reduced or eliminated. The other significant relationship is the relatively rapid initial assessment of the sign to be applied to the phase error signal. The order of magnitude difference in reaction rates is only one part of this relationship. The other factor that must be addressed is the time allowed for the controller to work between error magnitude assessments (as explained in section

[III.B. 2]). In this case, a reasonable reaction time was set at $T = 1$ sec. This time is a function of the adaptation rates of the LMS algorithms. If the controller does not reduce the magnitude of the disturbance in the time allotted (1 sec), then the error signal sign is reversed. If T is increased, the possibility of system fluctuation will be reduced at the expense of convergence rate and in extreme cases could significantly increase the structure vibration before effectively canceling it out.

The values listed in this section were used for all the data runs and dozens of other combinations of frequency, active element, and control node location. All results demonstrated stability and effectiveness with varying convergence times required. While performing demonstrations after the conclusion of this research, an unstable combination was found. The combination of frequency, element, node, and axis are summarized at the end of the experimental results [V.C. 11]. This discovery illustrates that the relationship demonstrated here is vestal, but not universal. Further experimentation is required to either correct this condition or fully document the instability.

C. SIMULINK / RTI

1. Simulink Controller

a. Overview

The first step in building the controller was to assemble a Simulink model. The Simulink model contains the processing connections necessary, implemented with block diagrams, to create the control law. The complete model is shown in Figure 16. Individual functional blocks are broken down and explained in the following sections.

37
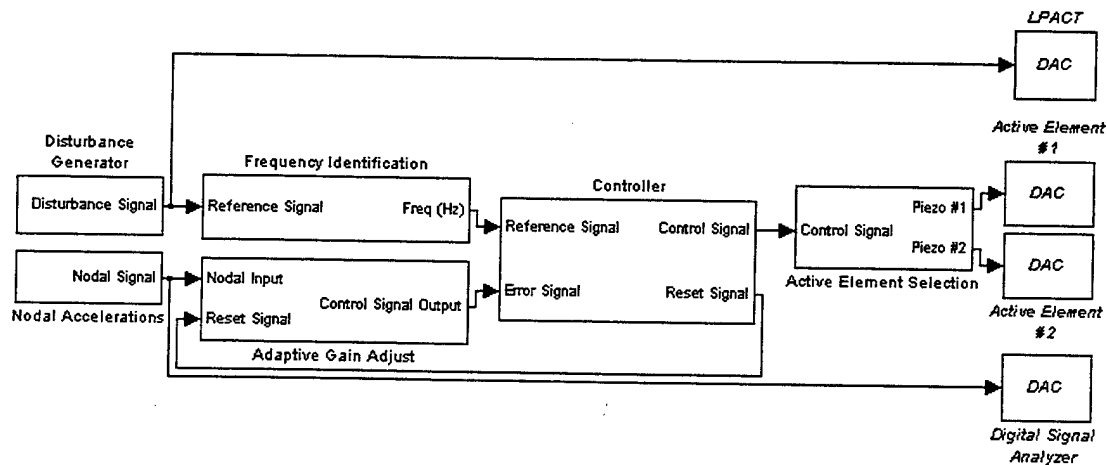
Figure 16. Adaptive Multi-Layer LMS Controller Overview

The nodal acceleration selected as the error signal for the controller is also sent directly to a DAC that was used to analyze the effectiveness of the controller in near real time. This allowed for analysis independent of the control law and without competing for system resources.

The dSPACE system relies upon the Simulink model for the selection of its sampling frequency. The sample input and signal output rates are both set at 1kHz, but the signal internal to the controller is often down sampled and/or buffered as explained in the following sections. This results in a multiple internal sample times ranging from 0.001 to 2 seconds. After the Simulink model was complete, the command "Tools> RTW Build" created a real-time program and object file that was executed by the CPU of the dSPACE system.

b. Disturbance Generator

The method of generating of the disturbance signal was designed to be adjustable from the dSPACE ControlDesk. Both the frequency and amplitude of the

disturbance can be adjusted using by modifying the "Disturbance Freq (Hz)" and the "Amplitude" values. The ability to turn off the disturbance was included as a separate gain factor. The default values are shown in Figure 17.
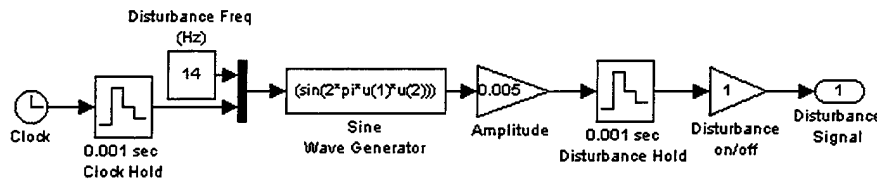
Figure 17. Disturbance Signal Generator

The signal is generated by,

$$D = A\sin(2\pi\omega t)$$
$$A \equiv \text{Amplitude}$$
$$\omega \equiv \text{Disturbance Freq (Hz)}$$
$$t \equiv \text{Clock}$$

(3.40)

Even though the clock signal is digitized to a 1 kHz sample rate for calculational purposes, the finial disturbance signal requires it's own 1 kHz hold in order to assure the correct synchronization with the other elements of the controller.

It was also noted that the clock signal would degrade over time, which compromised the reference signal to the phase adjust algorithm and the overall effectiveness of the controller. This was only observed during extended experimental runs and is a documented deficiency in the software package used for controller implementation [Ref. 18, p. 190].

c. Frequency Identification

This was initially constructed to use a reference signal from a sensor, not the digital signal from the disturbance generator. This requirement for additional signal

processing motivated both the input filter and the down sampling. This established the highest effective frequency of the controller at 33 Hz. After experimental data reveled the now obvious fact that as the controller reduced the disturbance signal by 30-50 dB, the signal to noise ratio for the frequency identification process increased to the point of ineffectiveness of the algorithm. This generated a significant error in the reference signal used for the phase adjustment and effectively prevented the controller from converging.
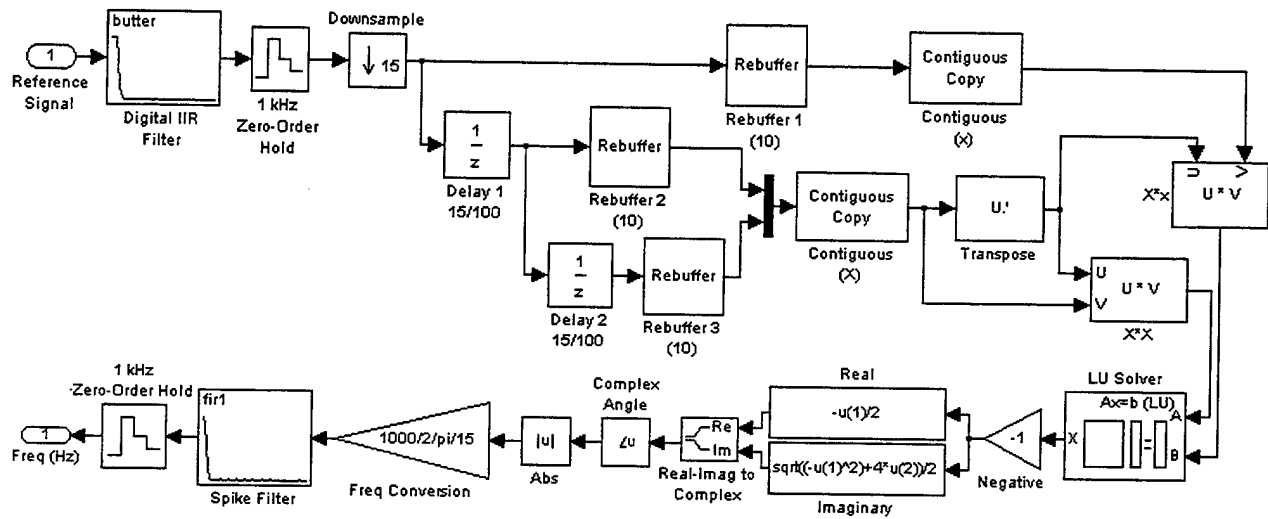
Figure 18. Frequency Identification

Although the reference signal was switched to the output of the signal generator, the algorithm was not changed. The minimum algorithm would not require either of the filters or 10 samples to determine the disturbance frequency and would therefore not be limited to the 33 Hz operational effectiveness limit. The "Contiguous Copy" blocks are required for the vector/matrix manipulation.

d. Nodal Accelerations

Each of the four accelerometers used on the selectable control nodes have three-axis capability. Each axis from the four accelerometers is fed into a 12-channel

40

Kistler Piezotron Coupler, Model 5124A, and then to a Trek 50/750 Voltage Amplifier.

Details of the equipment are included in Appendix A.
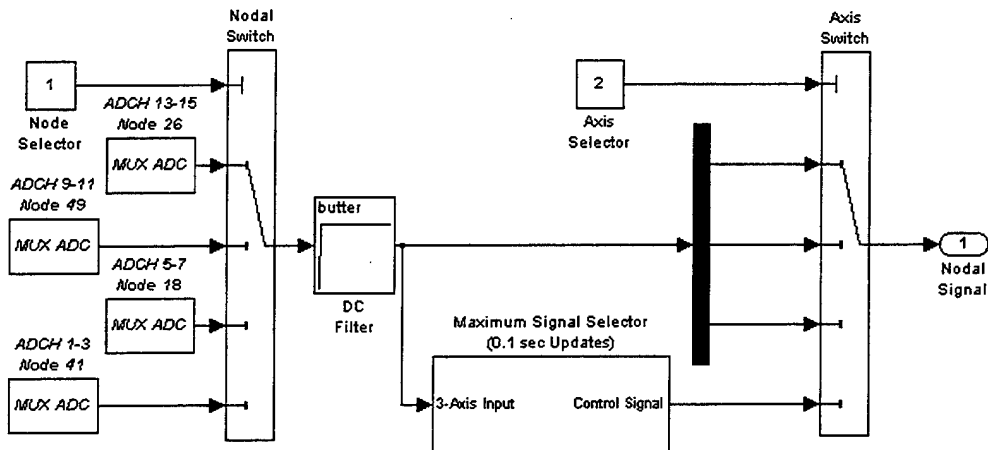
Figure 19. Control Node and Axis Selection

After the proper signal conditioning, the signals are used as the control signal input. The values of the constants "Node Selector" and "Axis Selector" are both controlled from the dSPACE ControlDesk. The "Nodal Switch" is controlled by the integer value of the "Node Selector" from 1 to 4 that corresponds to the desired node (Node 26 = 1, Node 49 = 2, Node 18 = 3, and Node 41 = 4). The "Axis Switch" is similarly controlled by the value of "Axis Selector" (X-Axis = 1, Y-Axis = 2, Z-Axis = 3, Max-Axis = 4) but includes an automatic selection option. The output from this sequence of switches is one of three axis signals originating from one of four nodal accelerometers.

It was found through several test runs that the input contained a DC bias that created a DC bias in the output and thus reduced the effective stroke of the active control element. This DC bias was removed with high-pass filter in the signal path in order to maximize the effectiveness of the controller. This need is consistent with the

41

results observed by the researchers at NRL, who used a second-order Butterworth filter to remove the DC bias [Ref. 6, p. 6]. A fourth-order filter was used for the NPS space truss. Higher order filters were tested to determine their utility and it was discovered that the higher-order did not lead to an appreciable increase in filtering, but did decrease the instantaneous response time.
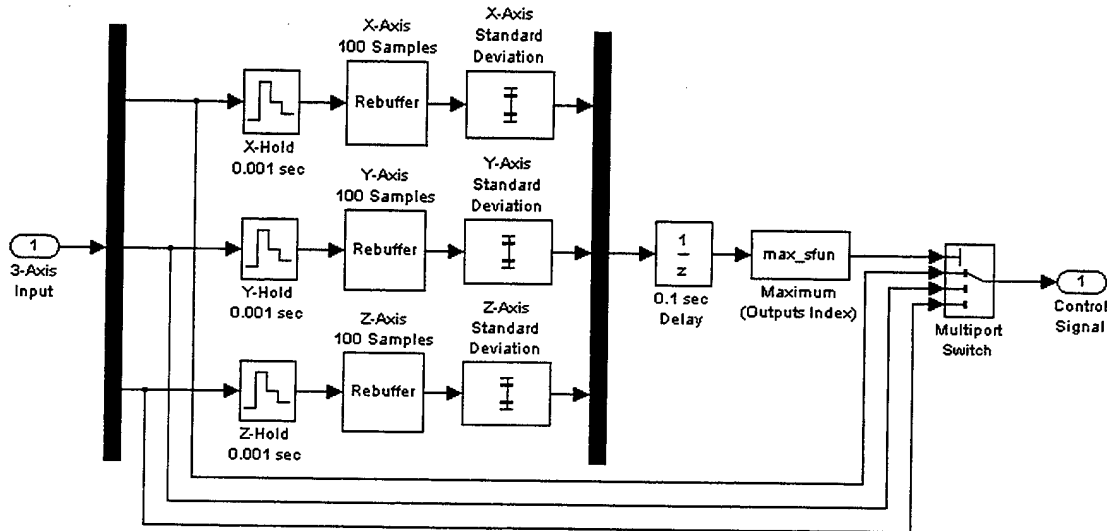
Figure 20. Automatic Maximum Amplitude Axis Selection

In general, minimizing a single axis disturbance using a random control location will result in an increase in the magnitude of at least one of the other axis. This motivated the rather simple option of having an algorithm automatically select the largest magnitude axis and use that signal as the controller error. Figure 20 shows the method used to determine the axis with the maximum amplitude disturbance. The standard deviation was used because it is proportional to the amplitude of a sinusoidal signal and the 100 sample buffer allowed for 0.1 second updates and covered enough of a 10 Hz disturbance signal to be effective. The "max_sfun" block outputs the index of the signal with the largest magnitude and is used to control the "Multiport Switch" that determines

42

the axis sent to the controller. This results in an instantaneous switching of the control signal as the amplitude of one of the signals drops below another. The controller tolerates this due to the set adaptation rates of the LMS algorithm. The use of this option predictably results in a steady state disturbance of equal magnitude in two of the control axis. This option was not used for evaluation of the controller due to large the effect on controller performance due to dependence on specific system response.

e. Adaptive Gain Adjustment

The adaptive gain adjust has the net effect of controlling the convergence rate of the entire controller. This element uses two main adaptive elements, but both use signals derived from the magnitude of the error signal used by the phase adjustment algorithm. This turned out to be one of the more complex sections of the controller, using both simple logic statements and LMS algorithms to adjust the gain while the controller was attempting to reduce the error. An overview of this function is shown in Figure 21.

43
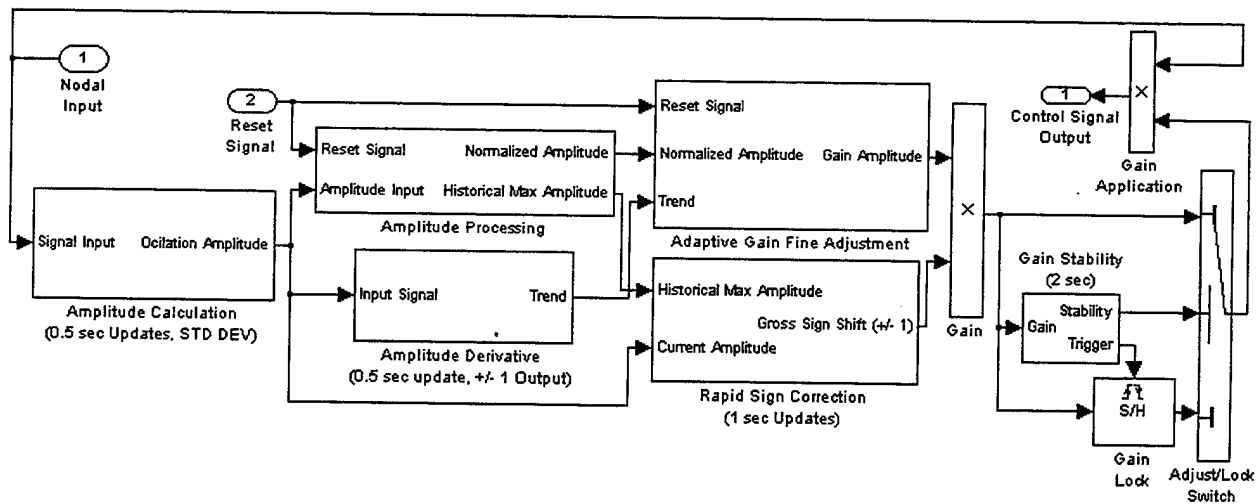
Figure 21. Adaptive Gain Adjustment

The "Control Signal Output" is simply the product of the "Nodal Input" and the calculated gain. If the controller is reducing the magnitude of the error signal, then the gain is increased, which increases the convergence rate of the phase adjust algorithm. Conversely, if the magnitude of the error is increasing, the gain is reduced, thus slowing the controller convergence rate. To derive a signal proportional to the disturbance magnitude, the standard deviation was calculated as shown in Figure 22.
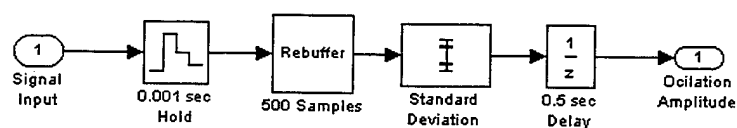
Figure 22. Amplitude Calculation

The LMS algorithm used to adjust the magnitude of the gain requires an error signal that oscillates around zero in order to converge. This was accomplished by using the product of the error magnitude and it's derivative. This produced a LMS step size that was positive and increasing in size when the error was increasing, and negative

44

and decreasing in size as the error was decreasing. To force the gain up as the error was

reduced, the sign of the derivative was reversed. Attempts to use the amplitude of the

derivative to increase the convergence rate resulted in unpredictable and thus undesirable

results. To correct for this, the derivative signal was used to determine the sign of the

error signal only and as noted before, the signs were reversed to allow for LMS

convergence.
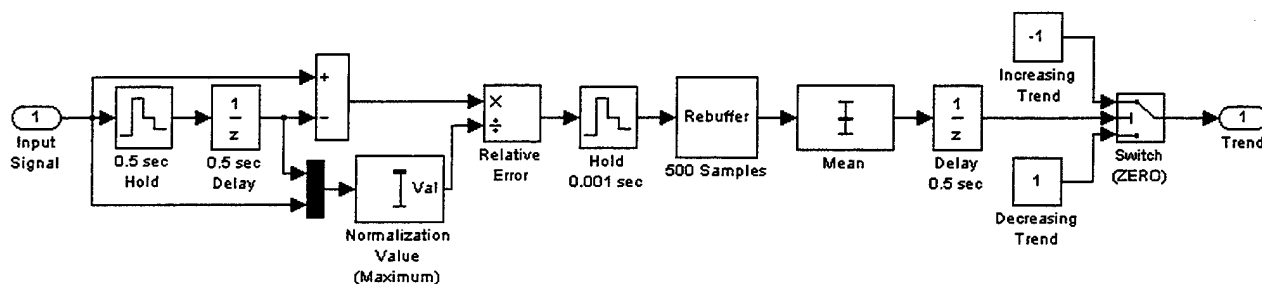
Figure 23. Amplitude Derivative

In order to further stabilize the convergence rate of the controller, the

amplitude of the error magnitude was normalized. The normalization value is referred to

as the "Historical Max Amplitude" and limits the magnitude of the error signal used to

adjust the gain LMS algorithm. In order to allow for multiple experimental runs without

reloading the program, a reset was included. The activation of this reset is either manual

from the dSPACE ControlDesk, or automatic based on the stability of the frequency

identification signal. Exact operation will be explained later, but the net effect on the

"amplitude Process" block is to trigger the "Hold Max Value" block continuously, but

assign a value of 1×10^{-10} in order to assure the first calculated amplitude will be greater

and replace the reset value.
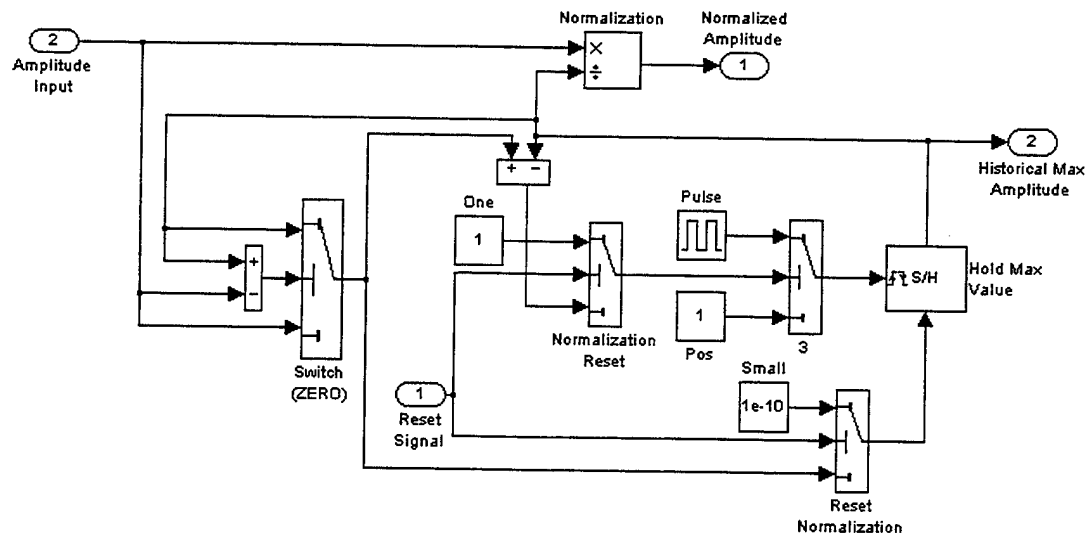
Figure 24. Amplitude Processing

When in normal operation, the historical maximum is determined by taking the difference of the current maximum and the "Amplitude Input" signal. If the input signal is smaller, then nothing happens. If the input signal is larger than the maximum, then it is switched to the input of the sample and hold block and the "Pulse" signal is aligned to the trigger. This replaces the output of the "Hold Max Value" block with the input signal. The maximum value is used directly as an output from this block and to normalize the "Amplitude Input" signal, as shown in Figure 24.

The adaptive gain adjust also contains a sign correction factor that is based on the historical maximum value compared to the current magnitude of the error and a time delay. The input to the algorithm is the "Current Amplitude" and the "Historical Max Amplitude" of the controller disturbance signal. The output is limited to either $+/-$ 1. The controller is allowed 1 sec to reduce the magnitude of error signal before the sign is reversed. This time delay is controlled by the pulse width of the "Trigger" to the "Hold the Sign" sample and hold block. The sign is reversed by a simple application of 1^{-n},

46

where n is a counter signal that is triggered by the same pulse generator that triggers the sample and hold, as shown in Figure 25.
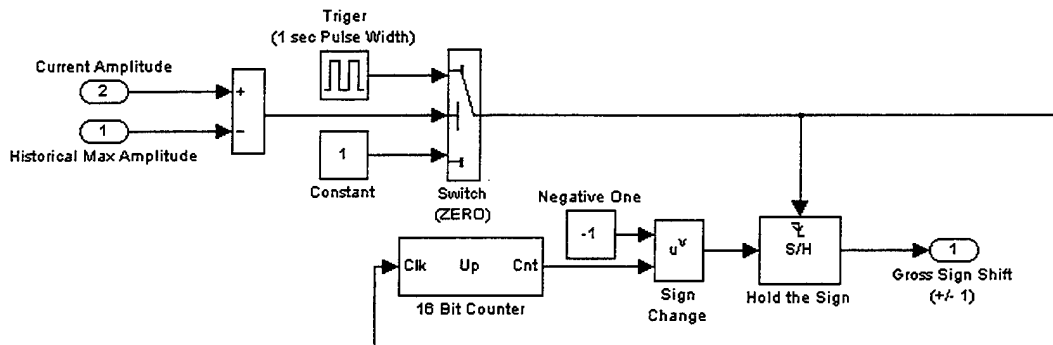
Figure 25. Rapid Sign Correction

The "Adaptive Gain Fine Adjustment" block controls the magnitude of the gain as seen in Figure 26. The values internal to the "Gain Adaptive Filter" are an initial tap value (w) of 400 and a step size (μ') of 1×10^{-5}. These values are reset by the same "Reset Signal" used to restore the initial values of the other control systems, based on wither manual override or frequency identification fluctuation.
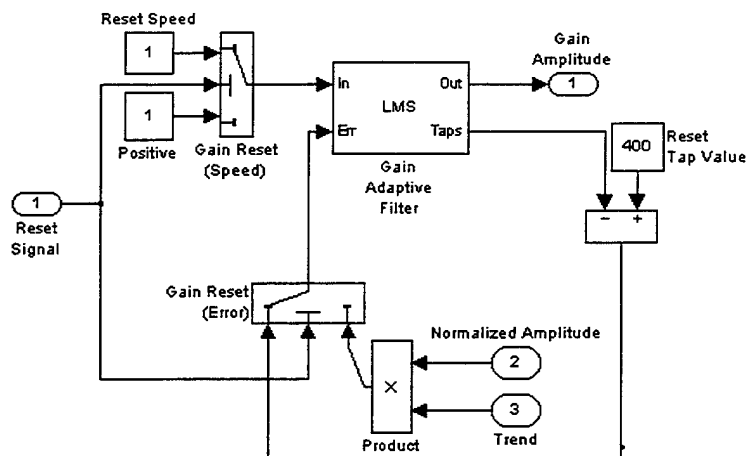
Figure 26. Adaptive Gain Fine Adjustment

47
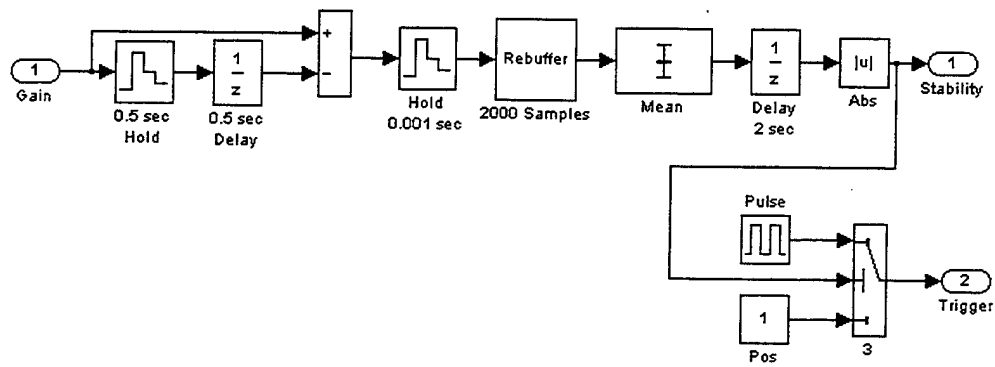
Figure 27. Gain Stability

The "Gain Stability" algorithm shown in Figure 27 was added to reduce the fluctuations of the LMS algorithm output after the controller has effectively converged. It was observed that the gain magnitude adjustment continually floated at, or near a convergence value. Unfortunately, this oscillation was reflected in the phase adjust LMS and resulted in the reduced effectiveness of the controller. To prevent this, a dead zone was built into the gain magnitude adjustment. The purpose of this block is to measure the fluctuation in the gain signal and produce a pulsed trigger if the average difference between four successive gain values is less than 4. When the trigger is pulsed, the sample and hold block labeled "Gain Lock" in Figure 21 will lock in the current gain value. The "Adjust/Lock Switch" is triggered by a gain stability value of 4 or less to switch the gain used to the output of the "Gain Lock" block.

f. Adaptive Phase Adjustment

The phase adjustment of the control signal is accomplished using a sine and cosine generated based on the output of the frequency identification block "Reference Signal." The same signal also is used to reset the controller presets if the disturbance frequency varies. The overview is shown in Figure 28.

48
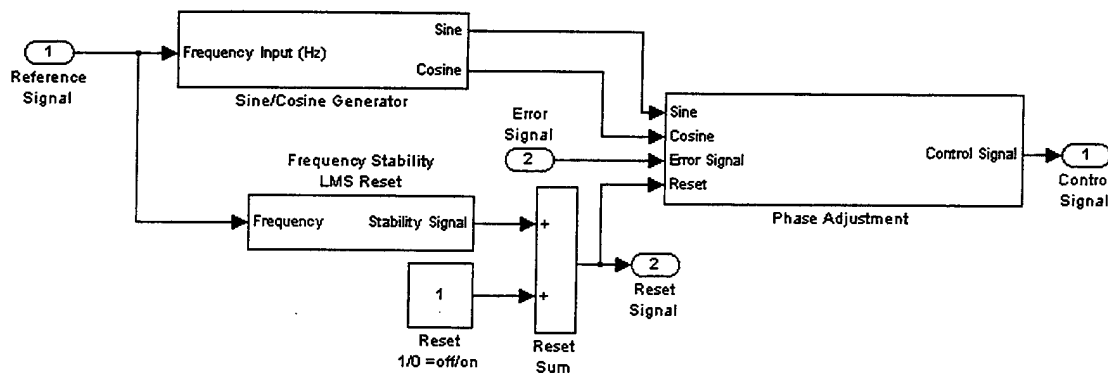
Figure 28. Controller

The "Reset Sum" block allows for either a manual or automatic reset of the controller. All of the reset switches associated with the LMS algorithms and the disturbance magnitude history have a set point of 1. If the reset signal is less than the set point, then the appropriate operating signal is allowed to pass. If the reset signal exceeds that set point, then the signals are switched to the appropriate values to restore the initial conditions to the controller.

The sine and cosine waves are produced as described in section [III.B. 1]. An additional gain factor was included in this section to allow for the controller output to be zeroed. Switching both the "Sine Switch" and the "Cosine Switch" to zero does this, forcing both phase adjustment LMS outputs to zero regardless of error signal or gain.
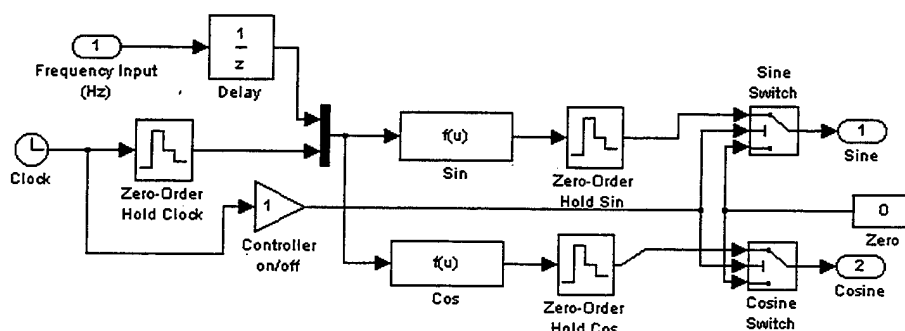
Figure 29. Sine/Cosine Generator

49

This controller requires steady reference signals, at the correct frequency, in order for the appropriate gains to be determined. If the reference signals fluctuate, the fluctuation tends to be amplified by the controller. To prevent this, the stability of the frequency identification signal is monitored. If the signal is fluctuation too fast, the controller resets and waits until the identification becomes stable. The "Frequency Stability LMS Reset" block shown in Figure 30 is tuned to allow only very minor fluctuation in the reference signal prior to resetting the controller. It was found experimentally that the controller was capable of tracking with very slowly changing disturbance frequencies, but this option was not explored by this research and in fact, the values of the stability reset were set to preclude most chance of this.
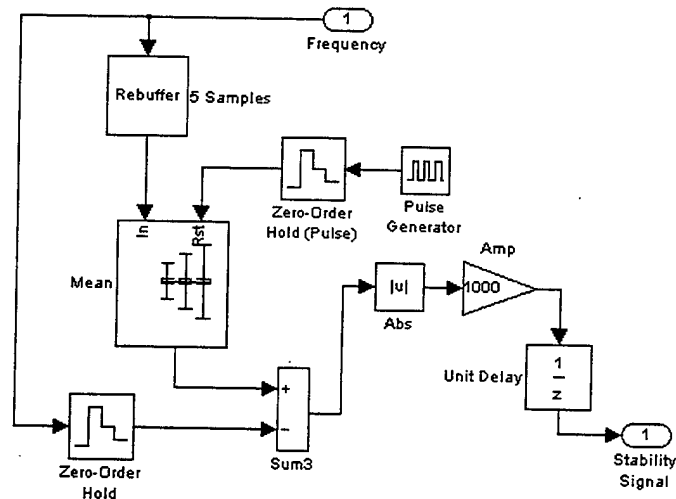
Figure 30. Frequency Stability LMS Reset

The reset is based on the difference between the mean of the previous 100 samples and the current frequency identified by the algorithm. If the magnitude of this difference is greater than 0.001 then the controller is reset. This block generates a signal

proportional to this difference with a gain factor that brings the output up to the required trip value for the controller reset switches. The mechanism for the reset can be seen in Figure 28.

Figure 31 shows the "Adaptive Phase Adjustment" block that is essentially a notch filter as explained in section [III.B.   1].   The addition of the various reset switches allows for the reference and error signals to be changed in order to force the "taps" back to their default value of zero. The step size (μ') used for these LMS blocks is 1×10^{-5}. This section also contains a provision to prevent an over voltage condition of the piezoelectric strut. The saturation limiter is configured to insure the control signal in maintained within the operation limits of the strut. The DC bias is included as part of the control signal in order to allow the maximum oscillation of the strut.
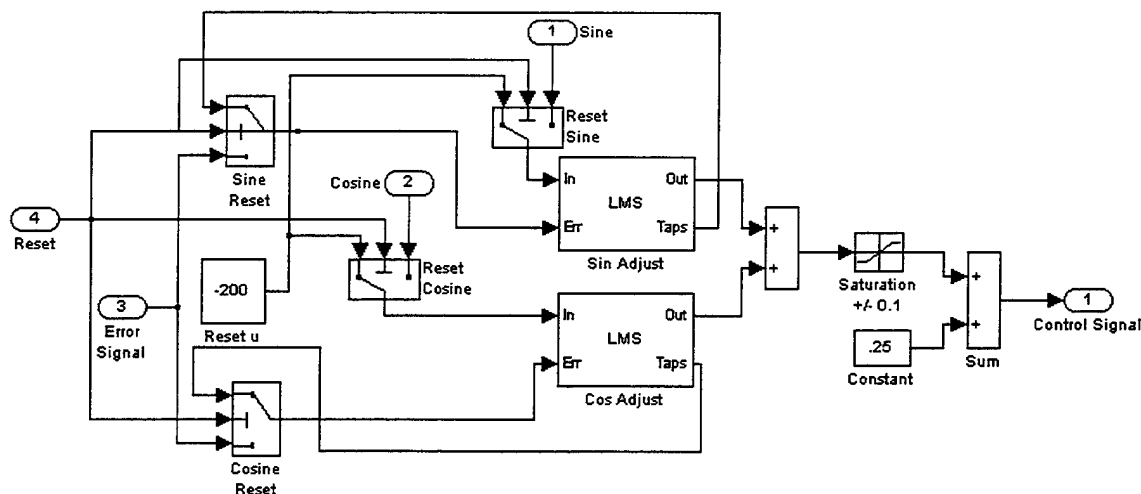
Figure 31. Adaptive Phase Adjustment

51

g. Active Element Selection

The last segment of the controller, prior to the digital to analog converter that directs the signal to the strut, is the "Active Element Selection" block. This block was included to allow for software switching between active elements. The same DC Bias is included in this feature to minimize the voltage fluctuation on the piezoelectric elements.
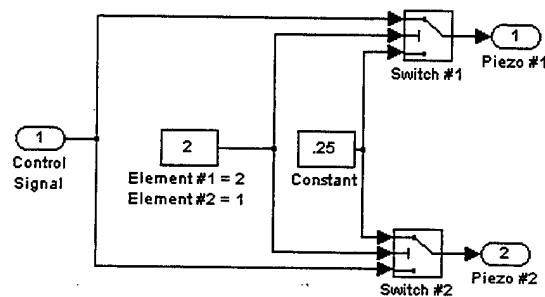
Figure 32. Active Element Selection

2. RTILIB

The interface from Simulink to dSPACE is found in the Real-Time Integration Simulink Library (RTILIB) and was accomplished the same was as previous control system experiments using the NPS Space Truss [Ref. 5]. The program is started by typing "rtilib" in the MATLAB command window, after Simulink is running [Ref. 18, p. 17]. The RTILIB contains the blocks required to provide the interface between the CPU and the I/O hardware. The RTILIB interface is shown in Figure 33.
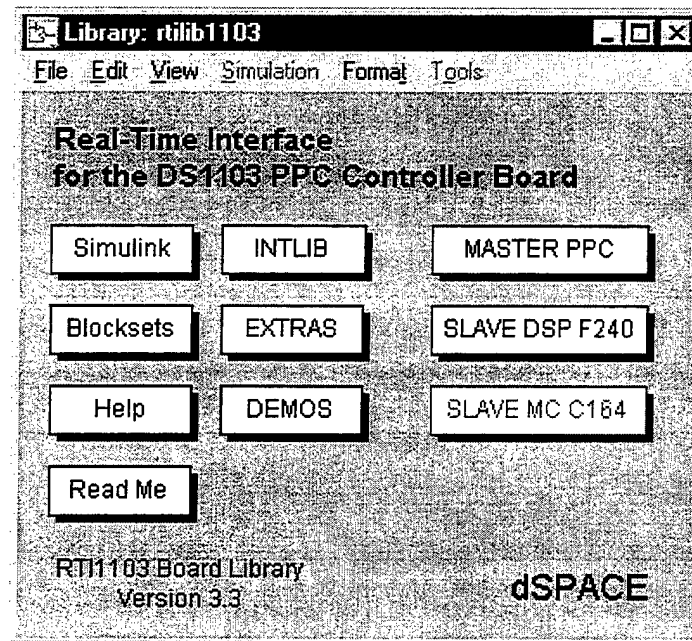
Figure 33. RTILIB Interface [Ref. 18, p. 18]

The blocks were selected and then "dragged and dropped" onto the Simulink model for integration. The I/O box connections are found under the "MASTER PPC" icon and there are twenty available inputs and eight outputs available to the user in dSPACE, accessible by three blocks, shown in Figure 34.
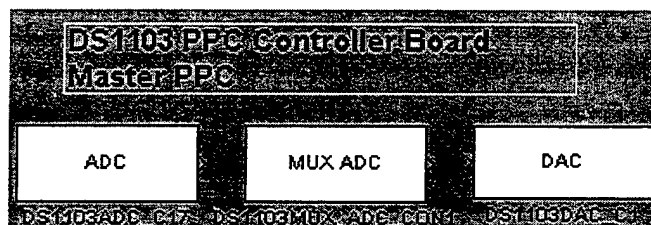
Figure 34. MASTER PPC I/O Connections [Ref. 18]

The ADC channels available are the ADC and MUX (Multiplexed) ADC. The MUX ADC is a series of four channels, with four multiplexed inputs each (ADCH 1-16). They can be used in Simulink as individual separated channels, or as a vectored input. The scalar ADC block is a single input, corresponding to the last four input channels (ACDH 17-20). There are eight output channels accessible with the DAC blocks (DACH

1-8) [Ref. 18, p. 24]. The I/O blocks, when connected to the I/O interface box, exhibit a 10:1 gain in value.

D.   dSPACE CONTROL DESK

ControlDesk also allows for grouping relevant files under an "experiment" and then accessing and manipulating the data loaded in the CPU. It also allows for running macros that automate the data taking process using the dSPACE macro language, Python [Ref. 19, pp. 13-14].

Using ControlDesk allows for the selection of variables for real-time display in on-screen instruments, and for entire program to be downloaded and executed by the CPU [Ref. 19, p. 31]. To create a working experiment, a program must be loaded into the CPU's memory, then an instrument panel may be built that will monitor and control the parameters and signals desired. The ControlDesk interface contains the main window, Navigator, and Tool Window that can be manipulated to allow a user to run his/her experiments. The Navigator provides access to load files into the CPU; the Tool window is used to create the interface using the program variables and several interface options. The Main window is used to monitor and control the simulation [Ref. 19, pp.43-50].

Instrument panels are built in the Tool window using a pull-down menu interface to D&D desired instrument on the main window. The user can choose between sliders, pointers, oscilloscopes, knobs, buttons...etc. to create the interface. There are various types of variables that can be assigned to each of these interface options. The variables are grouped according to their block location in the Simulink model used to create the program loaded into the CPU. The relevant types to this thesis are shown in Table 2.

Type	Description:
B:	Block Outputs
S:	Inputs of Signal Sinks
P:	Block Parameters

Table 2. dSPACE Variable Types [Ref. 20]

The controller layout used for the Adaptive Multi-layer LMS controller on the NPS Space Truss is shown in Figure 35. The large plot on the top of the Layout is an oscilloscope plot of the disturbance signal. The upper plot in the lower right-hand portion of the layout is the control signal to the actuator. The lower plot is to monitor the convergence of the LMS algorithms for both phase and gain adjustment. The actuator used for control is designated in the selection labeled "Active Control Element" located in the center of the panel. The "Gain Lock" LED is controlled by the stability signal generated by the "Gain Stability" block (section III.C. 1.e) and turns from yellow to green when the gain stops adjusting. The control node and axis are selected with buttons in the "Node and Axis of Interest" section located just left of center. The "Auto Axis" LED is controlled by the "Automatic Maximum Amplitude Axis Selection" block (section III.C. 1.d) and changes color depending on the relative magnitude of the disturbance and indicates RED when the X-axis is the largest, WHITE when the Y-Axis is the largest, and BLUE when the Z-Axis is the largest. The output from the "Frequency Identification" block (section III.C. 1.c) is displayed in by the digital readout labeled "Frequency Identification" located on the center, left-hand edge of the panel. The "Run/Reset" LED is controlled by the "Reset Sum" value (section III.C. 1.f) and turns green when the controller is active, and yellow when it is in standby either due to frequency identification instability, or manual override.
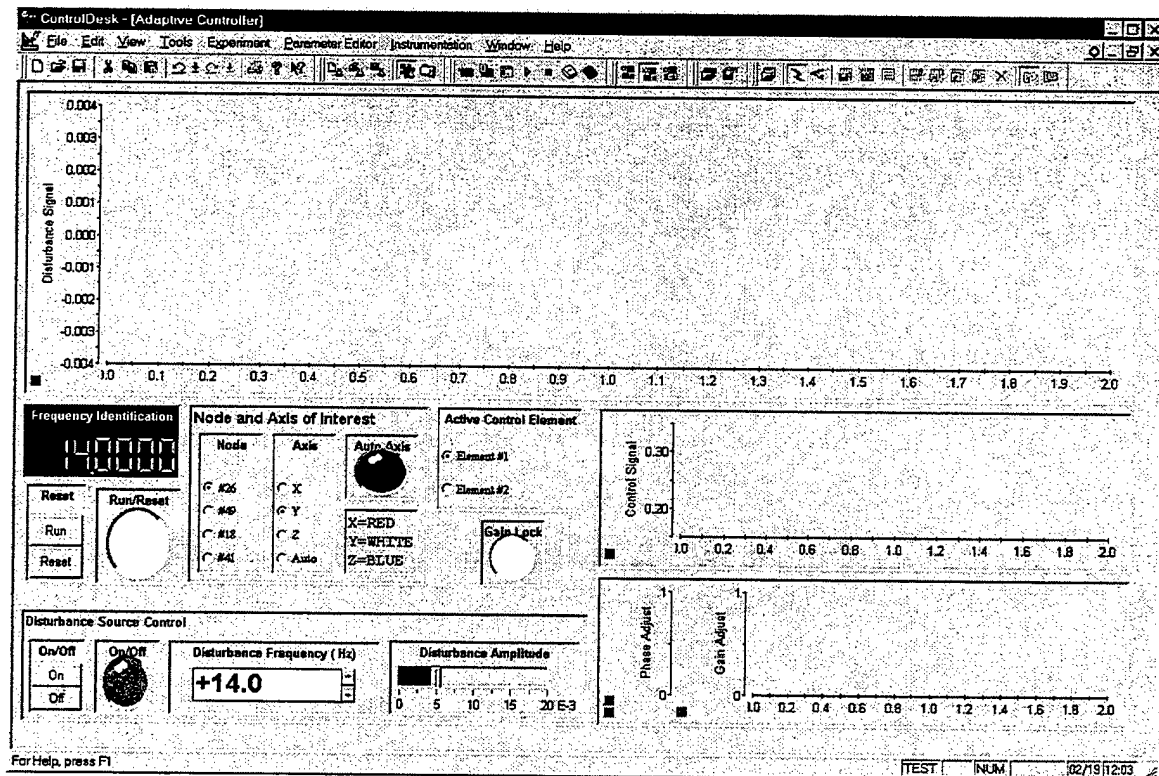
Figure 35. NPS Space Truss Controller Layout

The disturbance frequency and amplitude can be adjusted from the "Disturbance Source Control" block located in the lower left corner. The only adjustment required for the controller to function is to push the "Run" button on the "Reset" switch located to the left of the "Run/Reset" LED. All other controls change the disturbance properties, the control element location, or the location of the node and/or the axis where the vibration is to be minimized. The steps required to start and run the controller are included in Appendix D.

E.   AMPLIFIERS AND CONDITIONERS

As previously stated, the equipment used for this research is virtually identical to that used by Pantling [Ref. 5]. A notable exception to this is the addition of another active strut and the associated signal conditioners. The signals generated by the force

56

transducers are not used for this controller, but are still available if required for future research. These signals are fed into PCB Piezotronics Model 484B signal conditioner, which has a unity gain and a selectable bias (either 6.0 or 11.0 Volts, DC or AC). The four accelerometers mounted on the control nodes have three-axis capability. Each axis from the four accelerometers is fed into a 12-channel Kistler Piezotron Coupler, Model 5124A. The control signal is sent to a Trek 50/750 Voltage Amplifier. Details of the equipment are included in Appendix A.

The mini-calibration performed on the Trek amplifier by Pantling [Ref. 5] was determined to be sufficient for this research. The Trek was calibrated for a 20-time voltage gain.

THIS PAGE INTENTIONALLY LEFT BLANK

IV. CONTROLLED FINITE ELEMENT MODEL OF THE NPS SPACE TRUSS

A. ANSYS OVERVIEW

ANSYS is a finite element utility capable of modeling many different physical properties, using more than 100 types of elements. Systems that involve, mechanical, electromagnetic, thermal, piezoelectric and electric characteristics can be modeled. The options available with the software package are based on the licensing obtained from ANSYS. For the work in this thesis ANSYS version 5.6, Multiphysics was used.

The ANSYS preprocessor permits the creation and manipulation of a finite element model that can then be meshed into a finite element grid and acted upon with loads and restraints. The solver sub-program can be used to specify different solution types. For this thesis, a modal analysis was performed on the same model used for the transient analysis on the controlled model. The specifics of the ANSYS commands required are detailed in Reference 21.

B. ANSYS PARAMETRIC DESIGN LANGUAGE (APDL)

The ANSYS Parametric Design Language (APDL) is a macro language that enables a user to run command streams from an external file. This allows for a closed model that performs an actively controlled data run, requiring no input from the user save to establish initial parameters and start the simulation.

An APDL file is a text file that contains the commands, as they would be typed into the ANSYS command interface, with user-determined variables [Ref. 21, /INPUT, *SET] and is used in conjunction with the transient analysis capability to perform the

control law application. ANSYS allows the user to examine each step in a transient analysis and the APDL program can record these parameters to output files for analysis in the time domain.

The model routine automatically time-steps through a transient analysis, applying a sinusoidal force to the mass representing the LPACT. The control node displacement was also measured and the velocity and acceleration of that node estimated based on previous samples. The nodal acceleration was then used as the error signal for the controller section of the adaptive multi-layer LMS controller. The entire logic statement of the control algorithm was not included for this thesis for simplicity. The numerical control law was applied and the control voltage was calculated and applied to the chosen piezoelectric actuator. These varying forces were recalculated and applied at each step.

1. Controller Application

An example of the APDL files used in this thesis is included as Appendix E and is based on the finial APDL used by Pantling [Ref. 5]. There was no need for the digital filter used in Reference 5, so it was removed. The adaptive multi-layer LMS control algorithm, as it is applied to the NPS Space Truss, uses nodal acceleration to generate a disturbance reference signal. This is not a direct output of the ANSYS program, but the nodal displacement is. After each time step, the post-processor was used to obtain the vector displacement at the control node. Then the velocity is estimated using a backward difference, 2nd order derivative approximation.

$$\vec{V}_n = \frac{(\vec{\delta}_n - \vec{\delta}_{n-1})}{\Delta t}$$

where,   (4.1)

$(\delta_n - \delta_{n-1}) \equiv$ The vector change in displacement.

$\Delta t \equiv$ The time step used in the analysis.

The acceleration is calculated in the same manor, replacing the estimated velocity for the measured displacement and using the same time step.

$$\vec{A}_n = \frac{(\vec{V}_n - \vec{V}_{n-1})}{\Delta t}$$

where,   (4.2)

$(\vec{V}_n - \vec{V}_{n-1}) \equiv$ The vector change in velocity.

For the sake of simplicity, the gain portion of the adaptive multi-layer LMS control algorithm was not included in the simulation. This did require multiple runs to establish the optimal gain that should be applied to the controller, but the saved programming time. Further research in this area could incorporate the entire control system into the APDL file.

The controller uses the LMS algorithms developed in Reference 5 and outlined in section [III.B. 1], Adaptive Phase Adjustment. The basic equations are restated below:

$$CS_n = G\left[a_n \cos\left(2\pi f n \Delta t\right) + b_n \sin\left(2\pi f n \Delta t\right)\right]$$

where,

$CS_n \equiv$ Voltage applied to the piezoelectric element.

$G \equiv$ Constant gain factor due to hardware amplification.

$f \equiv$ Disturbance frequency in Hz.   (4.3)

$n \equiv$ Iteration counter.

$\Delta t \equiv$ The time step used in seconds.

$a_n \equiv$ The Cosine weighting factor.

$b_n \equiv$ The Sine weighting factor.

The weighting factors are updated each time step based on the calculated nodal acceleration (A_n) using the following equations:

$$a_{n+1} = a_n + \mu A_n \cos\left(2\pi f n \Delta t\right) \qquad (4.4)$$

and

$$b_{n+1} = b_n + \mu A_n \sin\left(2\pi f n \Delta t\right) \qquad (4.5)$$

The adaptation constant (μ) was determined by trial and error, running short simulations and evaluating the results until the initial trends were indicative of convergence. The finial run was then made using the predetermined value of μ.

After each time step is solved for the CS voltage was applied to the actuator element in the next time step. The control signal, weighting factors, nodal displacement, velocity, and acceleration were all captured for analysis.

C. NPS SPACE TRUSS MODEL

The FEM created in Reference 5 was used for this analysis with an additional active strut assembly replacing NPS Space Truss element 107. First the existing truss element was deleted. Then the piezoelectric element and force sensor were copied and reflected across a plane of symmetry located in the middle of the truss. Then the elements were rotated 90° around the geometric center of the span. Then a similar procedure was followed for the steel connecting elements. This effectively made the model look correct, but the mathematical formulation was incomplete.

The next step was to merge the coincident nodes created by copying and pasting the original active element over the previously existing nodes on the opposite side. This procedure also had to include the nodal junctions of the piezoceramic elements and the

62

steel support elements. After the nodes were merged, the boundary conditions had to be applied to the new piezoelectric elements. Boundary conditions do not copy with the elements. As with the previous model, a grounded condition was used to act as a reference to the applied voltage and then the displacement DOF's of the solid elements were coupled to the steel beam element nodes that contacted the piezoelectric model.

Details of the original model assembly can be found in Reference 5 and the actual component specifications are found in Appendix A. A summary of the properties used to model the piezoelectric properties is found in Table 3.

Property	Quartz	PZT
Stiffness	1.0 kN/μm	33.0N/μm
Sensitivity	11,420 mV/kN	-
Axial Elastic Modulus	100Gpa	142GPa
d_{33}	87.56e-9 m/V	500e-9 m/V
e_{33}	8756	7100

Table 3. Material Properties [From Ref. 5]

Figure 36 shows one of the active struts as modeled in the ANSYS FEM.
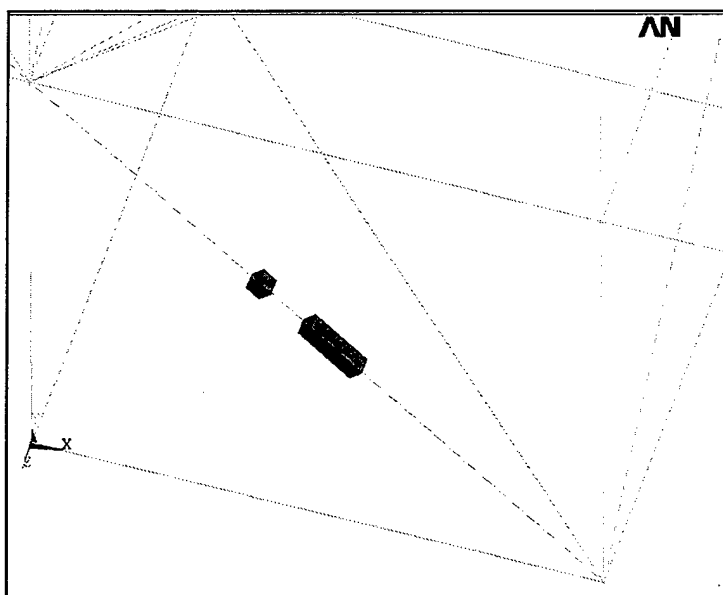
Figure 36. Active Strut Modeled in the NPS Space Truss [From Ref. 5]

63

The LPACT model was not modified, but the experimental results did show that the limits of the control authority of the installed elements could be exceeded by the LPACT at certain frequency and node combinations. This was addressed by reducing the amplitude of the reference signal to the LPACT. The same transfer function derived in Reference 5 was used to model the force applied by the LPACT in this research, however it was occasionally required to modify the amplitude by applying a gain factor (GF) in the FEM. This resulted in the following equation that was used in the APDL program:

$$AMP = (GF)(0.2037 * FREQ^2 - 7.0719 * FREQ + 68.3564) \text{ [lb/amp]} \quad (4.6)$$

The APDL macro program, "Act_truss.inp" that was used in the previous analysis [Ref. 5] was modified to become "Truss_Control.txt", which served as the root program for this analysis. The original program "Act_truss.inp" is included for reference in Appendix F and the modified version (set up to control the y-axis of Node 18, with 19Hz disturbance, using the second active element) is included in Appendix E.

The new version of ANSYS seemed to eliminate the stability problems that were experienced in previous research. No stability problems were encountered in any of the simulations that were not explained by incorrect gains being applied to the control algorithm.

V. COMPARISON OF EXPERIMENTAL RESULTS WITH ANSYS FINITE ELEMENT MODEL

A. METHODOLOGY

The purpose of these experiments is to demonstrate the performance of the controller developed in this thesis and to confirm the ability of an active FEM to predict the effectiveness of the algorithm. The flexibility of the controller made a full demonstration of its abilities infeasible. In order to show its general abilities, nine experiments were performed using a variety of frequency, control node, and active element combinations. Eight of the experimental combinations were also simulated in ANSYS for comparison. Although the adaptive gain portion of the controller is not included in the ANSYS model, the correct gains for the comparisons were determined on a trial and error basis using the results of short simulations to modify and tune the controller gain manually. A ninth experiment was run to compare the results of the adaptive multi-layer LMS controller with the previously used IDIFF controller.

The first four experiments were designed to demonstrate the versatility of the controller with respect to active element location, disturbance frequency, and control location. The first and second experiments control different nodes, axis, and frequencies using different active elements. The third and fourth experiments control different axis of the node that is the closest to the disturbance source with the same disturbance frequency, using different active elements. The next four experiments were done to demonstrate more challenging control situations. They use the first three modal frequencies predicted by the FEM, axis based on the displacement shown by modal analysis, and a randomly

chosen active element. The last experiment was done at the frequency, node and axis at which the IDIFF controller demonstrated the best performance.

Each experiment was run multiple times with nearly identical results in most cases. A representative set of results of each data is included either in the text, or in Appendix G.

B.   EXPERIMENTAL CONTROL SYSTEM

1. Experimental Setup

The nodal accelerations used as the controller system feedback were generated by one of four Kistler 8690C10 three-axis accelerometers. Two accelerometers were place at the ends of the truss, nodes 26 and 41. The other two were positioned near the midpoint of the truss arms, nodes 49 and 18. This configuration is the same as the one used in previous research, but the node numbering is not consistent. If direct comparison of results is desired, both the nodal numbering system and axis orientation should be verified.

A Kistler Piezotron Signal Conditioner, model 5124A was used as a signal conditioner for the accelerometers. It does not amplify the signal and only served to power the accelerometers and filter the output. Accelerometer drift that was experienced in previous research [Ref. 5] was removed using a high pass filter. This was not required in the past, because the signals were used only for spectral analysis. This controller uses the signals as feedback and would attempt to zero out the low frequency drift as well as the vibration and this could have lead to actuator saturation.

The dSPACE DS1103 digital signal processor received ADC inputs from the accelerometer signal conditioners. The control signal DAC output was feed to a TREK power supply, model 50/750 and then directly to the piezoelectric elements. A second DAC output was used to send the nodal acceleration signal to a Hewlett Packard HP 35665A Dynamic Signal Analyzer. This output was not required for the operation of the controller and only served to provide a visual signal representative of the performance of the controller that did not use the same computational resources as the control system.

The generation of the excitation signal for the LPACT was incorporated into the controller in order to facilitate a common dSPACE ControlDesk capable of controlling all required experimental parameters. This signal used a third DAC output from the DS1103 board.

Generic, off the shelf BNC connector cables of various lengths were used to make all connections. The experimental control system can be seen in Figure 37 and the description of connections is provided in Table 4.
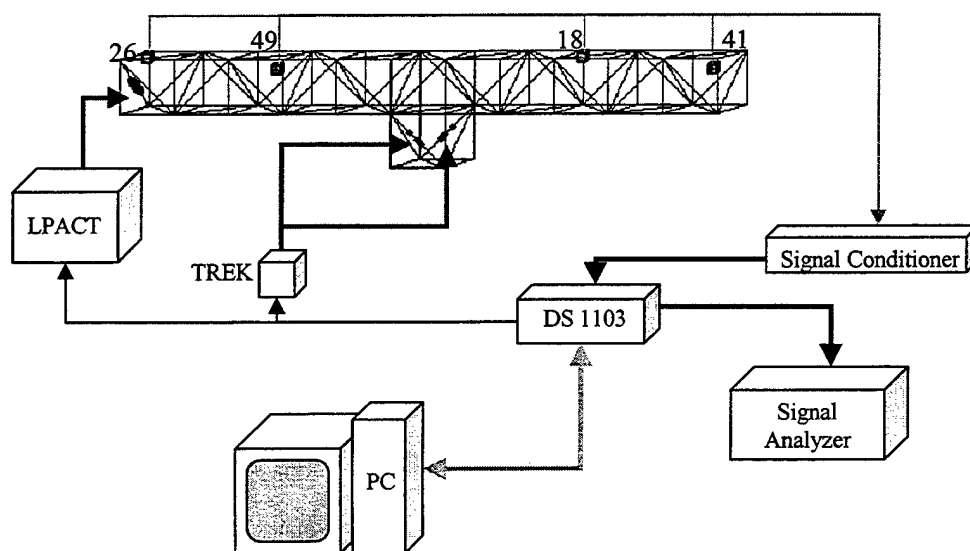
Figure 37. Experimental Layout

From Device	Connection	To Device	Connection
DS 1103	DACH 3	LPACT Driver	User Input
Accelerometers	Cable	Kistler Coupler 5124A	Input
Kistler Coupler 5124A	Output	DS 1103	ADCH 1-3,5-7,9-11,13-15
DS 1103	DACH 5	HP Signal Analyzer	Channel 1
DS 1103	DACH 1	TREK 50/750	INPUT 1
DS 1103	DACH 2	TREK 50/750	INPUT 2
TREK 50/750	OUTPUT 1	PI Piezo Actuator #1	Cable
TREK 50/750	OUTPUT 2	PI Piezo Actuator #2	Cable

Table 4. Cable Connections

The dSPACE ControlDesk used to run the experiments is called "Adaptive Conrtoller.cdx" and is located in the "C:\Space_Truss\Truss01" directory of the host computer. This ControlDesk was used to run the majority of the experiments and has an additional layout that allows the researcher to monitor all the nodal accelerations at once. A similar ControlDesk called "Data Capture.cdx" is located in the same directory and was used to save the data analyzed in this chapter. A separate ControlDesk was used in order to reduce the computational requirements of displaying all the nodal accelerations at one time. The Data Capture version does not include the monitoring layout. Both versions have all the controls required to vary the frequency, amplitude, control node, and active element used for each experiment (Figure 35).

After all the required connections are made and the equipment is powered up, the a Newport Vibration Control System Table should be "floated" on the compressed Nitrogen supports to lower the noise level prior to data collection. The ControlDesk is then loaded and the switch LPACT switch on the LPACT Driver is enabled. The remaining parameters can be manipulated via the ControlDesk with general security to equipment integrity, as the required signal limits have been built into the controls as hardware limits and cannot be exceeded without modifying the ControlDesk Layout.

After the required disturbance parameters are set, the control node and axis are chosen and the active element selected. The "Run/Reset" button activates the controller indicated by the "Run/Reset" button turning GREEN. Controller operation is monitored by the gain level values, the "Gain Lock" LED and the "Control" and "Disturbance" signal displays. Variations of the disturbance frequency or magnitude will automatically reset the controller and will be obvious by the "Run/Reset" button returning to YELLOW. After the frequency identification stabilizes, the controller will automatically return to "Run" unless manually overridden.

2. Modal Verification

The system modal frequencies have been verified with a Hewlett-Packard HP35665A Dynamic Signal Analyzer (DSA) [Ref. 5]. The results are shown below and correspond well with those predicted by the ANSYS FEM modal analysis.
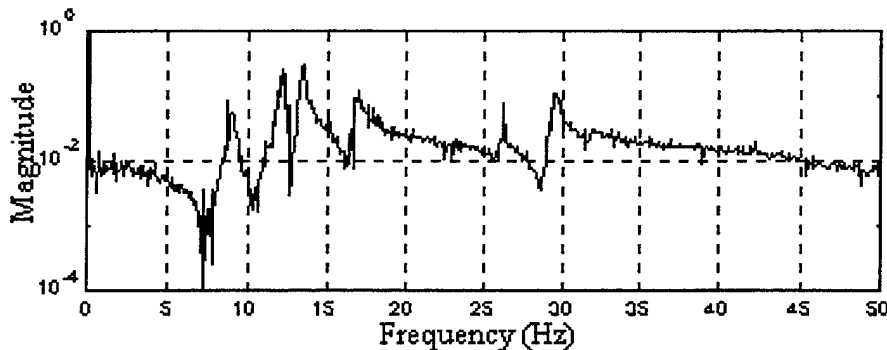
Figure 38. Frequency Response from Random Noise [From Ref. 5]

C. EXPERIMENTAL PARAMETERS AND RESULTS

1. Data Capture

Data capture was done using the Data Acquisition feature of dSPACE ControlDesk [Ref. 23]. A layout was added to the experiment to add the "Capture Settings" window shown in Figure 39.
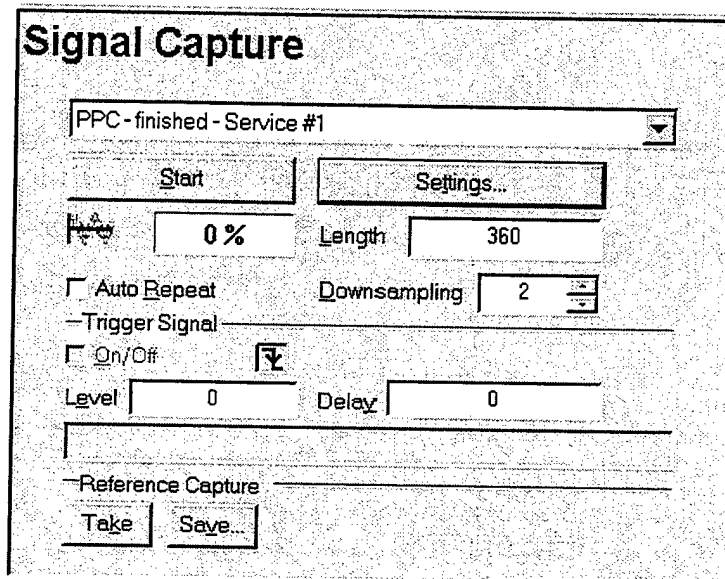
Figure 39. dSPACE ControlDesk Data Capture Window

The "PPC" block defines the set of variables that you wish to capture and the length defines the time in seconds to record the data. The data is selected for capture by defining the "Capture Settings" for the desktop display of that variable and then selecting that definition in the before mentioned "PPC" block. The data sample rate was down sampled for capture to reduce file size. The 500 Hz sample rate (1 kHz down sampled by 2) was more than sufficient to provide adequate resolution below 30 Hz.

The "Settings" button provides access to the acquisition options available. A "Simple Capture" with "Automatic Storage" was used for all data capture. These options

70

generate a "*.mat" file and allow the file name to be preset. The automatic storage facilitates setting up the experiment from start to finish prior to execution. Data was written directly to the working directory to be used for storage and manipulation by MATLAB.

The sample times used for each experiment were set to allow a continues data set to hold the steady state, transition, and equilibrium conditions of the controller at each set of experimental conditions. The limiting time was based on having enough samples before control and after it converged to allow for a meaningful FFT to be performed. The variable time was the time required for convergence. The data sets were typically 180 seconds, but they were extended up to 360 seconds if required to show system response to the controller. The parameters stored were the nodal acceleration, the controller gain, the sine LMS gain, the cosine LMS gain, and the control signal sent to the piezoelectric actuator. The program "PROCESS1.M," included as Appendix H, contains the code that was used to generate the plots for the first experiment. The same code was modified to use the sample length and file names to analyze the other experiments.

The required adjustments to the disturbance, control location, and control element were all done from the ControlDesk. All experiments used the same control logic and no adjustments were made to any gain or other controller parameter. The frequency response shown for each experiment represent the power spectrum of the nodal acceleration in g's that the controller was attempting to reduce.

2. Experiment 1 (19 Hz, Y-axis of Node 18, Piezo #2)

The first experiment performed as a baseline for the controller performance and not specifically to test stress its capabilities. The controller was set to "Reset" and the disturbance was set to its maximum amplitude at 19.0 Hz. The system was monitored with the HP Dynamic Signal Analyzer until the power spectrum had reach equilibrium. Then the data capture was started and allowed to run for approximately 15-20 seconds to allow for enough data to produce the uncontrolled power spectrum.

When the controller was placed in run, the adaptive values began to vary over time. This response was also recorded and is shown in Figure 40. After equilibrium was reached; the data captured continued from long enough to demonstrate stability and record the controlled system response. The time history of the disturbance signal and the control signal are shown in Figure 43 and the power spectrum of the frequency response of the acceleration in g's is shown in Figure 42.
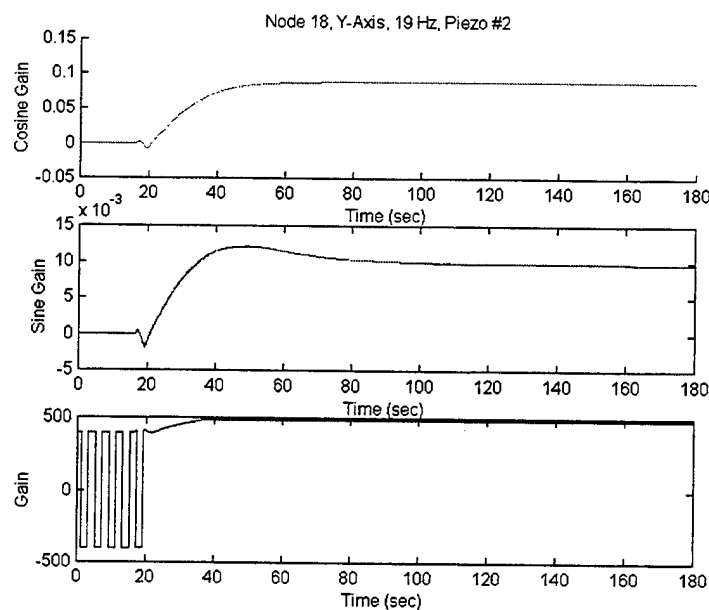
Figure 40. Exp. 1, Controller Gain Response

72
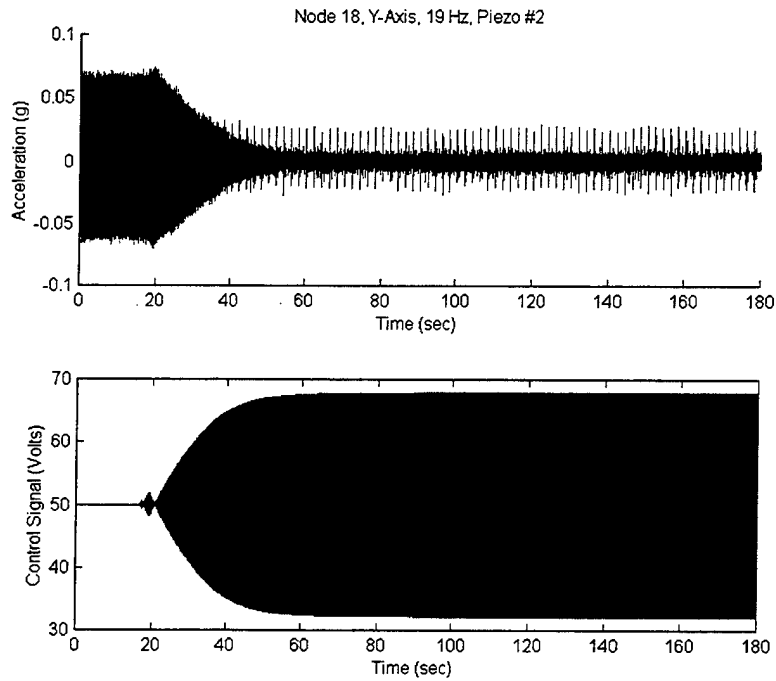
Figure 41. Exp. 1, System Response
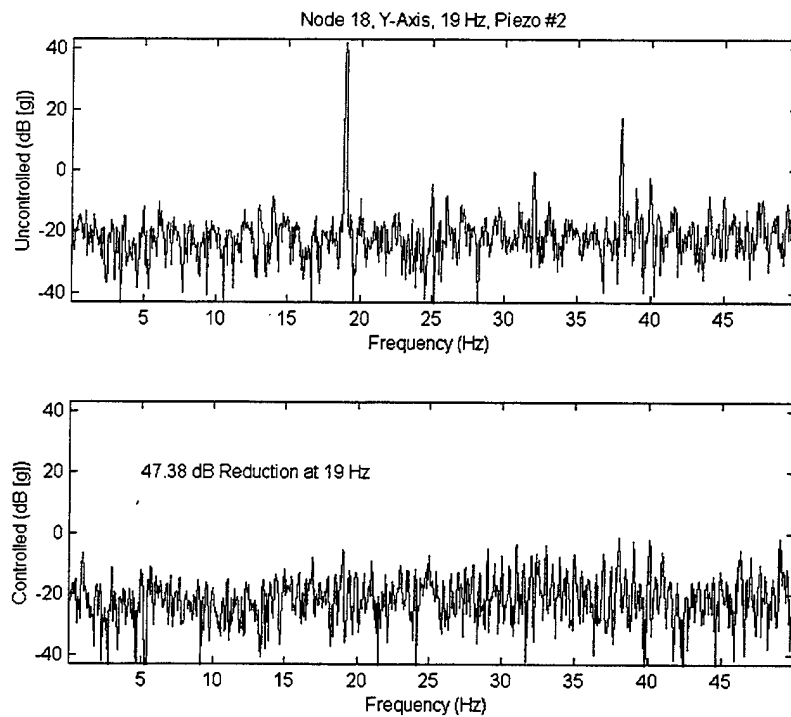
Figure 42. Exp. 1, Power Spectrum

This example showed a 47.38 dB reduction at the disturbance frequency. The limiting factor on the magnitude of the reduction was later demonstrated to be initial amplitude and control authority. The adaptive nature of the controller, if convergence is possible, will always take the control signal down to the noise level. This example also shows a marked drop in the first harmonic frequency, but this is not a design feature of the controller and was not expected.

3. Experiment 2 (15 Hz, Z-axis of Node 41, Piezo #1)

The second set of experimental conditions changes the all the base parameters including, active element, disturbance frequency, control node, and control axis. This was chosen to demonstrate the ability of the same control algorithm to be used at a different frequency, from a different location, and controlling a different parameter with no reduction in performance. The controller initially converges slightly faster with these conditions, but the finial power spectrum still shows a slight peak at 15 Hz. Even with the remaining peak, the controller reduced the nodal axial acceleration by 42.45 dB. The results of this experiment are shown in Figure 60, Figure 61, and Figure 62 of Appendix G.

4. Experiment 3 (12 Hz, X-axis of Node 26, Piezo #2)

These conditions were chosen because the LPACT is at the same end of the truss as Node 26 and the disturbance source is applied in a plane perpendicular to the x-axis. This makes the only significant contribution to acceleration in the x-direction due to rotation about the base due to the induced vibration. This signal is significantly smaller than the other two axis, which decreased the signal to noise ratio significantly as shown

in Figure 64 of Appendix G. This combination of control node and axis is also one of the worst cases for control authority due to the location and orientation of the active element. Regardless, the controller still reduced the signal by 23.07 dB and further reduction is expected if longer time is allowed for convergence. The system gain values were not fully stabilized even after about 2.5 minutes of adaptation. System gain values and power spectrum are included in Figure 63 and Figure 65 of Appendix G respectively.

5. Experiment 4 (12 Hz, Y-axis of Node 26, Piezo #1)

This set of conditions was chosen based on the results of the previous experiment. The axis of concern was shifted to the Y-axis in order to provide more control authority to the active element and reduce the signal to noise ratio. The shift from active element number two, to active element number one was only to verify that either position could control that nodal location. All other parameters were left identical. The signal strength was increased and but the vibration reduction was only slightly improved, showing a reduction of 25.24 dB. The system response is notably different for the two cases. Comparing Figure 63 and Figure 66 of Appendix G, shows the difference that disturbance magnitudes make on the convergence rates of the various adaptive components. In experiment 3, the signal was week and the gain values for sine and cosine were still approaching their equilibrium values after 3 minutes. In this experiment, the gains initially overshoot the optimal value and approach them in an oscillatory manor. A further reduction in both cases may have been realized if longer convergence time was allotted. The system response and power spectrum are shown in Figure 67 and Figure 68 of Appendix G.

6. Experiment 5 (1st Modal Freq, Y-axis of Node 26, Piezo #1)

The original intent of the controller was to adapt and control vibrations from 10 to 30 Hz, based on the assumption that the first modal frequency was introduced by the disturbance source only. Upon review of the mode shape predicted by the revised FEM model and the model frequencies of both the predicted and experimental results, it was decided that the first structural mode was 9.4 Hz. In fact, this frequency is exceptionally challenging due to the nonlinearities introduced by the disturbance source. The LPACT frequency response curve [Figure 10] shows its natural frequency at approximately 8.5 Hz with a significant increase in response below 10 Hz.

For all of the modal control experiments, node 26 was used as the control point. This node is the closest to the disturbance source and thus presented the greatest challenge to the controller. A disturbance of 9.4265 Hz was used for this experiment based on the first ANSYS modal frequency and the Y-axis (horizontal) because it had the largest signal to noise ratio prior to control. The active element used was still chosen randomly and for this experiment Piezo #1 was used.

The convergence rate of the controller was significantly slower for this experiment, possibly due to the nonlinearities and the fact that the first harmonic (~19 Hz) actually had about 20 dB more power than the disturbance frequency. The controller did manage to reduce the disturbance frequency by 18.80 dB with no noticeable affect on the harmonics [Figure 71 of Appendix G] even though the one of the base assumptions of the control algorithm was a linear system. The controller gain and system response plots are Figure 69 and Figure 70 of Appendix G, respectively. The power spectrum for this experiment is Figure 71 of Appendix G.

7. Experiment 6 (2nd Modal Freq, Y-axis of Node 26, Piezo #2)

For consistency, the only thing changed in this experimental condition was the disturbance frequency. The second mode was predicted by ANSYS to be 11.318 Hz and that was used as the disturbance source. Both active elements were used with the same results and the results included are those using Piezo #2.

These conditions also demonstrated strong nonlinearities. It is worth noting that the nonlinear nature of the structural response was not typical and these frequencies would not have been identified without the ANSYS analysis.

The controller was able to obtain a 41.54 dB reduction with a relatively slow convergence rate. The harmonics in this experiment did exhibit some net gain, but remained less than the original amplitude of the disturbance frequency. Again, the harmonic response is not included in the controller design and a linear system was assumed in its development. Experimental results are shown in Figure 72, Figure 73, and Figure 74 of Appendix G.

8. Experiment 7 (2nd Modal Freq, Z-axis of Node 26, Piezo #2)

Based on the bare truss modal analysis, the second modal frequency should be in the x-z plane and have no y component. This observation is obviously not the case due to the applied force in the experiments being in the y-z plane, but it did motivate the conditions set in this experiment. The conditions are the same as those in experiment 6, except that the Z-axis was selected for control.

The controller took a relatively long time to converge in this condition and showed only a 2.4 dB reduction over the 3-minute time frame used in all the previous

experiments. This situation was used to illustrate the continued ability of the controller to

adapt and improve results over time (until the gains reach there equilibrium values). The

data capture time was thus increased to 4-minutes and the reduction increased to 11.44

dB as shown in Figure 43.
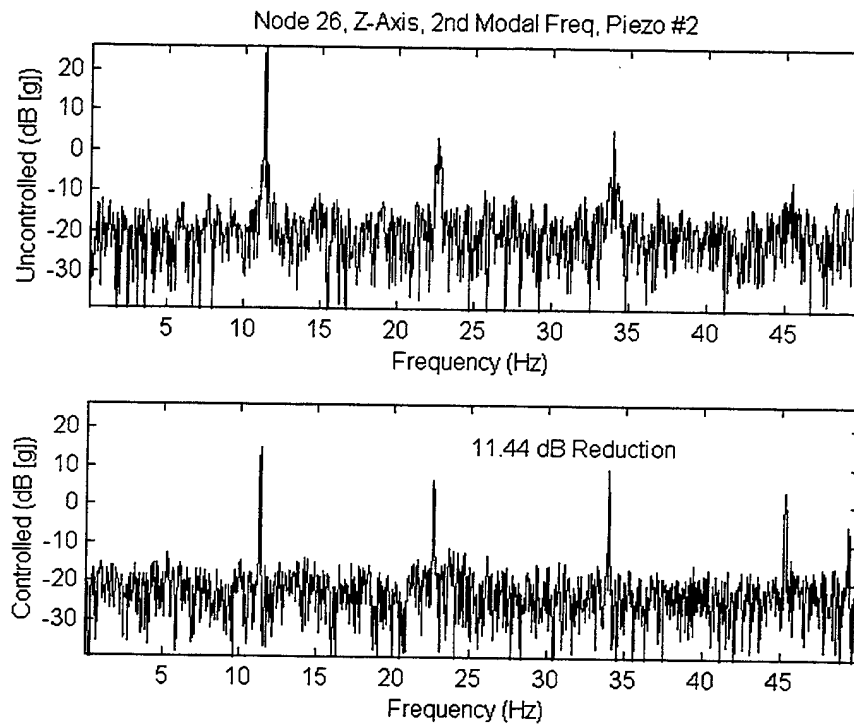
Figure 43. Exp. 7, 4-Minute Data Capture Power Spectrum

The data capture time was increased to 5 and 6 minutes in the next two

experiment sets. Representative samples showed a reduction of 19.6 dB and 21.3 dB

respectively and the power spectra are shown in Figure 44 and Figure 45.
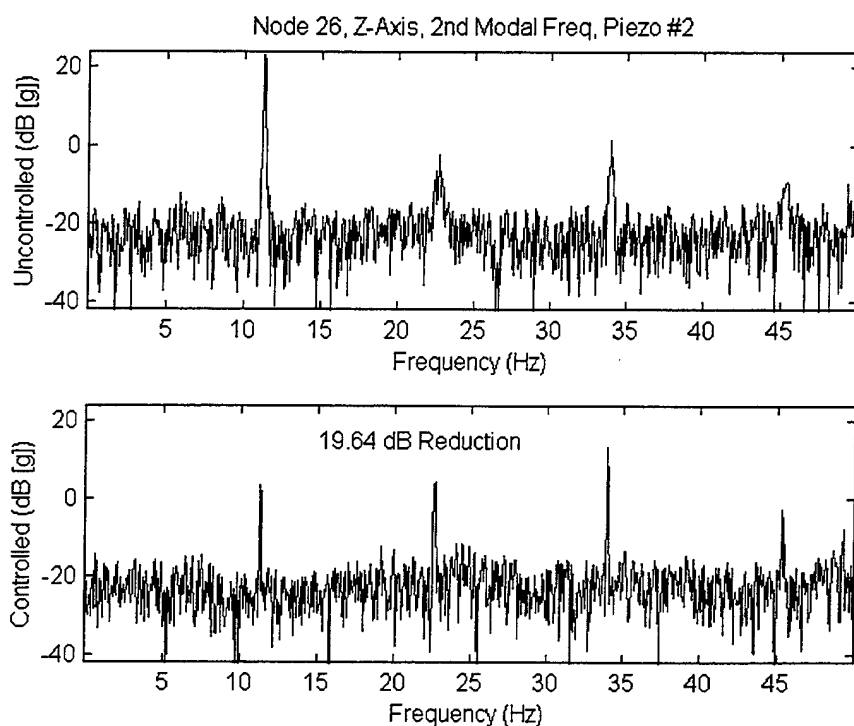
Figure 44. Exp. 7, 5-Minute Data Capture Power Spectrum
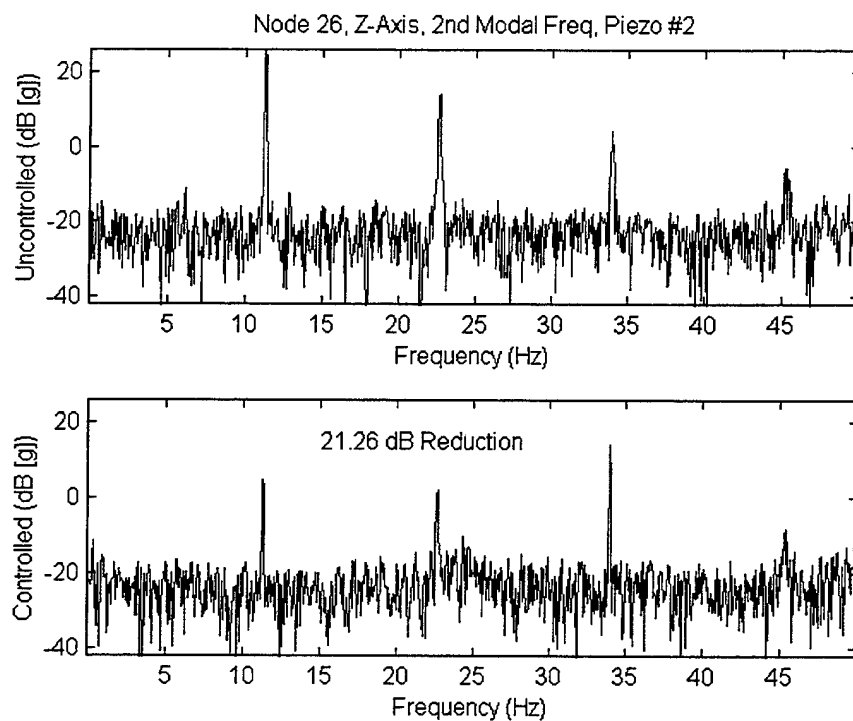
Figure 45. Exp. 7, 6-Minute Data Capture Power Spectrum

79

Further increases in data capture times were not pursued due to the large file sizes and data manipulation resources. It was also discovered while attempting to explain the slow convergence rate that the full truss model included in ANSYS showed this mode shape as a nearly linear displacement of the LPACT in the x-direction. This made the actual truss response less critical and the experimental set was concluded with a set of 6-minute data collection runs. A representative sample of the controller gain values and system response from the finial iteration show that the gains are still not fully converged indicating an improved response is possible given longer runs. These results are shown in Figure 75 and Figure 76 of Appendix G.

9. Experiment 8 (3rd Modal Freq, Z-axis of Node 26, Piezo #2)

After reexamining the results form the modal analysis, it was determined that the third modal frequency predicted by ANSYS corresponded closest to the bare truss second frequency and had the second greatest effect on the overall motion of the truss. The largest displacement in this mode was in the z-direction. The predicted frequency of 12.529 Hz also agreed with the second modal frequency determined experimentally Figure 38. The initial data capture time was once again 3-minutes, but the data showed that the gains had not fully reached equilibrium at the end of the run even though a reduction of 28.92 dB was realized at the disturbance frequency. Consequent data runs with a collection time of 4-minutes showed that the gains essentially reached equilibrium with a total reduction of 56.61 dB. Representative results are shown in Figure 77, Figure 78, and Figure 79 of Appendix G.

10. Experiment 9 (Controller Comparison)

The last set of experimental conditions was chosen to reproduce the conditions that resulted in the greatest vibration reduction using the IDIFF Controller on the same structure. Although the same active element was used and the same disturbance frequency was input, it is important to realize that the design intention of the previous controller was to actively dampen the vibration by interrupting the most significant conduction path. The adaptive multi-layer LMS controller is designed with the express purpose to counter any induced vibration at the control node by introducing a similar signal that is out of phase with the disturbance at that point. The controllers obviously have different applications, but are compared to show the advantage of this controller if the desired result is to reduce a single axis disturbance at a given node.

The best results shown in Reference 5 were noted on the z-axis of node 41 with a 13.81 Hz disturbance source. The active damping resulted in a reduction of 19.02 dB in that specific node [Ref. 5]. The same disturbance frequency was chosen for this experiment and the control signal was the acceleration from the z-axis of node 41. The same active element was also used for sake of comparison. The spectral analyses of the old and new controllers are shown in Figure 46 and Figure 47 respectively. It was also observed that the controller converged very quickly in this case and reduced the disturbance down to the noise level for a reduction of 57.26 dB. Based on these results, it is obvious that controller location is near optimal for that specific node and axis which also explains the performance of the active damping system. The gain and system responses are shown in Figure 80 and Figure 81 of Appendix G.
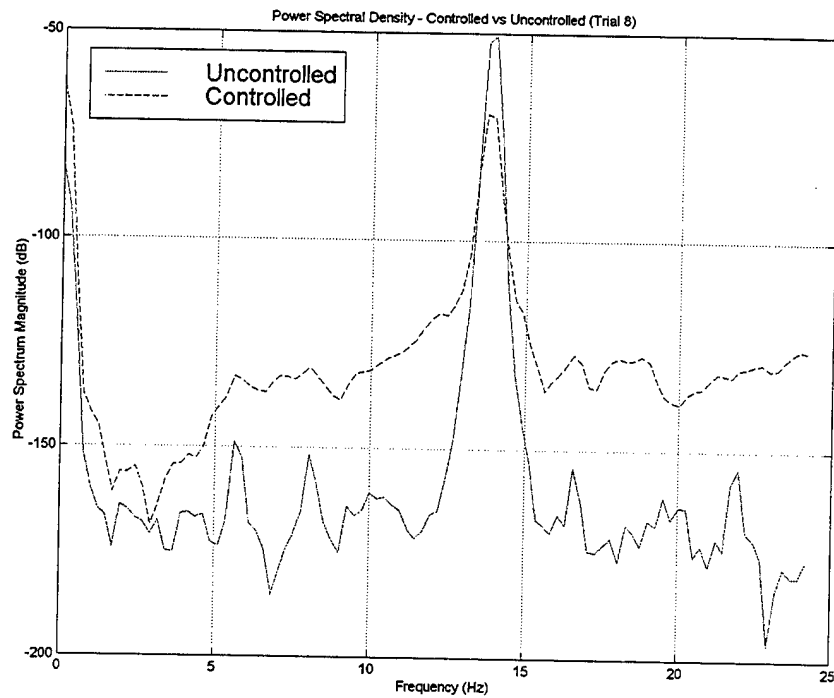
Figure 46. IDIFF Controller Results [From Ref. 5]
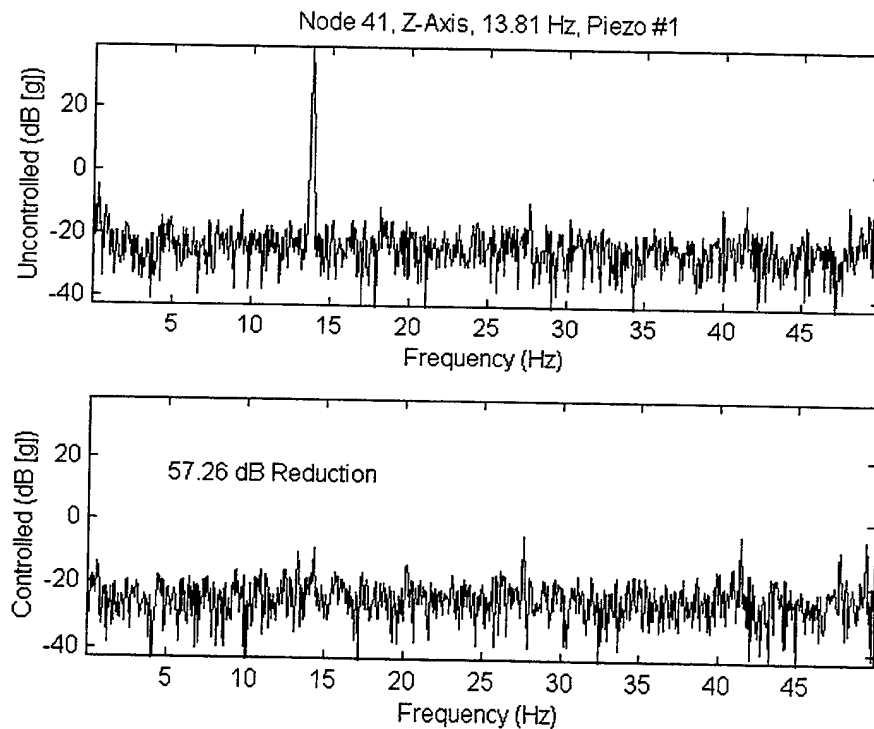
Figure 47. Exp. 9, Power Spectrum

11. Unstable Configuration

As noted in section [III.B. 4], there was one unstable system configuration revealed after the controller development. The discovery was made during a demonstration of the system under random conditions chosen by the observer. Ironically, the observer varied only one of three of the demonstration default values choosing the y-axis of node 41, with a 14 Hz disturbance signal. The exact cause of the instability was not determined, but it is suspected that it could be removed with further adjustment of the individual control element adaptation rates.

As noted in the analytical section this algorithm is theoretically capable of guaranteed convergence, but not guaranteed effectiveness. The addition of multiple adaptation rates was necessary to increase the applicability of this controller to random initial conditions, but sacrificed an order of magnitude on the potential convergence time of the phase adjust LMS algorithm. This effect is obvious by comparing the required time for convergence on the experimental and analytical models [Appendix I]. Increasing the adaptation rate of the gain magnitude LMS algorithm minimized this effect, but is also the likely source of this instability. Additional testing is required to evaluate, document, and correct this situation if possible.

D.   ANSYS FEM COMPARISON

1. Model Setup and Initiation

A modal analysis was done using ANSYS and the natural frequencies obtained were significantly different from the original bare truss modal frequencies. This was contributed to the added mass of the LPACT and control apparatus (~20% of the bare

83

truss mass). The first four natural frequencies obtained from the modified FEM are compared with the experimental frequencies obtained from the DSA [Ref. 5] in Table 5.

Mode	ANSYS Frequency	DSA Frequency
1	9.43	8.94
2	11.32	12.19
3	12.53	13.87
4	18.74	17.50

Table 5. Natural Frequencies of Truss With Active Components

Upon examining the mode shapes from the postprocessor, it was determined that the second natural frequency was essentially due to the 2.5 kg mass of the LPACT vibrating almost entirely in the x-direction. If the model is assumed to be accurate, then this mode is also nearly entirely contained in that single element and thus not controllable by the current system. Due to the position of the LPACT and the orientation of the force axis, this frequency can be detected by the system and subsequently controlled, however the control authority of the current configuration is minimal and thus leads directly to the long convergence times and reduced effectiveness demonstrated in the experimentation described in sections [V.C. 7] and [V.C. 8] which describe experiments six and seven respectively.

One factor that was not included in the ANSYS model was the active element preloaded required on the actual truss. The preload was done using shims to give a compressive bias for the piezoelectric actuator and then the control signal was added to a 50V DC signal that centered the piezoelectric element in the center of its operating band. In the ANSYS model, this effect was necessary due to the mathematical modeling of the SOLID5 elements, but a limiter was included to prevent the control signal from exceeding +/- 50V.

84

The simulations were run for times ranging from 5 to 50 seconds of simulated time. The time was varied based on capturing the optimal performance of the controller based on the convergence rate obtained for each set of experimental conditions. The longest data run (50 seconds) was extended to gather enough data points for a power spectrum analysis of the system before and after control. Other power spectra shown were generated with fewer data points, but were considered adequate for comparison. The time-step interval was set at $1/20^{th}$ the driving frequency.

The active control APDL macro, "TRUSS_CONTROL.TXT" [Appendix E], was used to vary the experimental parameters to match those used in truss experiments. The time required for each data run varied from approximately 15 minutes to several hours based on the number of iterations required by the combination of simulation time and time-step required. The files saved by the overarching APDL macro were ASCII files that contained the control node displacement, velocity, and acceleration as well as the actual control signal and controller gain values. A MATLAB algorithm was developed to process and display the data, included as Appendix J. A second algorithm was written to allow for comparison of the experimental and FEM results, included as Appendix K.

The different nodal numbering and axis definition used in the model had to be accounted for in the APDL file when duplicating the experimental conditions. The changes made include switching the Y-axis and Z-axis and verifying the node numbering. As previously discussed, the adaptive gain adjustment was not included, so an average of 3 abbreviated data runs were required to determine the proper gain to be applied to the controller for each set of experimental conditions. The simulated convergence rates were significantly faster due to the near optimal gains used and the removal of the layered

adaptive nature of the experimental control system. This was expected and is representative of the possibilities if a simplified controller were to be applied and tuned to specific situations. The equilibrium results in either the multi-layered controller or the tuned controller are the same, so the comparison is still a valid verification of the model response.

The results of each data run are included in Appendix L, and comparisons of the results are either shown in the text or in Appendix I.

2. Simulation 1 (19 Hz, Y-axis of Node 18, Piezo #2)

In this data run, the conditions of the first experiment were duplicated with a 19 Hz disturbance, controlling the y-axis of node 18, using element number two. To account for the variation in nodal numbering and axis definition, the APDL file was written to control the z-axis of node 49, which are the model equivalents to the experimental parameters. The value used for the controller gain (μ in the LMS algorithm) in this run was -0.045 and a 5 second acquisition time was sufficient to determine system response.

Simulation results of control node response, control signal, and adaptive LMS gains are shown in Figure 98, Figure 99, and Figure 100 of Appendix L. A comparison of the nodal acceleration is shown in Figure 48.
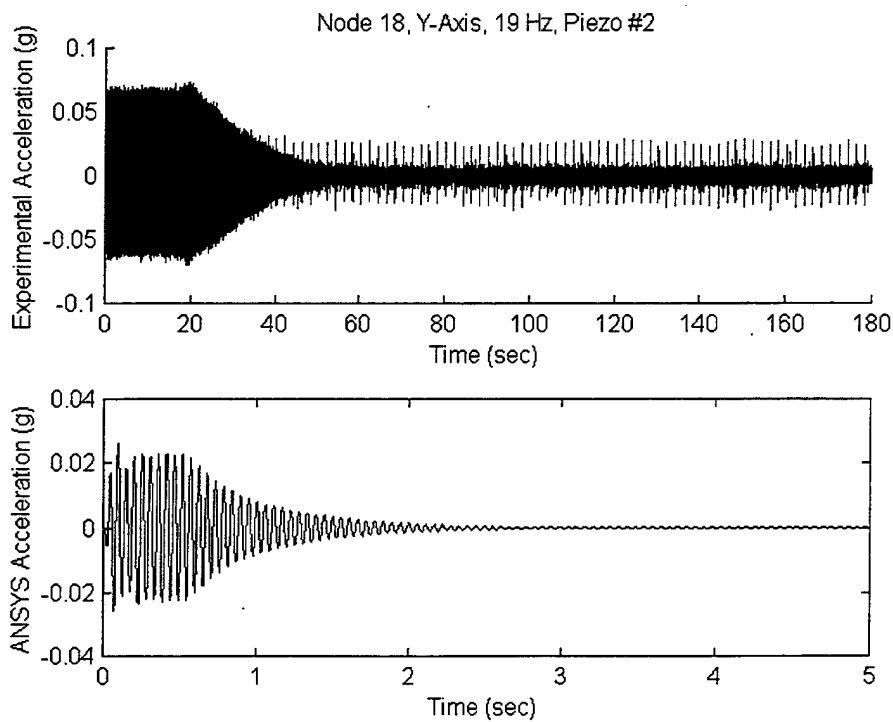
Figure 48. Case 1, Control Node Acceleration Comparison

No attempt was made to intentionally match the initial magnitude of the nodal accelerations felt by the control node. This was not deemed necessary due to the adaptive nature of the controller, but it does reflect in the magnitude of the resulting control signal and the rate of convergence. While the rate of convergence is typically a critical value, the process of manually determining the gain for the simulations removed the effect of magnitude on the convergence rate. If the entire control system were to be modeled, the signal strength would have to be match to predict the control system response correctly. The control signals generated by both the experimental and simulated cases are shown in Figure 49.
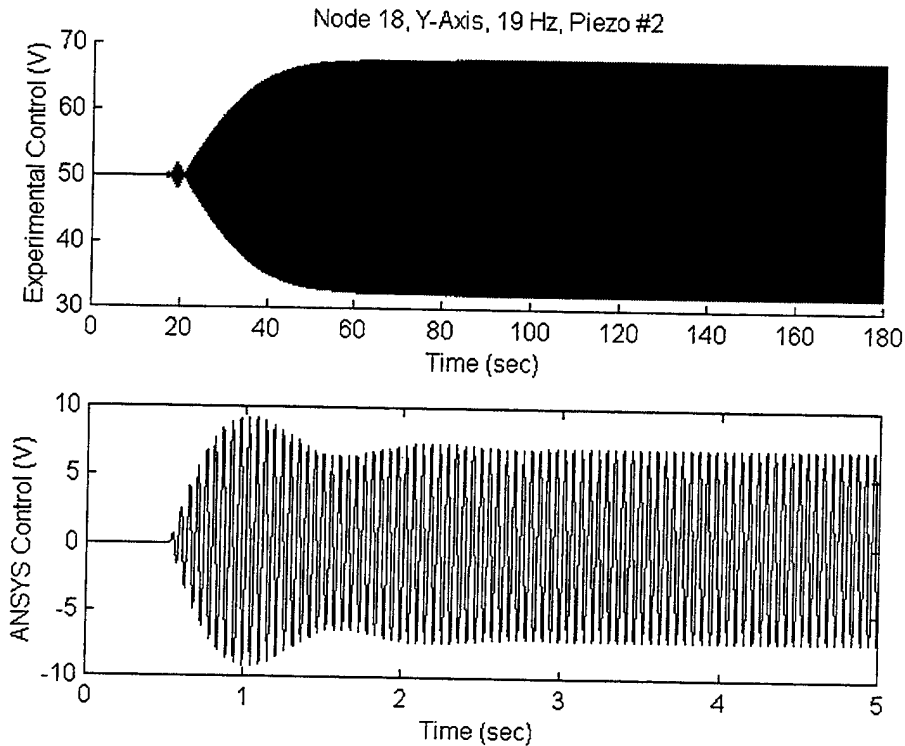
Figure 49. Case 1, Control Signal Comparison

The finial reduction in the nodal acceleration predicted by the FEM was 68.43 dB. The difference between this reduction and the 47.38 dB reduction realized in the first experiment was due to the difference in noise level. No signal noise was introduced into the FEM, so the noise level was effectively due to the mathematical precision of the computations. This difference supports the assumption that the control law is capable of reducing a specific frequency disturbance to the noise level, regardless of initial magnitude, if the system has sufficient control authority.

3. Simulation 2 (15 Hz, Z-axis of Node 41, Piezo #1)

The second simulation corresponds to the conditions of the second experiment, using a 15 Hz disturbance, controlling the z-axis of node 41, using element number one. The APDL file was written to control the y-axis of node 26, which are the model

equivalents to the experimental parameters. The value used for the controller gain (μ in the LMS algorithm) in this run was slightly higher than the first simulation, at –0.075 but a 5 second acquisition time was still sufficient to determine system response.

The simulation results are shown in Figure 101, Figure 102, and Figure 103 of Appendix L. A comparison of these results with the experimental data is shown in Figure 82 and Figure 83 of Appendix I. Due to the very rapid convergence of the LMS gains in this simulation, the reduction in vibration was greatly enhanced as the controller was allotted more time to "fine tune" the response and drive the signal down to the mathematical noise of the computational algorithm. The finial reduction shown in the simulation was 175.28 dB. The results of experiment number two showed a 42.45 dB reduction. Both are essentially the difference between the original signal and the applicable system noise.

4. Simulation 3 (12 Hz, X-axis of Node 26, Piezo #2)

The third simulation corresponds to the conditions of the third experiment, using a 12 Hz disturbance, controlling the x-axis of node 26, using element number two. The APDL file was written to control the x-axis of node 41, which are the model equivalents to the experimental parameters. The value used for the controller gain (μ in the LMS algorithm) in this run was the largest of any of the simulations, at 0.9, but a 5 second acquisition time was sufficient to determine system response. The large gain required for rapid convergence is an indication that the signal strength for the disturbance was weak. It was also necessary to reduce the magnitude of the disturbance signal by a factor of ½ in order to keep the disturbance from exceeding the control authority of the active element.

This reduction kept the control signal to within the +/- 50V operational limit. The amount of controller input required to minimize this nodal acceleration is consistent with the node shape and control element orientation, however inconsistent with the experimental results. This is credited to the orientation of the LPACT perpendicular to the control axis, thus minimizing the disturbance energy at the real control node and increasing the signal to noise ratio as noted in the experimental results section.

The simulation results are shown in Figure 104, Figure 105, and Figure 106 of Appendix L. A comparison of these results with the experimental data is shown in Figure 84 and Figure 85 of Appendix I. The finial reduction in the simulation was 73.39 dB and the experimental reduction was 23.07 dB.

5. Simulation 4 (12 Hz, Y-axis of Node 26, Piezo #1)

As before, this simulation mimics the conditions of the corresponding experiment, using a 12 Hz disturbance, controlling the y-axis of node 26, using element number one. The APDL file was written to control the z-axis of node 41, which are the model equivalents to the experimental parameters. The value used for the controller gain (μ in the LMS algorithm) in this run was at 0.005, which is the smallest value used. The 5-second acquisition time was not sufficient in this case to determine system response because of a relatively slow convergence rate. The simulation time was extended to 45 seconds and the controller gains were near, but not fully converged to equilibrium at the end of the simulation. The significantly reduced gain suggested that the magnitude of the disturbance in that axis was larger than the previous simulation. That was consistent with the mode shape and the measurements taken on the actual truss. The magnitude of the

90

disturbance signal again had to be reduced, this time by a factor of $^1/_3$ the original value in order to keep the disturbance from exceeding the +/- 50V operational limit of the actual active element. Both the experimental and simulated LMS gain factors approached their equilibrium values in an oscillatory manor as seen in Figure 87.

The simulation results are shown in Figure 107, Figure 108, and Figure 109 of Appendix L. A comparison of these results with the experimental data is shown in Figure 86 and Figure 87 of Appendix I. The finial reduction in the simulation was 26.06 dB and the experimental reduction was 25.24 dB.

6. Simulation 5 (1st Modal Freq, Y-axis of Node 26, Piezo #1)

This simulation possible explains the nonlinearities seen in experiment number five. The same conditions were input into the model (9.4265 Hz disturbance, controlling the y-axis of node 26, using Piezo #1), but no nonlinearities were noted either before or after the controller was activated. It is theorized that this is primarily due to the FEM model of the LPACT being a rigid part of an element. The failure of the harmonics frequencies to show up in a model that does not include the LPACT spring-mass interactions and the amplification of the second harmonic seen in the initial power spectrum of experiment number five both support this theory. As with previous simulations the APDL file was written to the FEM equivalent parameters, controlling z-axis of node 41. The value used for the controller gain (μ in the LMS algorithm) in this run was at -0.08 and the simulation time was set to 10 seconds.

The simulation results are shown in Figure 110, Figure 111, and Figure 112 of Appendix L. A comparison of these results with the experimental data is shown in Figure

88 and Figure 89 of Appendix I. The finial reduction in the simulation was 54.85 dB and the experimental reduction was 18.80 dB. The difference is contributed to the absence of harmonics in the model and the excitation of the disturbance frequency by the first harmonic in the experimental case.

7. Simulation 6 (2nd Modal Freq, Y-axis of Node 26, Piezo #2)

As noted in the experimental version of this simulation, the mode shape of this modal frequency is nearly entirely described by displacement of the LPACT mass in the x-direction. The simulation was run on the ANSYS model under the same conditions as experiment six, to test the model's ability to predict the controller response in a less than ideal control situation. The disturbance frequency was set to 11.318 Hz and element number two was used to control the y-axis of node 26. The APDL used the model equivalents of the z-axis of node 41. The controller gain (μ in the LMS algorithm) was determined to be -0.015 and the simulation time was extended to 45 seconds to allow for convergence.

The model again failed to predict the nonlinearities seen in the experimental case, but it did exhibit the same slow convergence and reduced effectiveness. These results seem to indicate that the harmonics do not directly affect the controller performance in this case. That may be true for the previous experiment as well, which would mean the only significant error on that evolution was the failure to model the mass-spring relationship of the LPACT. More testing is required to either confirm, or deny the discrepancy.

The simulation results are shown in Figure 113, Figure 114, and Figure 115 of Appendix L. A comparison of these results with the experimental data is shown in Figure 90 and Figure 91 of Appendix I. The finial reduction in the simulation was 32.42 dB and the experimental reduction was 41.54 dB.

8. Simulation 7 (2nd Modal Freq, Z-axis of Node 26, Piezo #2)

The simulation of these experimental conditions showed the same relatively slow convergence rate as seen in experiment seven. This slow convergence could not be corrected by adjustments to the gain, even though multiple attempts were made. The fastest convergence was an oscillatory approach to gain convergence. This approach was normally avoided due to the obvious proximity to instability. However, for the FEM simulation it was desirable to force the system to equilibrium and the absence of noise made the transition to instability predictable based on the graphs of the gain over time. Even with the optimal gains and a 45 second data capture simulation time, the gains were still not fully converged. The simulation was stopped at this time because similarity between system and model response had been verified.

The simulation introduced an 11.318 Hz disturbance and controlled the z-axis of node 26, using element number two. The APDL file was written to control the y-axis of node 41, which are the model equivalents to the experimental parameters. The value used for the controller gain (μ in the LMS algorithm) in this run was at -0.005.

The simulation results are shown in Figure 116, Figure 117, and Figure 118 of Appendix L. A comparison of these results with the experimental data is shown in Figure

92 and Figure 93 of Appendix I. The finial reduction in the simulation was 18.29 dB and the best experimental reduction was 21.26 dB.

9. Simulation 8 (3rd Modal Freq, Z-axis of Node 26, Piezo #2)

The last set of conditions used to test the simulation was also used to generate power spectra both before and after model control. The previous power reductions were calculated based on similar spectra that were calculated with significantly reduced resolution. The spectra generated in this simulation are included in this thesis and required an expended simulation time of 50 seconds for data capture. The exact time for the simulation is not known because it was run overnight, but it was in excess of 3 hours in real time.

The conditions of the 8th experiment were duplicated with a 12.529 Hz disturbance, controlling the z-axis of node 26, using element number two. To account for the variation in nodal numbering and axis definition, the APDL file was written to control the y-axis of node 49, which are the model equivalents to the experimental parameters. The value used for the controller gain (μ in the LMS algorithm) in this run was 0.005. The magnitude of the disturbance source was reduced to 25% of the full strength magnitude in order to keep the controller within operating limits. This turned out to be over conservative and the control signal stayed below +/- 20 volts (+/- 50 V max).

The power spectrum of the FEM during this simulation shows that it did predict the second tonal frequency, but it failed to show the first. The difference in noise level between the two spectra is attributed to the linear approximation (reverse difference approximation) used in the calculation of the nodal velocities and accelerations based on

FEM calculated displacements. The plot shows the power spectrum of the nodal acceleration, which is used as the input to the controller in both the real and simulated experiments.
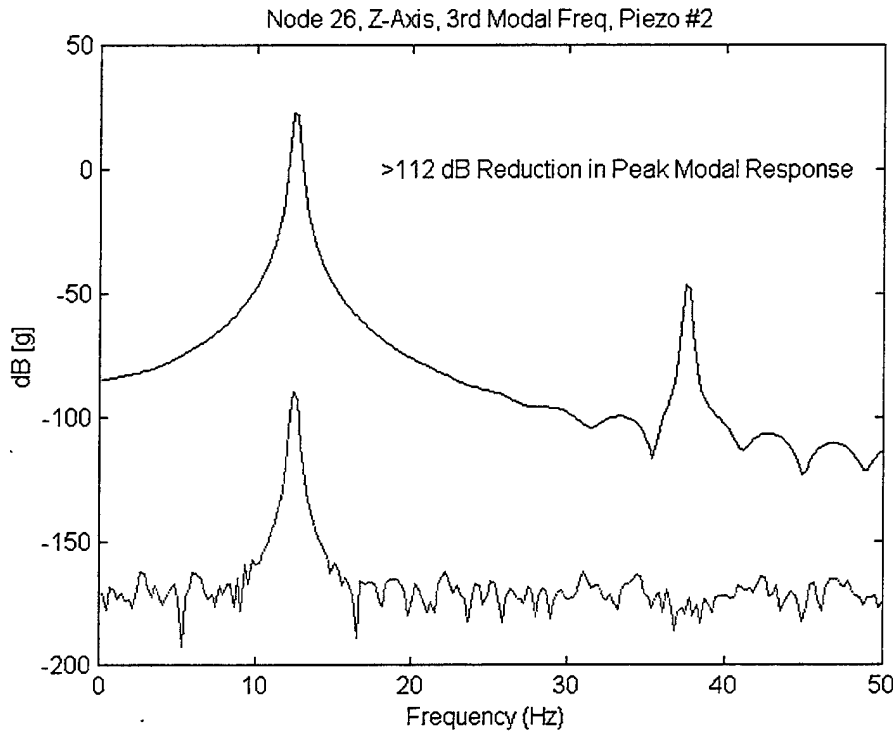
Figure 50. Simulation 8, Power Spectrum Before & After Control

The magnitude of the reduction exhibited in this simulation was due mostly to the initial magnitude of the disturbance and the length of time allowed for convergence. From Figure 50, it appears that another 70 dB of reduction may have been realized (assuming that the mathematical floor noise level had stabilized) if the controller was allowed to continue adapting. This is not the case because of the nature of the adaptive LMS. The controller gains will converge, but will never stop "hunting" for the correct value. This introduces slight variation in the control gain that will always prevent a perfect cancellation, if any signal noise is present. The difference between a reduction of

112 dB and 182 dB in the power of an actual vibration with an initial power on the order of 20 dB is not considered significant for most applications. The simulated system response and LMS gain values for this simulation are shown in Figure 51 and Figure 52 respectively.
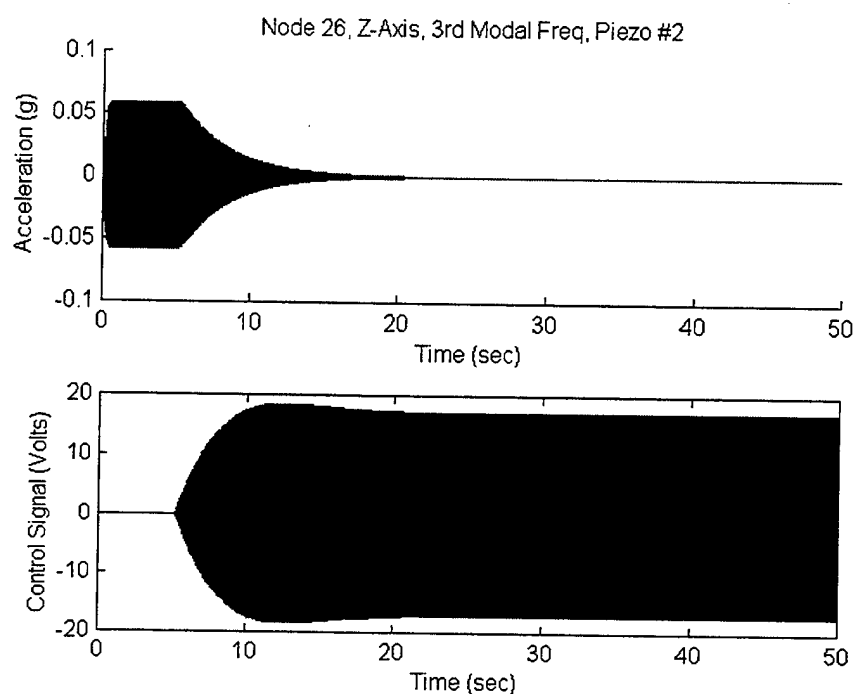
Figure 51. Simulation 8, System Response

96
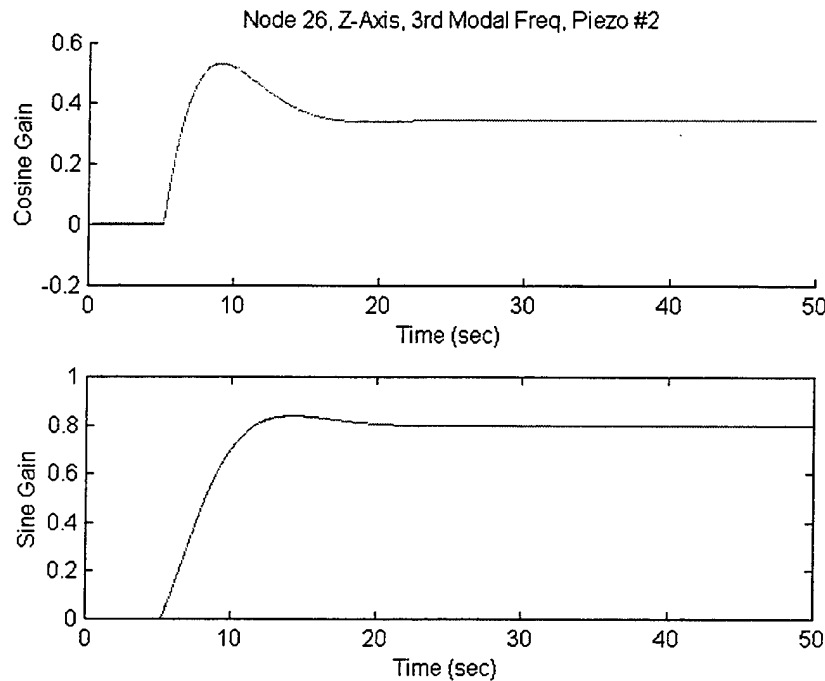
Figure 52. Simulation 8, Controller Gains

A comparison of these results with the experimental data is shown in Figure 94,

Figure 95, Figure 96, and Figure 97 of Appendix I. The finial reduction in the simulation

was 112.3 dB and the best experimental reduction was 56.61 dB.

10. Comparison and Summary of Results

A summary of the different cases is presented in Table 6. These figures

demonstrate that the controller is able to adapt to various frequencies and structural

configurations. The validation of the FEM should include similarity of the system

responses shown in Appendix I and not just the vibration reductions stated in this table.

The adaptive nature of this controller makes the reduction in vibration a function of the

signal-to-noise ratio, controller gain, and the time allotted for controller gains converge.

It may be desirable in future research to prove that the reductions (both analytical and

experimental) converge to near the signal-to-noise ratio as the convergence time goes to infinity.

Case Number	Disturbance Frequency (Hz)	Control Element	Control Node (#/axis)	Analytical Gain	Analytical Reduction (dB)	Experimental Reduction (dB)
1	19	2	18/Y	-0.045	68.43	47.38
2	15	1	41/Z	-0.075	175.28	42.45
3	12	2	26/X	0.9	73.39	23.07
4	12	1	26/Y	0.005	26.06	25.24
5	9.4265	1	26/Y	-0.08	54.85	18.80
6	11.318	2	26/Y	-0.015	32.42	41.54
7	11.318	2	26/Z	-0.005	18.29	21.26
8	12.529	2	26/Z	0.005	112.3	56.61
9	13.81	1	41/Z	N/A	N/A	57.26

Table 6. Summary of Results

The option to tune to the ANSYS model of the controller also demonstrated the controller's ability to converge faster if the application is specified and frequency specific. This was not expressly demonstrated in the experimental version, but was observed in the early stages of controller development. The addition of the automatic frequency identification and adaptive gain features were designed to improve versatility at the expense of convergence rate, without affecting the steady state performance of the controller.

During the development of the Adaptive Multi-Layer LMS Controller, hundreds of experiments were conducted on the NPS Space Truss. Using this experience made the optimal gains that were manually determined in the ANSYS model a relatively simple task. That was because the empirical response of the FEM to variations in disturbance frequency and magnitude had the same affect on the required gain as the actual truss system. To quantify the accuracy of its prediction of LMS gain values, further

experimentation must be performed which matches the analytical disturbance force and uses a more precise method of calculating nodal acceleration in the model. There would also have to be representative noise added to the FEM signals used as controller input and output.

THIS PAGE INTENTIONALLY LEFT BLANK

VI.   FUTURE RESEARCH

A.   IMPACT ANALYSIS

1. Background

High-speed motion photography can capture the structural response of impacts such as a bullet hitting a flack jacket. Those types of images motivated this approach to impact analysis. They clearly capture a structural response to the impact besides the axially transmission of energy through the material. The difference between these forms of propagation allows them to be differentiated and utilized independently.

An analysis of structural impacts using installed accelerometers should be possible using cross correlations with known reference signals. The analysis output would include impact location, energy, and angle. This would provide the ability to rapidly evaluate the potential damage done by unexpected impacts.

2. Analysis Technique

The reference signals required for this analysis are three orthogonal impacts at each sensor. Two variations of each reference impact should saved, one normalized with respect to the energy of impact and the other with respect to the peak response. These signals are representative of each nodes response to a unit impact in a specific direction. The peak-normalized data is to be used to evaluate the location and angle of impact by comparing the characteristic shape of the responses and the delay times. The impact-normalized signals are used to determine the magnitude of the impact.

101

The analysis can take two different approaches based on sample frequency. The material response is characterized by the transmission of relatively high frequency vibration through the structure. In the NPS Space Truss, this energy is transmitted axially through every element of the truss. This correctly implies multiple paths and high-speed propagation. The rate of propagation is estimated by using the material properties of the structure. For the NPS Space Truss, this is Aluminum.

$$V = \sqrt{\frac{E}{\rho}} = \sqrt{\frac{7 \times 10^{10} \left(\frac{N}{m^2} \right)}{2.7 \times 10^3 \left(\frac{kg}{m^3} \right)}} \approx 5{,}100 \; \frac{m}{sec} \qquad (6.1)$$

Based on this propagation rate, a delay time can be estimated based on the size of the structure in order to access the required sample time to capture the signal. For this estimation, a straight-line path is used and structural reflections are ignored. The maximum dimension of the truss is 3.67 meters and the distance between nodes is 0.33 meters. The sensors are only attached to nodes, thus:

$$Delay_{end-end} = \frac{3.67m}{5{,}100 \frac{m}{sec}} \approx 0.7 \; msec$$

$$Delay_{node-node} = \frac{0.33m}{5{,}100 \frac{m}{sec}} \approx 0.06 \; msec \qquad (6.2)$$

Assuming that 10 samples are required for resolution between delay times, this leads to required sample rates on the order of:

$$Freq_{end-end} = \frac{10 \; samples}{0.7 \; msec} \approx 14 \; kHz$$

$$Freq_{node-node} = \frac{10 \; samples}{0.06 \; msec} \approx 150 \; kHz \qquad (6.3)$$

While obtainable, these sample rates are higher than those that are widely available on current spacecraft. It is therefore desirable to use the other method of energy transmittance through the structure in order to reduce the required sample rates. The natural frequency and mode shapes of the structure as a whole dominate the structural transmittance. The propagation rates of this energy are estimated based on the mode shape of the structure. For this order of magnitude estimation, it is assumed that the NPS Space Truss responds as a bare truss and the mode shapes predicted by both MATLAB and ANSYS FEM analyses are used as a basis. From those mode shapes, it is assumed that the path length of the 1st and 2nd modes is approximately 4 times the length of the truss. Similarly, the 3rd and 4th modes have path lengths of about ½ that distance or 2 times the truss length. These estimations are based on Figure 53 and Figure 54.
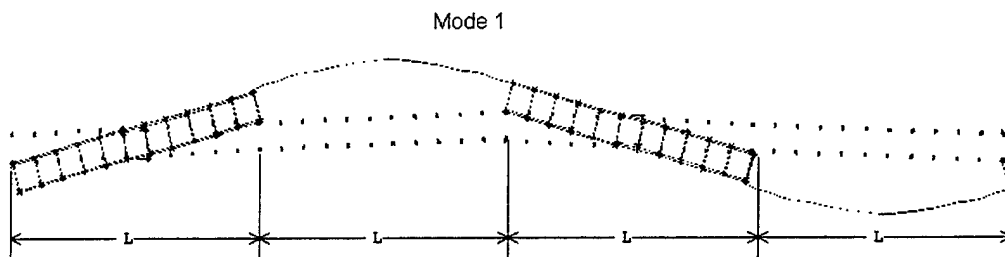
Figure 53. Extrapolation of Mode 1
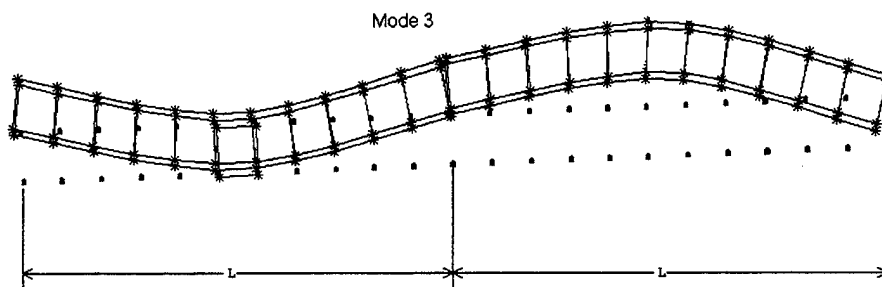
Figure 54. Extrapolation of Mode 3

The natural frequencies of the first two modes are both about 10 Hz and the second two modes are about 20 Hz. These numbers are expected due to the symmetry of the T-Shaped, NPS Space Truss. Using the nodal frequencies and the extrapolated path length to estimate propagation rates results in the following calculations:

$$V = (\text{Freq})(\text{Wave Length})$$

$$V_{1-2} = (f_{\text{mode 1}})(4L) = (10 \text{ Hz})(4)(3.67 \text{ m}) \approx 150 \text{ }^{m}\!/\!_{\text{sec}} \tag{6.4}$$

$$V_{3-4} = (f_{\text{mode 2}})(2L) = (20 \text{ Hz})(2)(3.67 \text{ m}) \approx 150 \text{ }^{m}\!/\!_{\text{sec}}$$

Based on this much slower propagation rate, a new delay time can be estimated using the same basis as before. The delays of structurally transmitted energy are as follows:

$$Delay_{end-end} = \frac{3.67\text{m}}{150\,^{m}\!/\!_{\text{sec}}} \approx 25 \text{ msec}$$

$$Delay_{node-node} = \frac{0.33\text{m}}{150\,^{m}\!/\!_{\text{sec}}} \approx 2 \text{ msec} \tag{6.5}$$

The longer delay times reduce the required sample rate to:

$$Freq_{end-end} = \frac{10 \text{ samples}}{25 \text{ msec}} \approx 400 \text{ Hz}$$

$$Freq_{node-node} = \frac{10 \text{ samples}}{2 \text{ msec}} \approx 5 \text{ kHz} \tag{6.6}$$

These rates may be able to be further reduced if the required resolution can be obtained with fewer than 10 samples.

3. Application

There are four, 3-axis accelerometers and two single axis accelerometers mounted on the NPS Space Truss. The single axis sensors are positioned at an angle such that x, y,

and z-axis accelerations are all measured. The cross correlations are done using the peak normalized impact signals from each of the sensors. This corresponds to the peak normalized reference signals from known impacts in an attempt to compare only the shape of the response. The magnitude is determined in a different process.

The cross correlations contain information on both the relative delay of the signals and there approximation of the reference signal. The delays are required in order to determine the location of impact and the quality of the comparison is used to determine the direction of impact. The "sharper" the cross correlation, the better the fit an impact signal is with the reference. Several methods were attempted to quantify this "sharpness", but none provided consistent results. Assuming that this can be accomplished, the relative fit can be used to determine the approximate angle of impact by compiling a unit vector of those quantities.

The delay times are the key to estimating the location of impact. It is assumed that the system has a preset minimum sensitivity level set to trigger the data collection. The first sensor to meet, or exceed this level becomes the trigger node. The distance from the impact to the trigger node is unknown. The delay times determined from the cross correlations from the other sensors measure the time from the trigger to the energy reaching the relative sensors.
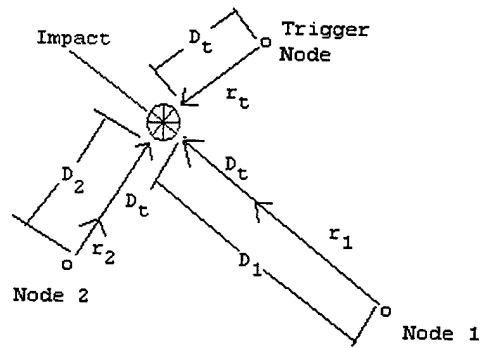
Figure 55. Impact Layout

An appropriate propagation rate is used, based on the method of energy transmission that you are measuring. With the delay times found using a cross correlation, the magnitudes of r_1 and r_2 can be calculated as follows:

$$|r_1| = V(\Delta t_1)$$
$$|r_2| = V(\Delta t_2)$$

(6.7)

The impact location is assumed to be a point located at (x, y, z) and the sensor locations are all known and numbered appropriately. With that information, the distance from impact to sensor number "n" is:

$$D_n = \sqrt{(x - x_n)^2 + (y - y_n)^2 + (z - z_n)^2}$$

(6.8)

The distance from any node is also equal to the distance measured using the delay time, plus the distance the energy traveled before reaching the trigger node:

$$D_n = D_T + |r_n|$$

(6.9)

The result is "n" equations with the impact location and trigger distance as unknowns. The trigger distance (D_T) is a constant for all these equations, so by minimizing the deviation in D_T, you localize the impact location. The result is a point

106

that corresponds to an estimate of the impact location (x, y, z). The larger the number of sensors used for the localization, the smaller the error (limited by the error in measuring the delay times).

$$D_T = \sqrt{\left(x - x_n\right)^2 + \left(y - y_n\right)^2 + \left(z - z_n\right)^2} - V(\Delta t_n) \tag{6.10}$$

The last characteristic of the impact is the energy. This analysis uses only the signal with the best correlation to a known impact. A method of evaluating the quality of a cross correlation is suggested to quantify this. The closest signal is then compared to the energy normalized reference signal. The peak response of the raw signal is divided by the energy normalized peak response to give an estimation of the actual impact energy. The units of the signal compared are irrelevant because they cancel out.

$$\text{Impact Energy} = \frac{\text{Peak Response}}{\text{Ref Peak(energy}^{-1})} \tag{6.11}$$

4. Preliminary Testing

Initial data sets, collected using only 4 of the sensors and a sample rate of 1 kHz were not sufficient to produce any meaningful results. That data run did provide the required information to develop the information discussed above.

The next data set was taken at 10 kHz, in an attempt to capture some of the structural energy. All 6 sensors were used for this set, resulting in 15 channels of data being captured (14 from sensors and one from the impact hammer). The volume of data limited the sample time to only 0.2 seconds per impact. This size can be increased, but at the time it seemed sufficient. A dozen known impacts were used to attempt to develop a method of weighting the cross correlations in such a manner as to permit the required

calculations. Using various methods of weighting the cross correlations of this data, results varied in accuracy from <1m to 3m from impact location. Based on the size of the structure, this was meaningless. The impact angle and force were more accurate. Force was used instead of energy due the ease of measuring force. Further data manipulation could be used to solve for impact energy after the method is established. The direction was typically accurate to less than 30° in spherical coordinates and the force was within 15%. The results prompted another set of experiments in an attempt to isolate the structural response and clarify the resulting resolution of the cross correlation delay times.

The third and final data set was taken from all 6 sensors at 1 kHz sample rate. The sample size was extended to capture 4 seconds of data and a software filter was built into the processing to allow low pass filtering at various corner frequencies. A Butterworth filter was used with a corner frequency of 30 Hz in order to capture the first 4 modes and filter out the high frequency noise. The delay times derived from this setup were inconsistent and the suspected causes are addressed in the next section.

Further research into this question is precluded due to a lack of time, facilitated by the early transfer of the principle investigator.

5. Required Analysis

The quality of the cross correlation is used to determine the angle of impact and could also be used to weight the accuracy of the time delay signals. The methods tried thus far have been inconsistent with respect to determining relative signal similarity. The next method tried should be an initial data fit to a normal distribution curve. Because all

signals are peak normalized prior to correlation, the standard deviation of the distribution should be related to the quality of the signal match.

For these developmental experiments, the impact hammer sensor was always used to trigger the data collection (both reference and impact signals). This should have resulted in positive delay times for each node, and a zero delay if the impact was located at the sensor node. This was not the case and the delay times were often negative. The most significant of the errors suspected in causing this is the method of collecting the reference data sets. A sample rate equivalent to the impact sample rate was always used. This seemed logical at the time, but introduced an unexpected error. The time of impact has to be captured to high accuracy in order to be a useful tool in correlation. The hammer trigger was observed to start consistently at the trigger level of 0.05 volts, but often at the down side of the peak. This resulted in delays long enough to cause negative correlations when compared to actual impact signals. To correct this, the trigger level should be lowered and the sample time of the reference sets increased to at least 10 times the impact sample rate with a recommended rate of 150 kHz. The resulting data should be down sampled to correspond to the sample rates used for analysis, but only after the initial capture. This will minimize the error introduced in determining the time delay.

Another problem discovered in this data set is the lack of resolution between sensors on neighboring nodes. This is lead to and is consistent with the assumption that a 5 kHz sample rate would be required to resolve nodal differences using structural response [Equation (6.6)].

The ability of the single axis accelerometers to resolve the angular difference between impacts is also questionable. The technique developed to determine the

109

significance of the cross correlations may prove this a mute point and they do serve as useful data points in determining both impact location and energy, regardless of angular resolution.

B.   VIBRATION SUPPRESSION

1. Simultaneous Suppression of Multiple Frequencies

The current configuration of the NPS Space Truss includes two active elements that have already been proven to be capable of controlling several different nodes and axes. This significantly reduces the implementation requirements of developing a suppression system capable of acting on two frequencies at the same time. Variations on this theme include controlling either the same node or different nodes and axes.

The most useful application of this process would also include a frequency identification technique capable of high resolution (+/- 0.01 Hz) and amplitude classification. This would allow the most significant disturbance frequencies to be automatically identified and suppressed.

2. Suppression of Multiple Signals

The signal used to generate the control system error has to contain both amplitude and phase information. There is no requirement that the signal be from a single sensor. It may be possible that by manipulating the signals from various sensors, you could develop a method of reducing a combination of disturbance effects.

There have been rudimentary attempts to minimize the total system energy, with no significant reduction. This outcome is predictable due to the inherent nature of

suppression introducing energy into the system. The equilibrium conditions were consistently low amplitude and often resulted in structural effects at the noise level. Combinations that included only specific nodes and/or axes were not tried but should produce measurable reductions related to the specific location of the nodes, frequency, control element, and axis chosen.

THIS PAGE INTENTIONALLY LEFT BLANK

VII. CONCLUSIONS AND RECOMMENDATIONS

The Adaptive Multi-Layer LMS Controller has been shown to be both flexible and capable of reducing a disturbance signal to the level of system noise, but there can be significant drawbacks to its application. If the control element is placed randomly in a structure and set to suppress an equally random point and axis, the controller will attempt to apply ANY force required to drive the nodes response to the disturbance to zero (noise level). The actual control of the node is due to the structural amplification of the force applied by the control element (a piezoelectric element in this case). If the controller has to excite the x-axis to reduce the z-axis, it will. This can result in significantly increased off axis vibration and possible an increase in total nodal vibrational energy.

The ANSYS FEM has a feature that allows visualization of the structural response over time, during actual controller application. The output is a ".avi" file that plays like a movie. By amplifying the magnitudes of the displacements by 5,000 times, it becomes clear that the controller uses the structural response to the control signal for nodal control. For instance, if the ay-axis is being used as a control reference, the steady state condition will show that the controller has excited either the x-axis or z-axis to counter the LPACT disturbance. This technique of system modeling can be used to analyze the system response prior to implementation to avoid component damage.

The best application of the suppression system would be a single axis disturbance with the active element positioned in the system to introduce energy into that specific axis only. The next best thing is to determine the best physical location of the control element to minimize the energy introduced into the system that is orthogonal to the nodal

signal being minimized. In either case, the relative location of the active element must be optimized with respect to the control node and axis, but no modification to the control law is required. If the active element location is optimized, then it may be possible to significantly simplify the control law.

LIST OF REFERENCES

1. dSPACE GmbH, *DS1103 PPC Controller Board Installation and Configuration Guide*, dSPACE GmbH, Germany, March 1999

2. *ANSYS Theory Reference*, Section 11.1, ANSYS 5.5 Online Help, SAS, IP, Inc.

3. The Math Works, *MATLAB Ref Guide*, The Math Works, October 1992

4. Bertran, E.; Montoro, G., "Adaptive Suppression of Narrow-Band Vibrations", *5th International Workshop on Advanced Motion Control*, June-July 1998, pp. 288-292

5. Pantling, Carey M., *Active Vibration Control Method for Space Truss Using Piezoelectric Actuators and Finite Elements*, Master's Thesis, Naval Postgraduate School, Monterey, California, December 1999

6. McClelland, Robert, Lim, Tae W., Bosse, Albert B. and Fisher, Shalom, "Implementation of Local Feedback Controllers for Vibration Suppression of a Truss Using Active Struts", *Proceedings of the SPIE 1996 Symposium on Smart Structures and Materials*, pp. 452-461, February 1996

7. NRL Code 8200 Interoffice Memo from Bosse, Albert to Shatzer, Blaine, "NPS Truss Assembly," 13 March 1997

8. *NRL Space Truss Assembly Schematics*, January 1997

9. *Newport Vibration Control System Instruction Manual*, Newport Corporation, Irvine, CA 1991

10. Holland, Richard, *Design of Resonant Piezoelectric Devices*, page 10, Massachusetts Institute of Technology Press, 1969

11. Bronowicki, Allen J., *Smart Structures, Work in Progress Report*, p. 3, TRW Space and Electronics Group, Spacecraft Technology Division, 14 September, 1994

12. *Piezo Performance Test Procedures and Documents (Technical Note TN 59E/2)*, Physik Instrumente, Waldbronn, Germany, 12 February 1997

13. Project 95-C-5003 Task 4, Report Number 3614-004-2, *Finite Element Modeling of Smart Structures*, p. 40, MRJ, Inc. 1996

14. Johnson, Scott E. and Vlattas, John, *Modal Analysis and Active Vibration Control of the Naval Postgraduate School Space Truss*, Master's Thesis, Naval Postgraduate School, Monterey, California, June 1998

15. PCB Piezotronics, "PCB Piezotronics Products – PFS Division 208B02," [http://www.pcb.com/products/pfs/pfs208b02.html]

16. *LPACT and Electronics User Manual*, Planning Systems Incorporated, Melbourne Controls Group, Melbourne, FL, 1997

17. Andberg, Brent K., *"Modal Testing and Analysis of the NPS Space Truss,"* Master's Thesis, Naval Postgraduate School, Monterey, California, September 1997

18. dSPACE GmbH, *Real-Time Interface (RTI and RTI-MP) Implementation Guide*, dSPACE GmbH, Germany, March 1999

19. dSPACE GmbH, *ControlDesk Experiment Guide*, dSPACE GmbH, Germany, March 1999

20. dSPACE GmbH, "Variable Description File", *dSPACE Help Desk (On-Line Help)*, From ControlDesk Version 1.0, dSPACE GmbH, Germany, 1999

21. SAS IP, Inc., *ANSYS Commands Ref*, Tenth Edition, Available as On-Line Help, SAS IP, Inc.

22. Physik Instrumente, "P842, P-843 Preloaded Open & Closed Loop LVPZT Translators," [http://www.physikinstrumente.com/pztactuators/1_16t.html]

23. dSPACE GmbH, *MLIB/MTRACE MATLAB-dSPACE Interface and Trace Libraries*, dSPACE GmbH, Germany, March 1999

24. PCB Model 208B02 S/N 15021 Calibration Data Sheet, PCB Piezotronics, 5 Mar 1998

APPENDIX A. NPS SPACE TRUSS CHARACTERISTICS AND COMPONENTS

Mass Properties of the Bare and Modified Truss:

Part Name	No. In Bare Truss	No. In Mod Truss	Component Masses (kg)	Mass Bare Truss (kg)	Mass Mod. Truss (kg)
Node Balls	52	52	0.0663	3.445	3.445
Longerons	100	100	0.0448	4.475	4.475
Diagonals	61	58	0.0522	3.181	3.025
LPACT Strut	0	1	2.2760	0.000	2.276
Active Strut	0	2	0.2900	0.000	0.580
Screw	322	322	0.0019	0.607	0.607
Total Mass Truss				11.708	14.408

Table 7. NPS Space Truss Mass Properties
[After Ref. 13 and the addition of a second active strut.]

Bare Truss Natural Frequencies

Mode Number	Modal Testing [Ref. 13]	MATLAB FEM	ANSYS
1	14.64	14.13	14.25
2	16.26	15.44	15.57
3	30.41	28.72	28.93
4	33.97	32.04	32.26
5	62.93	60.23	60.76
6	74.54	72.24	72.93
7	80.66	79.71	81.67
8	101.01	97.41	96.61
9	126.23	120.21	115.41
10	135.97	129.68	122.26

Table 8. NPS Space Truss Bare Natural Frequencies

Property	Aluminum	Steel
Outer Radius	3.968 mm	3.975 mm
Inner Radius	3.078 mm	Solid
Inertia	$1.242e\text{-}10 \ m^4$	$1.957e\text{-}10 \ m^4$
Cross-sectional Area	$1.96856e\text{-}5 \ m^2$	$4.96e\text{-}5 \ m^2$

Table 9. Truss Element Properties

117

COMPONENTS

Piezoelectric Translation Model P-848-30 S/N

Signal [Volts]	Expansion [Microns]	Contraction [Microns]	Hysteresis [Microns]	Hysteresis [Percent]
0.00	0.00	0.00	0.00	0.00
1.00	3.48	6.43	2.94	5.98
2.00	7.58	12.55	4.97	10.12
3.00	12.16	18.38	6.21	12.64
4.00	17.20	23.86	6.66	13.56
5.00	22.53	29.06	6.53	13.28
6.00	27.96	33.90	5.95	12.10
7.00	33.44	38.38	4.94	10.05
8.00	38.83	42.43	3.61	7.34
9.00	44.05	46.07	2.02	4.11
10.00	49.14	49.14	0.00	0.00

Table 10. Expansion and Contraction Data for Model P-843.30 [From Ref. 12]

Open Loop Travel (0-100V)	45 μm +/- 20%
Closed Loop Travel	45 μm
Stiffness	33 N/μm +/- 20%
Force Generation (Blocked)	1500 N +/-20%
Push/Pull Force Capability	800/300 N
Torque Limit (at tip)	350 mNm
Capacitance	5.4μF +/- 20%
Dynamic Operating Current Coefficient	15 μA/(Hz-μm)
Unloaded Resonant Frequency	10 kHz +/- 20%
Operating Temperature Range	-20 to +80 °C
Mass (w/o cables)	53 g
Length	73 mm

Table 11. P-843.30 Operating Characteristics [Ref. 22]

118

Item	Value
Force Constant (K_f)	5.5 lb/amp
Max. Current	1 amp
Coil Resistance	9 ohms
Flexure Natural Frequency (ω_n)	8 to 10 Hz
Flexure Modal Damping(ξ)	~3 % (or critical) without force loop, up to >100% with force loop on
Stroke	±0.2 inches
Stroke at 10 Hz for 3 lbs. output force	0.1 inches
Gravity Offset Spring Rate	2.4 lb/in
Allowable Strut Diameter	1.000 ± 0.01"
LPACT Envelope	3.8" OD x 4.86" height (including strut clamp and accelerometers)
LPACT Total Weight	4.0 lb.
LPACT Proof Mass Weight	2.9 LB
LPACT Model (low frequency) (refer to Figure 2 for measured FRF from current to force of LPACT)	$$\frac{Output Force(lb)}{Current \text{ Command}(amp)}$$ $$= \frac{K_f s^2}{s^2 + 2\xi\omega_n s + \omega_n}$$
Servo Amp Model	$$\frac{Current \text{ (amp)}}{Servo \text{ Command (V)}} = K_a = 0.1 \frac{amp}{V}$$
Force Loop Model (see section 3.3 for definition of terms)	$$\frac{Servo \text{ Amp Voltage Command (volts)}}{Pr \text{ oof Mass Accel (g)}}$$ $$= \frac{K_{pre} K_{rt} K_{force} s^2}{(s + w_{pre})(s + w_{rt})^2}$$
Rate Loop Model (see section 3.3 for definition of terms)	$$\frac{Servo \text{ Amp Voltage Command (volts)}}{Primary \text{ Accel}(g)}$$ $$= \frac{K_{pre} K_{rt} K_{rate} w_{rate} S_r s^2}{(s + w_{pre})(s + w_{rt})^2 (s + w_{rate})}$$

Table 12. LPACT Characteristics

119

| Cable Assembly cable	connect to LPACT Electronics (all on rear panel)	connect to LPACT Component
Black Coax	'To Coil' (banana plug to BNC adapter)	6" Blue Pigtail from coil (BNC)
Blue Coax marked with Red Tape	'From Secondary Accelerometer' (BNC)	Secondary Accelerometer on Proof Mass (microdot)
Blue Coax	'From Primary Accelerometer' (BNC)	Primary Accelerometer on Co-Locate Ring (microdot)

Table 13. LPACT Electronics Connectivity Guidelines [From Ref. 16]
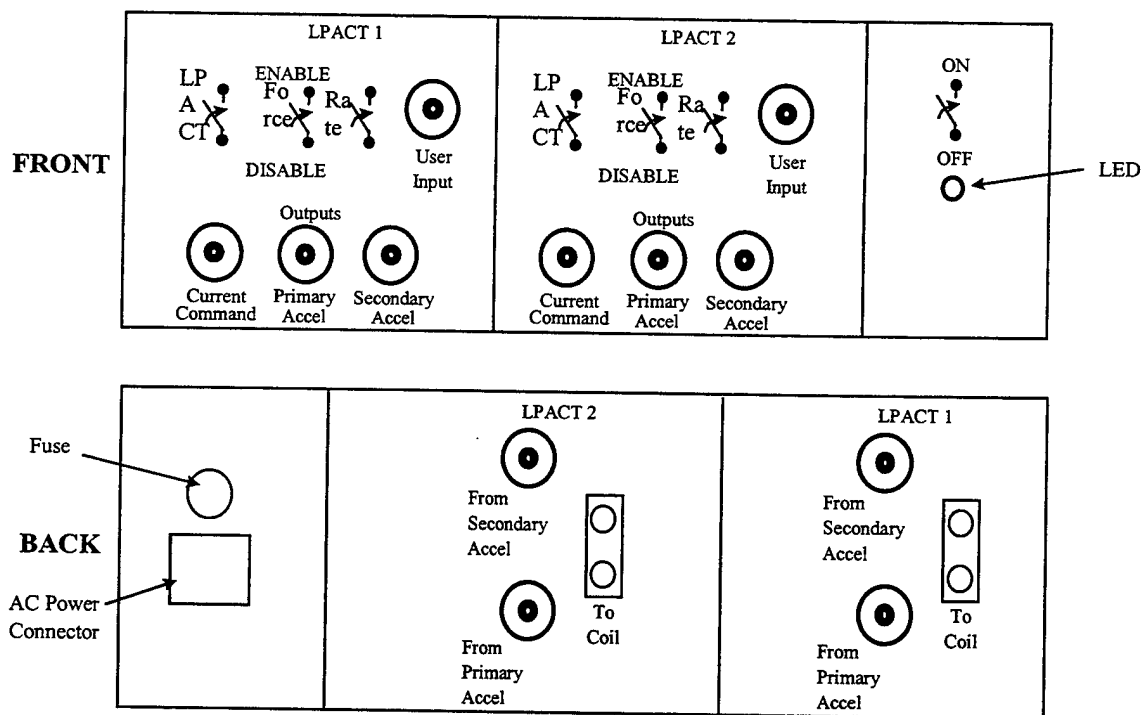
Figure 56. LPACT Control Electronics Rear Panel [From Ref. 16]

120
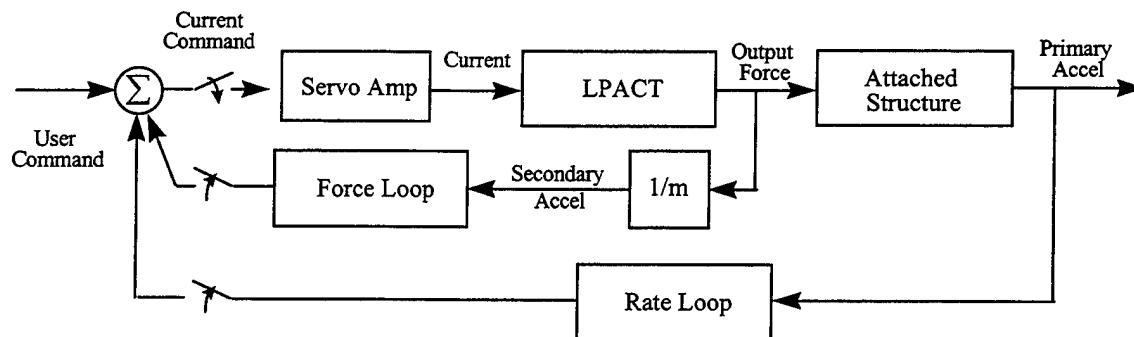
where m = mass of proof mass (2.9 lb)

Figure 57. LPACT System Level Block Diagram [From Ref. 16]

PCB Piezotronics Model 208B02 General Purpose ICP Force Sensor S/N 15021

Sensitivity (Specification)	50 mV/lb (11240 mV/kN)
Sensitivity (Measured)	50.80 mV/lb [Ref. 24]
Dynamic Range	-10 lb to 100-lb
Stiffness	1.0 kN/μm
Temperature Range	-54 to 121 °C
Sensing Element	Quartz

Table 14. PCB Model 208B02 Operating Characteristics [Ref. 15]

PCB® Piezotronics Type 484B Signal Conditioner S/N 2086

Notes
Unity Gain
Set CPLG to DC & Bias to 6 V

Kistler Instrument Corp. Accelerometers:
(Note: g = 9.807 m/s^2)

Type	Serial Number	+ x-axis	+ y-axis	+ z-axis	
8690C10	C112398	495	490	494	mV/g
8690C10	C112399	487	490	490	mV/g
8690C10	C112400	499	500	494	mV/g
8690C10	C112401	497	491	505	mV/g

Kistler Instrument Corp. Signal Conditioners (Multi-Channel Couplers):

Type	Serial Number
5124A (twelve channel)	C74930

121

Trek Voltage Amplifier:

Type   Serial Number   Notes
Trek 50/750   none   Required calibration on 10 September 1998.
                                     Mini-cal to verify setting and linearity
                                     Performed by author on 2 July, 1999
                                     Two channels that can be used with both active
                                     struts.

dSPACE GmbH, Germany, S/N 3192

CPU   Motorola PowerPC running at 300 Hz
Memory   128MB RAM
Input Channels   20 ADC
Ouput Channels   8 DAC 0-10V

Hewlett Packard HP 33120A Signal Generator S/N
settings

Hewlett Packard HP 54601A Digital Oscilloscope S/N 3134A02713
Four Channels
Frequency response up to 100 MHz

Hewlett Packard HP 35665A Dynamic Signal Analyzer S/N
hookups and settings

SOFTWARE DOCUMENTATION

Program	Version
MATLAB	5.2.1430
dSPACE RTI1103	3.3
dSPACE MLIB/MTRACE	3.1.1
dSPACE ControlDesk	1.0
ANSYS/Multiphysics	5.5.2

Table 15. Software Documentation

APPENDIX B. TRUSS_MODES.M

```
%--------------------------------------------------------------------%
% Modified from Example 8.9.5,"The Finite Element Method using MATLAB"%
% Young W. Kwon & Hyochoong Bang, 1997 CRC Press LLC                 %
% Modified by LT Carey M. Pantling                                   %
% Modified by LT Timothy A. Barney                                   %
% Eigenanalysis of NPS Space Truss                                   %
% Bulids systems mass and stiffness matrices for integating with     %
% active controls and plots the mode shapes.                         %
%                                                                    %
% Variable descriptions                                              %
%    coord = global x,y and z coordiates of each node                %
%    nd = nodal connection vector                                    %
%    k = element stiffness matrix                                    %
%    kk = system stiffness matrix                                    %
%    m = element mass matrix                                         %
%    mm = system mass matrix                                         %
%    ff = system force vector                                        %
%    index = vector containing system dofs associated with each element%
%    bcdof = vector containing dofs associated with boundary conditions%
%    bcval = vector containing boundary condition values associated  %
%            with the dofs in 'bcdof'                                 %
%--------------------------------------------------------------------%


% NPS Space Truss
clear;
nel=161;                % number of elements
nnel=2;                 % number of nodes per element
ndof=6;                 % number of dofs per node
nnode=52;               % total number of nodes in system
sdof=nnode*ndof;        % total system dofs

load nps_coord.dat;     %  52 by 3, 52 nodes x,y,z
load nps_node.dat;      %  161 by 2, 161 elements, node1 node2
load nps_bcdof.dat ;    %  24 by 2, 24 degrees constrained

coord=nps_coord;
nd=nps_node;
bcdof=nps_bcdof(:,1);
bcval=nps_bcdof(:,2);

% all units in standard metric units
el=70E9;                '% GPa     elastic modulus
area=1.9686982E-5;  % m^2     cross-sectional area
xi=1.242217E-10;    % m^4     moment of inertia of cross-section
rho=2800;           % kg/m^3 mass density per volume

ff=zeros(sdof,1);       % initialization of system force vector
kk=zeros(sdof,sdof);    % initialization of system matrix
mm=zeros(sdof,sdof);    % initialization of system matrix
index=zeros(nel*ndof,1); % initialization of index vector
```

```
for iel=1:nel                      % loop for the total number of elements
    index=feeldof(nd(iel,:),nnel,ndof); % extract system dofs associated
                                    % with the element

% compute element stiffness and mass matrices
  [k,m]=feframe3(el,xi,area,rho,coord(nd(iel,1),:),coord(nd(iel,2),:));
 kk=feasmbl1(kk,k,index); % assemble element matrix into system matrix
 mm=feasmbl1(mm,m,index);
end

% add the concentrated masses at the nodal translation dof
for iel=1:nnode
    start=(iel-1)*ndof+1;
    fini=start+2;
    % add lumped masses for the node points
    mm(start:fini,start:fini)=mm(start:fini,start:fini)+(0.0663)*eye(3);
    % kg added to each node as concentrated mass
end

% apply boundary conditions
% remove for simulink analysis, as this prevents m matrix inversion
[kk,mm,ff]=feaplyc2(kk,mm,ff,bcdof,bcval);
[V,D]=eig(kk,mm);
fsol=diag(D);

for index=1:size(fsol)
    output(index,:)=[index fsol(index)];
end

%%%%%%%%%%%%%%%%%%%%%%%%%%%%%%%%%%%
% Plots the first 4 mode shapes. %
%%%%%%%%%%%%%%%%%%%%%%%%%%%%%%%%%%%

% First Mode Shape
figure(1);
amp=2.0;
mode=V(:,256);
disp=nps_coord;
for index=1:nnode
    start=(index-1)*6+1;
    disp(index,1)=disp(index,1)+amp*mode(start);    % x-coord
    disp(index,2)=disp(index,2)+amp*mode(start+1);  % y-
    disp(index,3)=disp(index,3)+amp*mode(start+2);  % z-
end
disp=real(disp);
% form the line combinations
plot3(disp(1:2,1),disp(1:2,3),disp(1:2,2),'b*-');
hold on
plot3(nps_coord(1:2,1),nps_coord(1:2,3),nps_coord(1:2,2),'r.');
view(-30,20);
axis([-2 3 -1 2 -1 2]);
plot3(disp(3:14,1),disp(3:14,3),disp(3:14,2),'b*-');
plot3(nps_coord(3:14,1),nps_coord(3:14,3),nps_coord(3:14,2),'r.');
view(-30,20);
axis([-2 3 -1 2 -1 2]);
```

```matlab
plot3(disp(15:26,1),disp(15:26,3),disp(15:26,2),'b*-');
plot3(nps_coord(15:26,1),nps_coord(15:26,3),nps_coord(15:26,2),'r.');
view(-30,20);
axis([-2 3 -1 2 -1 2]);
plot3(disp(27:28,1),disp(27:28,3),disp(27:28,2),'b*-');
plot3(nps_coord(27:28,1),nps_coord(27:28,3),nps_coord(27:28,2),'r.');
view(-30,20);
axis([-2 3 -1 2 -1 2]);
plot3(disp(29:40,1),disp(29:40,3),disp(29:40,2),'b*-');
plot3(nps_coord(29:40,1),nps_coord(29:40,3),nps_coord(29:40,2),'r.');
view(-30,20);
axis([-2 3 -1 2 -1 2]);
plot3(disp(41:52,1),disp(41:52,3),disp(41:52,2),'b*-');
plot3(nps_coord(41:52,1),nps_coord(41:52,3),nps_coord(41:52,2),'r.');
view(-30,20);
axis([-2 3 -1 2 -1 2]);
% cross ties
for index=1:26
    line(1,:)=disp(index,:);
    line(2,:)=disp(index+26,:);
    plot3(line(:,1),line(:,3),line(:,2),'b*-');
end
% verticals
for index= [1 2 27 28]
    line(1,:)=disp(index,:);
    line(2,:)=disp(index+7,:);
    plot3(line(:,1),line(:,3),line(:,2),'b*-');
end
for index= 3:14
    line(1,:)=disp(index,:);
    line(2,:)=disp(index+12,:);
    plot3(line(:,1),line(:,3),line(:,2),'b*-');
end
for index= 29:40
    line(1,:)=disp(index,:);
    line(2,:)=disp(index+12,:);
    plot3(line(:,1),line(:,3),line(:,2),'b*-');
end
hold off
title('Mode 1');
print -djpeg mode4ml.jpg

% Second Mode Shape
figure(2);
amp=2.0;
mode=V(:,257);
disp=nps_coord;
for index=1:nnode
    start=(index-1)*6+1;
    disp(index,1)=disp(index,1)+amp*mode(start);    % x-coord
    disp(index,2)=disp(index,2)+amp*mode(start+1); % y-
    disp(index,3)=disp(index,3)+amp*mode(start+2); % z-
end
disp=real(disp);
% form the line combinations
```

125

```
plot3(disp(1:2,1),disp(1:2,3),disp(1:2,2),'b*-');
hold on
plot3(nps_coord(1:2,1),nps_coord(1:2,3),nps_coord(1:2,2),'r.');
view(-30,20);
axis([-2 3 -1 2 -1 2]);
plot3(disp(3:14,1),disp(3:14,3),disp(3:14,2),'b*-');
plot3(nps_coord(3:14,1),nps_coord(3:14,3),nps_coord(3:14,2),'r.');
view(-30,20);
axis([-2 3 -1 2 -1 2]);
plot3(disp(15:26,1),disp(15:26,3),disp(15:26,2),'b*-');
plot3(nps_coord(15:26,1),nps_coord(15:26,3),nps_coord(15:26,2),'r.');
view(-30,20);
axis([-2 3 -1 2 -1 2]);
plot3(disp(27:28,1),disp(27:28,3),disp(27:28,2),'b*-');
plot3(nps_coord(27:28,1),nps_coord(27:28,3),nps_coord(27:28,2),'r.');
view(-30,20);
axis([-2 3 -1 2 -1 2]);
plot3(disp(29:40,1),disp(29:40,3),disp(29:40,2),'b*-');
plot3(nps_coord(29:40,1),nps_coord(29:40,3),nps_coord(29:40,2),'r.');
view(-30,20);
axis([-2 3 -1 2 -1 2]);
plot3(disp(41:52,1),disp(41:52,3),disp(41:52,2),'b*-');
plot3(nps_coord(41:52,1),nps_coord(41:52,3),nps_coord(41:52,2),'r.');
view(-30,20);
axis([-2 3 -1 2 -1 2]);
% cross ties
for index=1:26
    line(1,:)=disp(index,:);
    line(2,:)=disp(index+26,:);
    plot3(line(:,1),line(:,3),line(:,2),'b*-');
end
% verticals
for index= [1 2 27 28]
    line(1,:)=disp(index,:);
    line(2,:)=disp(index+7,:);
    plot3(line(:,1),line(:,3),line(:,2),'b*-');
end
for index= 3:14
    line(1,:)=disp(index,:);
    line(2,:)=disp(index+12,:);
    plot3(line(:,1),line(:,3),line(:,2),'b*-');
end
for index= 29:40
    line(1,:)=disp(index,:);
    line(2,:)=disp(index+12,:);
    plot3(line(:,1),line(:,3),line(:,2),'b*-');
end
hold off
title('Mode 2');
print -djpeg mode4ml.jpg

% Third Mode Shape
figure(3);
amp=2.0;
mode=V(:,258);
```

```
disp=nps_coord;
for index=1:nnode
    start=(index-1)*6+1;
    disp(index,1)=disp(index,1)+amp*mode(start);    % x-coord
    disp(index,2)=disp(index,2)+amp*mode(start+1);  % y-
    disp(index,3)=disp(index,3)+amp*mode(start+2);  % z-
end
disp=real(disp);
% form the line combinations
plot3(disp(1:2,1),disp(1:2,3),disp(1:2,2),'b*-');
hold on
plot3(nps_coord(1:2,1),nps_coord(1:2,3),nps_coord(1:2,2),'r.');
view(-30,20);
axis([-2 3 -1 2 -1 2]);
plot3(disp(3:14,1),disp(3:14,3),disp(3:14,2),'b*-');
plot3(nps_coord(3:14,1),nps_coord(3:14,3),nps_coord(3:14,2),'r.');
view(-30,20);
axis([-2 3 -1 2 -1 2]);
plot3(disp(15:26,1),disp(15:26,3),disp(15:26,2),'b*-');
plot3(nps_coord(15:26,1),nps_coord(15:26,3),nps_coord(15:26,2),'r.');
view(-30,20);
axis([-2 3 -1 2 -1 2]);
plot3(disp(27:28,1),disp(27:28,3),disp(27:28,2),'b*-');
plot3(nps_coord(27:28,1),nps_coord(27:28,3),nps_coord(27:28,2),'r.');
view(-30,20);
axis([-2 3 -1 2 -1 2]);
plot3(disp(29:40,1),disp(29:40,3),disp(29:40,2),'b*-');
plot3(nps_coord(29:40,1),nps_coord(29:40,3),nps_coord(29:40,2),'r.');
view(-30,20);
axis([-2 3 -1 2 -1 2]);
plot3(disp(41:52,1),disp(41:52,3),disp(41:52,2),'b*-');
plot3(nps_coord(41:52,1),nps_coord(41:52,3),nps_coord(41:52,2),'r.');
view(-30,20);
axis([-2 3 -1 2 -1 2]);
% cross ties
for index=1:26
    line(1,:)=disp(index,:);
    line(2,:)=disp(index+26,:);
    plot3(line(:,1),line(:,3),line(:,2),'b*-');
end
% verticals
for index= [1 2 27 28]
    line(1,:)=disp(index,:);
    line(2,:)=disp(index+7,:);
    plot3(line(:,1),line(:,3),line(:,2),'b*-');
end
for index= 3:14
    line(1,:)=disp(index,:);
    line(2,:)=disp(index+12,:);
    plot3(line(:,1),line(:,3),line(:,2),'b*-');
end
for index= 29:40
    line(1,:)=disp(index,:);
    line(2,:)=disp(index+12,:);
    plot3(line(:,1),line(:,3),line(:,2),'b*-');
```

127

```
end
hold off
title('Mode 3');
print -djpeg mode4ml.jpg

% Fourth Mode Shape
figure(4);
amp=2.0;
mode=V(:,259);
disp=nps_coord;
for index=1:nnode
    start=(index-1)*6+1;
    disp(index,1)=disp(index,1)+amp*mode(start);    % x-coord
    disp(index,2)=disp(index,2)+amp*mode(start+1); % y-
    disp(index,3)=disp(index,3)+amp*mode(start+2); % z-
end
disp=real(disp);
% form the line combinations
plot3(disp(1:2,1),disp(1:2,3),disp(1:2,2),'b*-');
hold on
plot3(nps_coord(1:2,1),nps_coord(1:2,3),nps_coord(1:2,2),'r.');
view(-30,20);
axis([-2 3 -1 2 -1 2]);
plot3(disp(3:14,1),disp(3:14,3),disp(3:14,2),'b*-');
plot3(nps_coord(3:14,1),nps_coord(3:14,3),nps_coord(3:14,2),'r.');
view(-30,20);
axis([-2 3 -1 2 -1 2]);
plot3(disp(15:26,1),disp(15:26,3),disp(15:26,2),'b*-');
plot3(nps_coord(15:26,1),nps_coord(15:26,3),nps_coord(15:26,2),'r.');
view(-30,20);
axis([-2 3 -1 2 -1 2]);
plot3(disp(27:28,1),disp(27:28,3),disp(27:28,2),'b*-');
plot3(nps_coord(27:28,1),nps_coord(27:28,3),nps_coord(27:28,2),'r.');
view(-30,20);
axis([-2 3 -1 2 -1 2]);
plot3(disp(29:40,1),disp(29:40,3),disp(29:40,2),'b*-');
plot3(nps_coord(29:40,1),nps_coord(29:40,3),nps_coord(29:40,2),'r.');
view(-30,20);
axis([-2 3 -1 2 -1 2]);
plot3(disp(41:52,1),disp(41:52,3),disp(41:52,2),'b*-');
plot3(nps_coord(41:52,1),nps_coord(41:52,3),nps_coord(41:52,2),'r.');
view(-30,20);
axis([-2 3 -1 2 -1 2]);
% cross ties
for index=1:26
    line(1,:)=disp(index,:);
    line(2,:)=disp(index+26,:);
    plot3(line(:,1),line(:,3),line(:,2),'b*-');
end
% verticals
for index= [1 2 27 28]
    line(1,:)=disp(index,:);
    line(2,:)=disp(index+7,:);
    plot3(line(:,1),line(:,3),line(:,2),'b*-');
end
```

```
for index= 3:14
    line(1,:)=disp(index,:);
    line(2,:)=disp(index+12,:);
    plot3(line(:,1),line(:,3),line(:,2),'b*-');
end
for index= 29:40
    line(1,:)=disp(index,:);
    line(2,:)=disp(index+12,:);
    plot3(line(:,1),line(:,3),line(:,2),'b*-');
end
hold off
```

THIS PAGE INTENTIONALLY LEFT BLANK

APPENDIX C. NPS SPACE TRUSS MODE SHAPES

The first four mode shapes obtained with MATLAB are presented first. This model does not include the added mass of the LPACT or the active elements and results in symmetric shapes. The deformed shapes are shown with the undeformed node locations for comparison. The first four mode shapes generated by ANSYS are presented second, with both the deformed and undeformed shapes. The ANSYS model includes the LPACT and active element masses and stiffness characteristics.

Mode 1   Mode 2

Mode 3   Mode 4
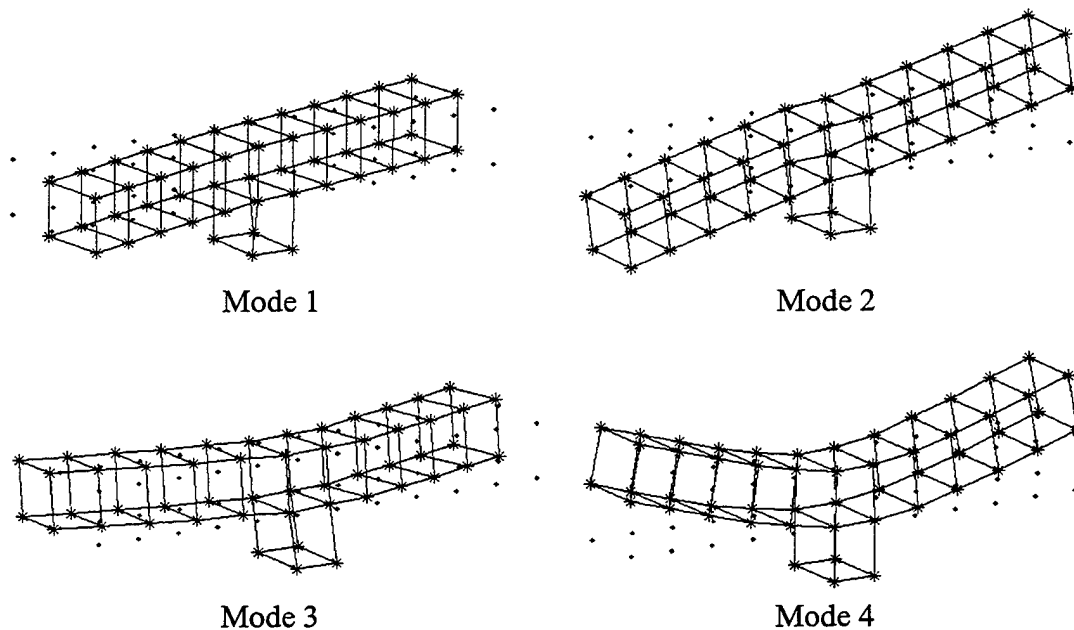
Figure 58. NPS Space Truss Mode Shapes with MATLAB

The mode shapes generated by ANSYS are shown with both the deformed and undeformed states. The undeformed states appear as light gray lines in the following figures.

MODE 1
(9.427 Hz)

MODE 2
(11.318 Hz)

MODE 3
(12.529 Hz)

MODE 4
(18.744 Hz)
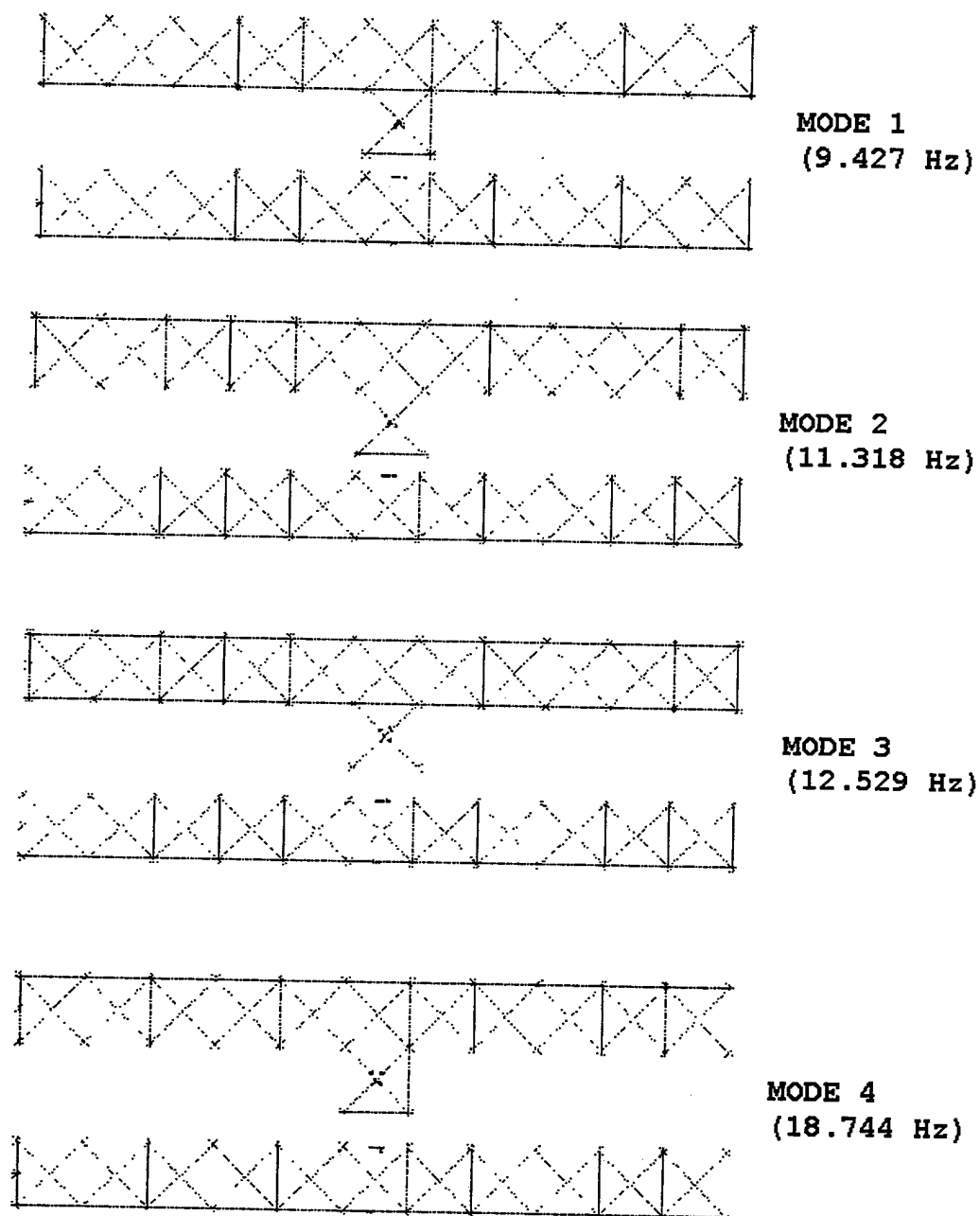
Figure 59. NPS Space Truss Mode Shapes with ANSYS

132

APPENDIX D. CONTROLLER OPERATION

To start and run the controller, the following steps must be followed (all on the NPS space truss computer in the Smart Structures Laboratory):

- Initiate ControlDesk using the ▨ icon either on the desktop of the toolbar, or by using the menu Start>Programs>dSPACE>ControlDesk

- Open the Experiment using the command File > Open Experiment. Select C:\Space_Truss\Truss01\Adaptive Controller.cdx.

- Load the controller to the CPU by using the ▨ icon on the toolbar. Select the program C:\Space_Truss\Truss01\Finished.ppc.

- Ensure the Edit Mode is selected from the toolbar (verify the Edit mode button depressed) ▨. The three buttons are Edit, Test and Animate mode respectively.

- Start the CPU (depress the green triangle on the toolbar).

- Select the Animate mode to enable the display.

- The disturbance and controller may be turned on and off with the push buttons as previously described.

THIS PAGE INTENTIONALLY LEFT BLANK

APPENDIX E. TRUSS_CONTROL.TXT

```
! ****************************************************
! * Truss Control APDL Program for ANSYS version 5.6     *
! * Constant Frequency, 19 Hz Disturbance from LPACT      *
! * Applied to the NPS Space Truss Active Controlled Model *
! * Controlling the Z-Axis of Node 49 [Lab Node 18, Y-Axis] *
! * Using Piezo #2 [Voltage Applied to Node 86]           *
! * Written by LT Carey M. Pantling                       *
! * Modified by LT Timothy A. Barney                      *
! * With assistance by Sheldon Imaoka                     *
! * Last Modified 2 March 2001                            *
! ****************************************************

finish

! First Load Truss model with mesh and BC's

! ***********************************
! * Increase the Max Result Set Size *
! ***********************************

/config,nres,10000

! *******************
! * Define Variables *
! *******************

*set,LMSADAPT,-0.045     ! Control Node Displacement Value
*set,FREQ,19.0          ! LPACT Disturbance Frequency
*set,PV,86              ! Node to apply Piezo Voltage
!                       (Node 67 = Piezo #1, Node 86 = Piezo #2)
*set,CTLNODE,49         ! Set Control Node Sensor Location
!                       (Node 41 = Lab Node 26)
!                       (Node 18 = Lab Node 49)
!                       (Node 49 = Lab Node 18)
!                       (Node 26 = Lab Node 41)
*set,STRTTIME,0.0       ! Start time = 0.0 seconds
*set,FINITIME,5.0       ! Finish Time in seconds

*set,DDISP1,0.0         ! Previous Nodal Displacement
*set,DDISP2,0.0         ! Current Nodal Displacement
*set,DVELO1,0.0         ! Previous Nodal Velocity
*set,DVELO2,0.0         ! Current Nodal Velocity
```

135

```
*set,CS,0.0                          ! Control Signal to Piezo, initial zero
*set,G3,0.0                          ! Control Signal Amplification to Piezo

TIMESTEP=1/FREQ/20        ! Defines the Timestep
*set,PI,acos(-1)
*set,APLNODE,75              ! The Node Where the LPACT is Located
finish


! ********************************************
! * Generate Disturbance Signal at 20 Steps per Period *
! ********************************************


*set,NUMSTEP,nint(FINITIME/TIMESTEP)
*set,FORCFUN,
*set,FFP,
*dim,FORCFUN,array,NUMSTEP   ! Array for Forcing function
!                                          Used as Input (indexed)
*dim,FFP,table,NUMSTEP       ! Table for Plotting
!                                          Used as Output (not indexed)


! ---------------------------------------------------------------------
! - Calculate Disturbance Magnitude Based on FREQ and LPACT Response -
! ---------------------------------------------------------------------


*set,MAG,0.05437*FREQ**2-1.8874*FREQ+18.2439      ! (N) force from LPACT


! ----------------------------------------------
! - Create a Table for the Disturbance Force -
! ----------------------------------------------


*do,ICOUNT,1,NUMSTEP
  FORCFUN(ICOUNT)=sin(2*PI*FREQ*((ICOUNT-1)*TIMESTEP))*MAG
  FFP(ICOUNT)=sin(2*PI*FREQ*((ICOUNT-1)*TIMESTEP))*MAG
*enddo

*set,NODEDISP                       ! Tracks the Control Node Displacement
*dim,NODEDISP,table,NUMSTEP  ! Creates an Array to Get Displacement
*set,CSCheck                        ! Tracks the Control Output Signal
*dim,CSCheck,table,NUMSTEP   ! Gets the Control Signal


! --------------------------
! - Included for Output Data -
! --------------------------


*set,MYDISP,                        ! Tracks the Node Displacement
```

136

```
*set,MYVELO,                        ! Tracks the Node Velocity
*set,MYACEL,                        ! Tracks the Node Acceleration
*set,MYCOSINE,                      ! Tracks the Cosine Weighting Factor
*set,MYSINE,                        ! Tracks the Sine Weighting Factor
*dim,MYDISP,table,NUMSTEP           ! Gets the Node Displacement
*dim,MYVELO,table,NUMSTEP           ! Gets the Node Velocity
*dim,MYACEL,table,NUMSTEP           ! Gets the Node Acceleration
*dim,MYCOSINE,table,NUMSTEP         ! Gets the Cosine Weighting Factor
*dim,MYSINE,table,NUMSTEP           ! Gets the Sine Weighting Factor


! ***********************
! * Do loop for Each Time Step *
! ***********************


! -----------------------------------------------------------
! - Clears any Constraints on Nodes 67 and 86 -
! -----------------------------------------------------------


/prep7
ddele,67,volt
ddele,86,volt
finish


! -----------------------
! - ANSYS Model Solution -
! -----------------------


*do,ICOUNT,1,NUMSTEP
  *set,CURRTIME,STRTTIME+ICOUNT*TIMESTEP      ! Set Current Time
!                                             (Actually the End of Current Time Step)
  /solu                                 ! Enter the Solution Processor
  *if,ICOUNT,eq,1,then
    antype,trans,new                    ! Start New Transient Analysis
  *else
    antype,trans,rest                   ! Restart or Continue Transient Analysis
  *endif
  time,CURRTIME                         ! Set Current Time for ANSYS Solution
  deltim,TIMESTEP                       ! Set Delta-t
  f,APLNODE,fy,FORCFUN(ICOUNT)*0.707          ! Apply Force to APLNODE
Node (LPACT)
  f,APLNODE,fz,FORCFUN(ICOUNT)*0.707          ! Apply Force to APLNODE
Node (LPACT)
  d,PV,volt,CS                          ! Apply CS Voltage to PV Node
  allsel,all                            ! Select Everything to Prepare for Solve
  solve
```

```
finish

! ----------------------------------------------------
! - Turns on Controller After Initial Transient -
! ----------------------------------------------------

    *if,ICOUNT,ge,200,then              ! Turns on Control at Specified Step
      G3=20.0
    *endif
    *if,ICOUNT,le,200,then
      *set,SINEWT,0.0
      *set,COSINEWT,0.0
    *endif


! ------------------------
! - ANSYS Post Processor -
! ------------------------

    /post1                              ! Enter Post Processor
    *get,NODEDISP(ICOUNT),node,CTLNODE,u,z  ! Get the Control Node Displacement
    finish

! ****************************************************
! * Control Law implementation, for next time step *
! ****************************************************

    *set,DDISP1,DDISP2                  ! Saves Last Control Node
Displacement
    *get,DDISP2,node,CTLNODE,u,z        ! Reads Current Control Node
Displacement
    *set,DVELO1,DVELO2                  ! Saves Last Control Node Velocity
    *set,DVELO2,(DDISP2-DDISP1)/TIMESTEP    ! Calculates Current Mean Velocity
    *set,DACEL,(DVELO2-DVELO1)/TIMESTEP     ! Calculates Current Mean
Acceleration
    MYDISP(ICOUNT)=DDISP2               ! Tracks Displacement Values
    MYVELO(ICOUNT)=DVELO2              ! Tracks Velocity Values
    MYACEL(ICOUNT)=DACEL              ! Tracks Acceleration Values


! -----------------------------
! - Updates Control Signal -
! -----------------------------

    SINEWT=SINEWT+LMSADAPT*DACEL*sin(2*PI*FREQ*((ICOUNT-
1)*TIMESTEP))        ! Sine Weight
```

138

```
COSINEWT=COSINEWT+LMSADAPT*DACEL*cos(2*PI*FREQ*((ICOUNT-
1)*TIMESTEP))        ! Cosine Weight
TERM1=SINEWT*sin(2*PI*FREQ*((ICOUNT-1)*TIMESTEP))        ! Sine Term
TERM2=COSINEWT*cos(2*PI*FREQ*((ICOUNT-1)*TIMESTEP))     ! Cosine Term
CS=G3*(TERM1+TERM2)                    ! New Control Voltage

MYCOSINE(ICOUNT)=COSINEWT          ! Tracks the Cosine Weighting Factor
MYSINE(ICOUNT)=SINEWT              ! Tracks the Sine Weighting Factor

*if,CS,gt,50,then                  ! Voltage Limiter, Based on Actual Piezo
  CS=50
*endif
*if,CS,lt,-50,then
  CS=-50
*endif

CSCheck(ICOUNT)=CS                 ! Tracks the Control Signal for Output

*enddo                             ! Ends the Loop, Ready for Next Time Step

! ***********************
! * Plot the Results to the Screen *
! ***********************

/erase
*vplot,,NODEDISP(1)

! *****************************************
! * Generates Output Files for:                *
! * Control Signal - "zCSoutput.out"           *
! * Control Node Displacement - "zNdisp.out"    *
! * Control Node Velocity - "zNvelo.out"        *
! * Control Node Acceleration - "zNacel.out"    *
! * Cosine Weighting Factor - "zCosine.out"     *
! * Sine Weighting Factor - " zSine.out"        *
! *****************************************

*cfopen,zCSoutput,out,
*vwrite,CSCheck(1),
(E10.3)
*cfclos
*cfopen,zNdisp,out,
*vwrite,MYDISP(1),
(E10.3)
*cfclos
```

```
*cfopen,zNvelo,out,
*vwrite,MYVELO(1),
(E10.3)
*cfclos
*cfopen,zNacel,out,
*vwrite,MYACEL(1),
(E10.3)
*cfclos
*cfopen,zCosine,out,
*vwrite,MYCOSINE(1),
(E10.3)
*cfclos
*cfopen,zSine,out,
*vwrite,MYSINE(1),
(E10.3)
*cfclos
```

APPENDIX F. ACT_TRUSS.INP

```
! ************************************************
! * act_truss_3.inp                            *
! * used in getting the fresh truss on line    *
! * Truss Control APDL Program for ANSYS version 5.5  *
! * For simple sinusoidal disturbances         *
! * Applied to the NPS Space Truss Active Controlled Model *
! * Written by LT Carey M. Pantling            *
! * Last Modified 14 Oct 1999                  *
! ************************************************


! First Load Truss model with mesh and BC's


! ********************
! * Define Variables    *
! ********************


eplot                    ! gives something to look at while waiting


! *set command will define and clear variables
*set,FREQ,11.75          ! disturbance frequency
*set,CS,0.0              ! control signal to piezo, initial zero
*set,PV,68              ! Piezo voltage node# for application
*set,RS,                ! read signal from piezo, defined only
*set,SV,60              ! Sensor voltage node# for detection
*set,G1,300             ! Control gain constants, see below
*set,G2,100
*set,G3,0.0
*set,OLDRS,0.0          ! the old RS, IC 0.0
*set,OLDINT,0.0         ! old integral, IC 0.0
*set,OLDFINT,0.0        ! old filtered integral
*set,OLDDBL,0.0         ! prev DI, IC 0.0
*set,OLDFDBL,0.0        ! old filtered DI
*set,STRTTIME,0.0       ! Start time = 0.0 seconds


! set to more reasonable later
*set,FINITIME,4.0       ! Finish Time in seconds

TIMESTEP=1/FREQ/20       ! TIMESTEP
*set,PI,acos(-1)
*set,DISPNODE,25                ! node 26 real truss for reading the output
*set,APLNODE,53                 ! the node where the LPACT is located
finish
```

```
! ****************************************************
! * Set up load disturbance, at least 20 steps per period *
! ****************************************************

*set,NUMSTEP,nint(FINITIME/TIMESTEP)
*set,FORCFUN,
*set,FFP,
*dim,FORCFUN,array,NUMSTEP          ! array for forcing function
*dim,FFP,table,NUMSTEP              ! table for plotting
! arrays for input (indexed), tables for output(non indexed)


! create a magnitude based upon the frequency, from the LPACT chart
*set,MAG,0.05437*FREQ**2-1.8874*FREQ+18.2439  ! (N) force from LPACT


! Make a table for the force disturbance
*do,ICOUNT,1,NUMSTEP
  FORCFUN(ICOUNT)=sin(2*PI*FREQ*((ICOUNT-1)*TIMESTEP))*MAG
  FFP(ICOUNT)=sin(2*PI*FREQ*((ICOUNT-1)*TIMESTEP))*MAG
*enddo


*set,NODE26Y
*dim,NODE26Y,table,NUMSTEP     ! creates an array to get displacement
*set,CSCheck                   ! tracks the control output signal
*dim,CSCheck,table,NUMSTEP     ! gets the control signal
*set,RSCheck                   ! tracks the read signal
*dim,RSCheck,table,NUMSTEP     ! copies the sensed signal


! these may be deleted, and not be required to be copied, included for error checking
! *set,INTcheck
! *dim,INTcheck,table,NUMSTEP
! *set,DBLcheck
! *dim,DBLcheck,table,NUMSTEP
! *set,FINTchk
! *dim,FINTchk,table,NUMSTEP
! *set,FDBLchk
! *dim,FDBLchk,table,NUMSTEP


! **************************************
! * Do loop for loading at each time step        *
! **************************************

*do,ICOUNT,1,NUMSTEP
! Set current time (actually, end of current step)
  *set,CURRTIME,STRTTIME+ICOUNT*TIMESTEP
```

142

```
/solu                                      ! enter the solution processor
*if,ICOUNT,eq,1,then
  antype,trans,new                         ! Start new transient analysis
*else
  antype,trans,rest                        ! Restart or continue transient analysis
*endif
time,CURRTIME                              ! set current time for ANSYS solution
deltim,TIMESTEP                            ! set delta-t
f,APLNODE,fy,FORCFUN(ICOUNT)*0.707         ! apply force to APLNODE node
(LPACT)
f,APLNODE,fz,FORCFUN(ICOUNT)*0.707         ! apply force to APLNODE node
(LPACT)
d,PV,volt,CS                               ! apply CS voltage to PV node
allsel,all                                 ! select everything to prepare for solve
solve
finish
*if,ICOUNT,gt,200,then                     ! turns on control at specified step
  G3=20.0
*endif


/post1                                     ! enter post processor
*get,RS,node,SV,volt                       ! get sensor voltage
RSCheck(ICOUNT)=RS                         ! saves current RS in table
*get,NODE26Y(ICOUNT),node,DISPNODE,u,y     ! get the tip displacement
finish


! ********************************************
! * Control Law implementation, for next time step    *
! ********************************************


*set,INT,OLDINT+(RS+OLDRS)/2*TIMESTEP              ! approx the integral
*set,FINT,0.95*OLDFINT+INT-OLDINT                  ! digital high pass filter
*set,DBLINT,OLDDBL+(FINT+OLDFINT)/2*TIMESTEP       ! second integral
*set,FDBL,0.95*OLDFDBL+DBLINT-OLDDBL               ! digital high pass filter!
! INTcheck(ICOUNT)=INT                             ! copies the terms for examination
! FINTchk(ICOUNT)=FINT
! DBLcheck(ICOUNT)=DBLINT
! FDBLchk(ICOUNT)=FDBL
OLDRS=RS                                           ! cycle the terms to old values
OLDINT=INT
OLDFINT=FINT
OLDDBL=DBLINT
OLDFDBL=FDBL
CS=(G1*FINT+G2*FDBL)*G3                            ! CS=RS*(G1/s+g2/s^2)*G3
```

143

```
*if,CS,gt,60,then                        ! voltage limiter
  CS=60
*endif
*if,CS,lt,-60,then
  CS=-60
*endif
CSCheck(ICOUNT)=CS                       ! save for output

*enddo                                   ! ends the loop, ready for next time step

! *********************
! * Plot the results to screen *
! *********************
/erase
*vplot,,NODE26Y(1)


! *********************************************
! * Write RSCheck results to text file "ATR_e#_r#.out" *
! *   and NODE26Y results to ATN.                      *
! *   and CSCheck results to ATS.                      *
! *********************************************
*cfopen,AR_e1_r1,out,
*vwrite,CSCheck(1),
(E10.3)
*cfclos
*cfopen,AN_e1_r1,out,
vwrite,NODE26Y(1),
(E10.3)
*cfclos
*cfopen,AS_e1_r1,out,
vwrite,NODE26Y(1),
(E10.3)
*cfclos
```

APPENDIX G. EXPERIMENTAL RESULTS
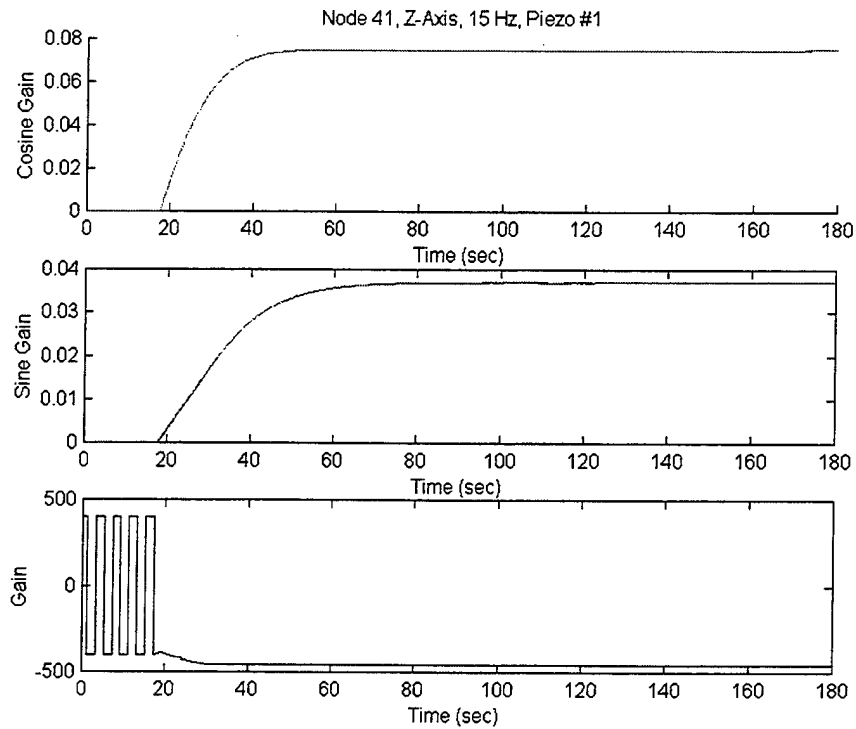
Figure 60. Exp.2, Controller Gain Response
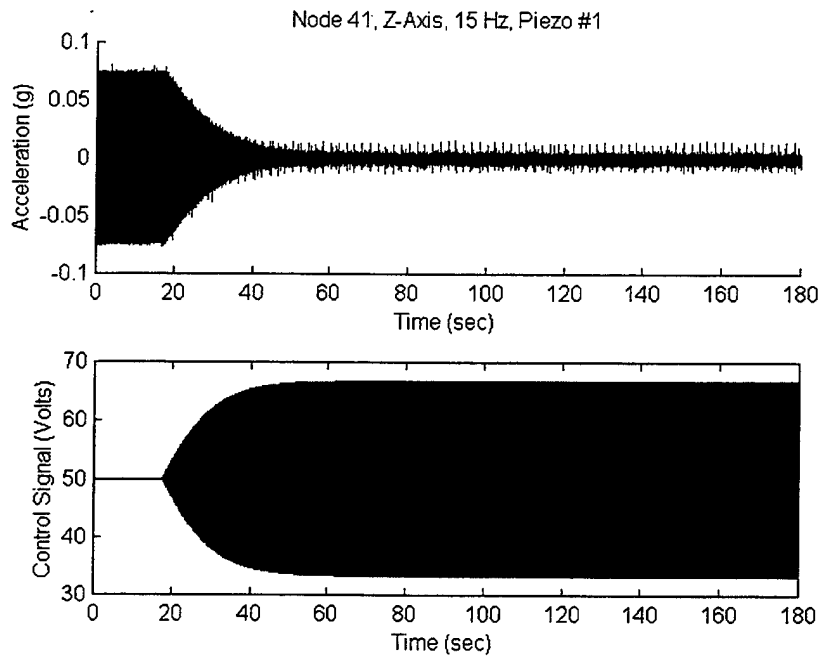
Figure 61. Exp. 2, System Response

145
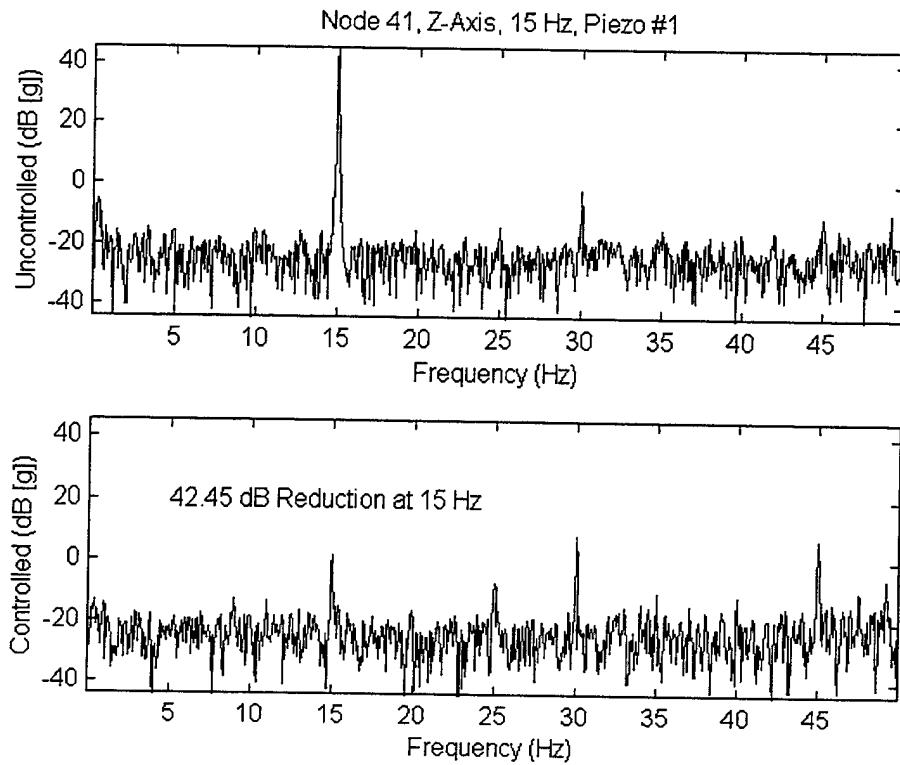
Figure 62. Exp. 2, Power Spectrum
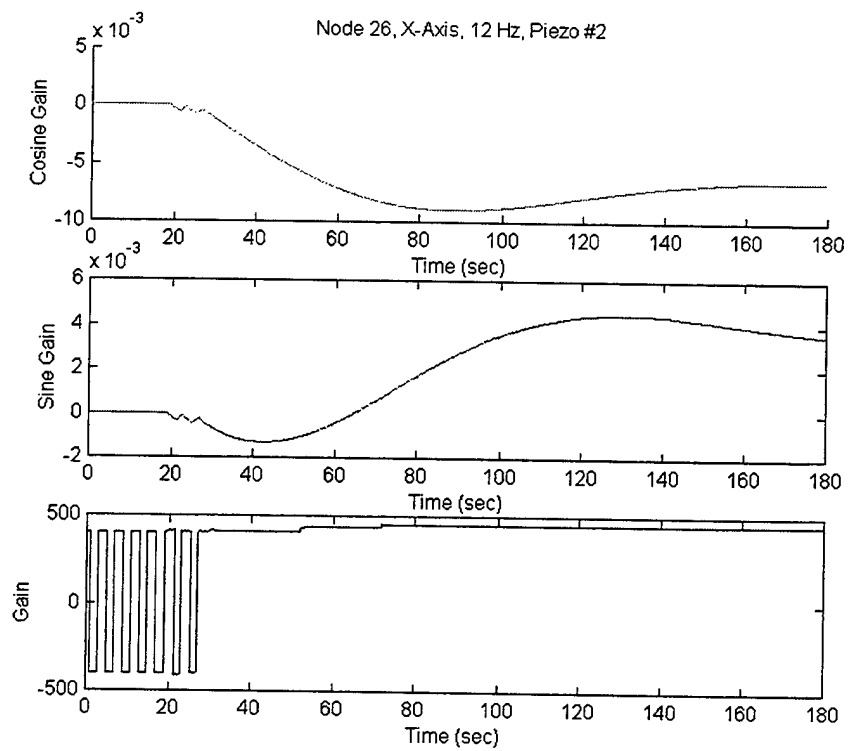
Figure 63. Exp. 3, Controller Gain Response

146
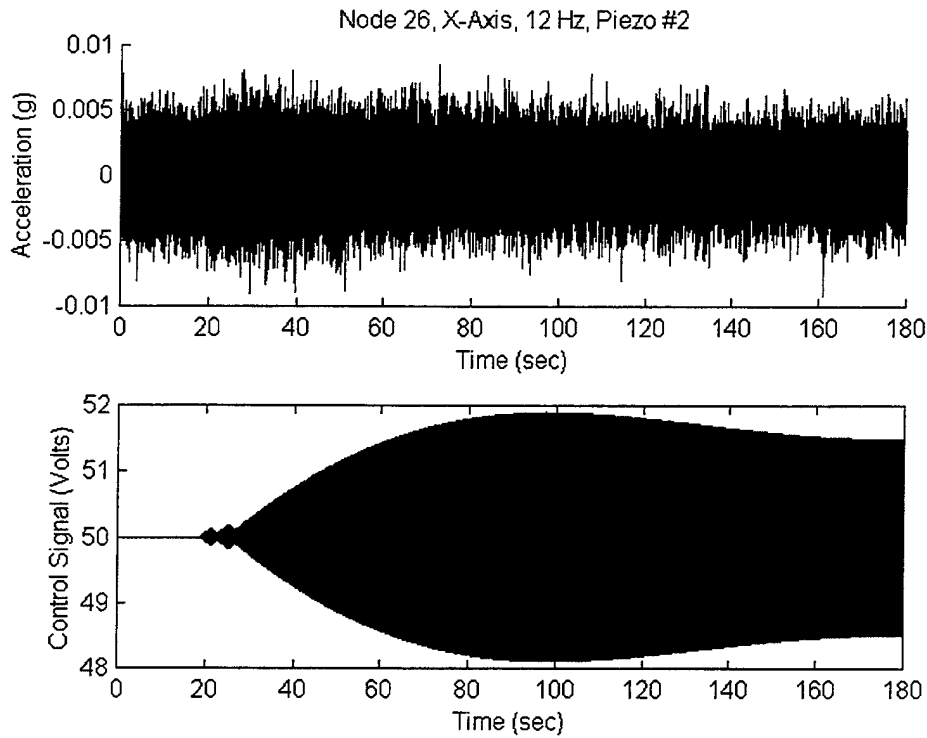
Figure 64. Exp. 3, System Response
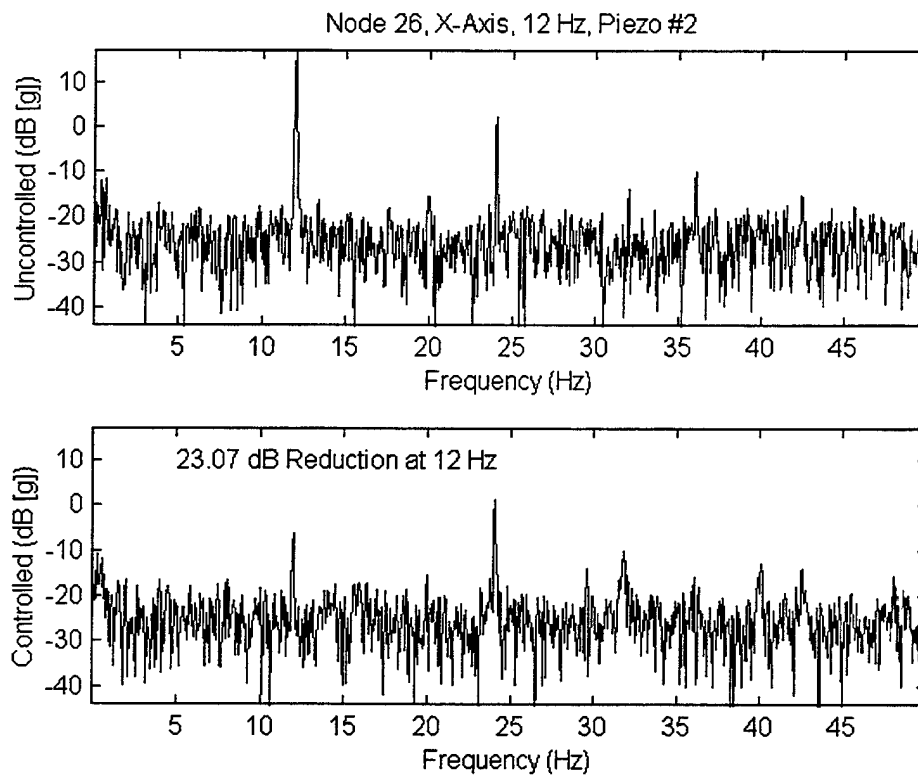
Figure 65. Exp. 3, Power Spectrum

147
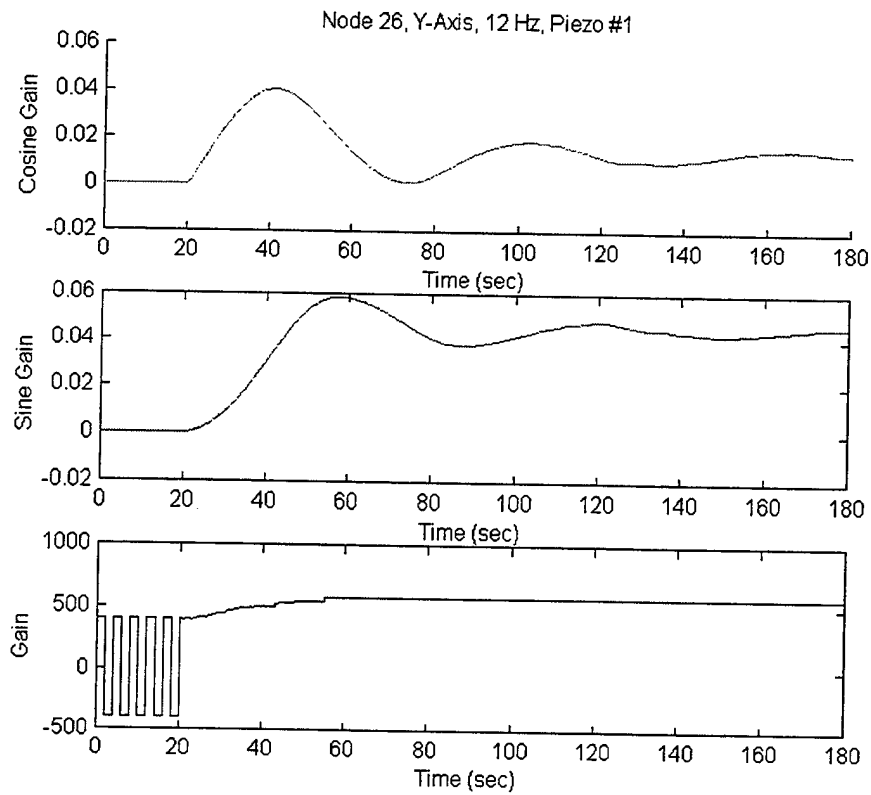
Figure 66. Exp. 4, Controller Gain Response
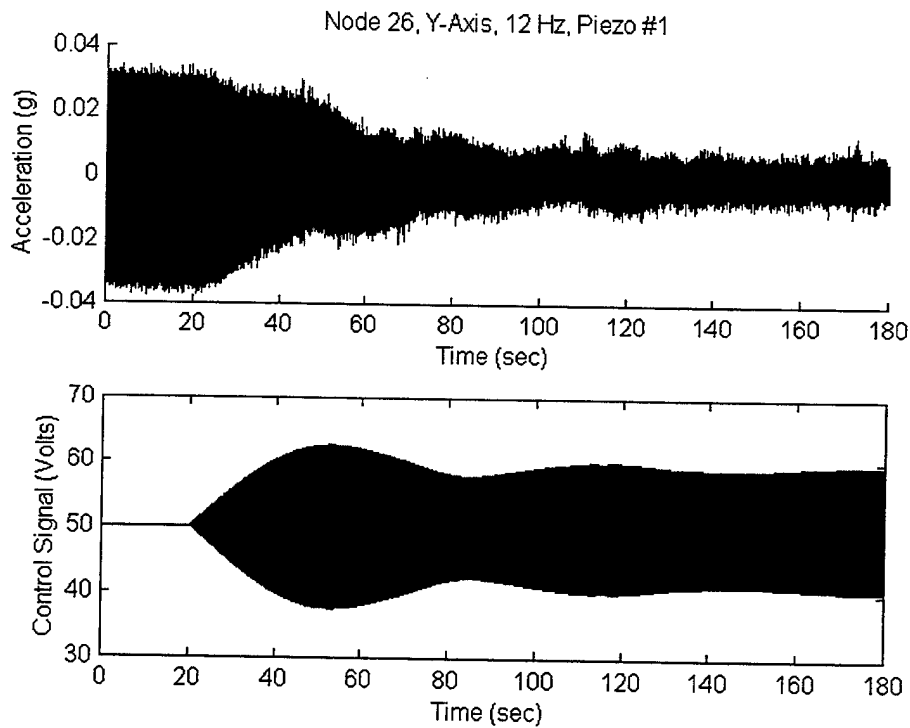
Figure 67. Exp. 4, System Response

148
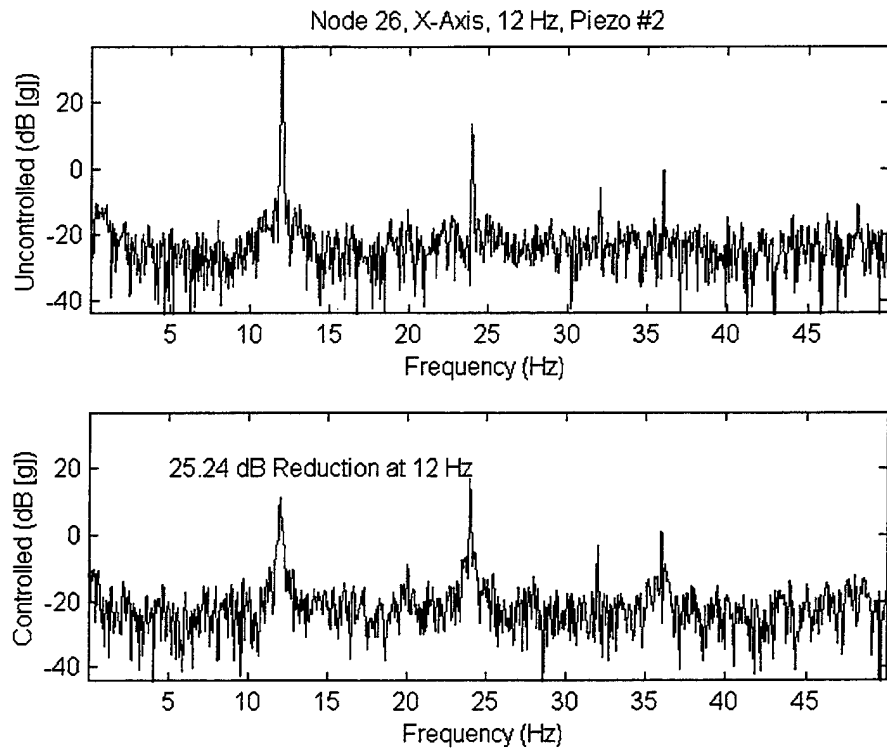
Figure 68. Exp. 4, Power Spectrum
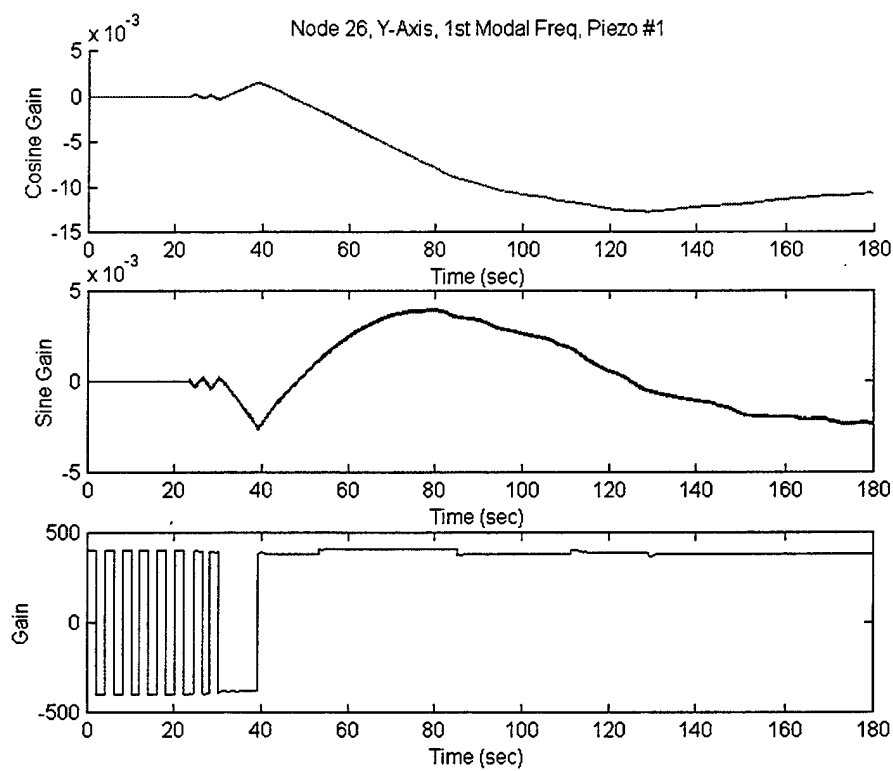
Figure 69. Exp. 5, Controller Gain Response

149
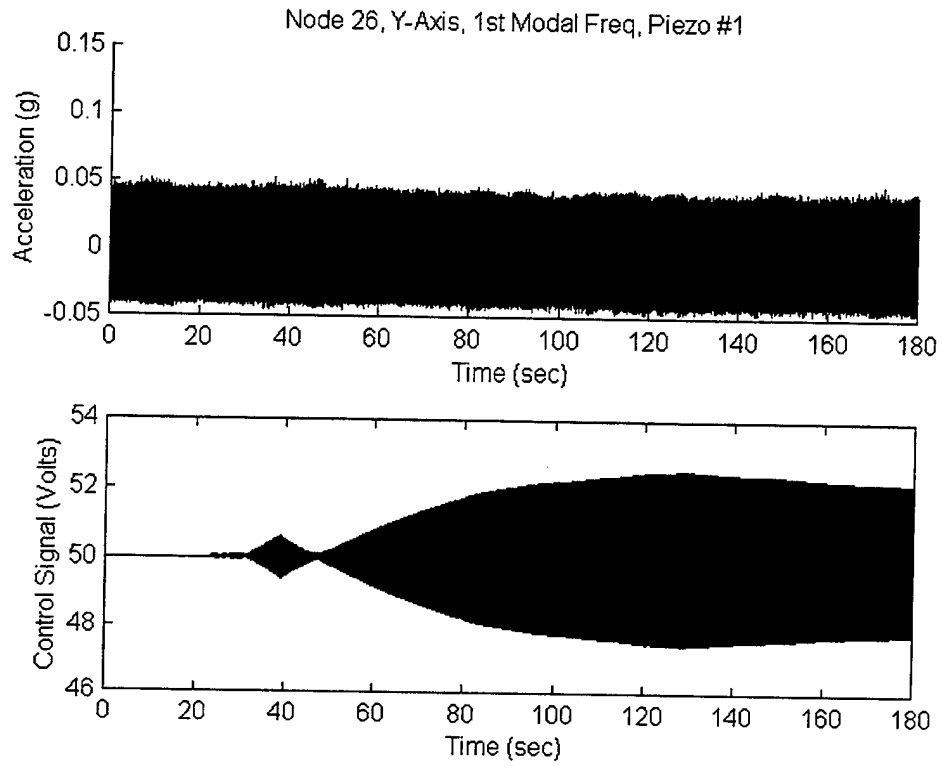
Figure 70. Exp. 5, System Response
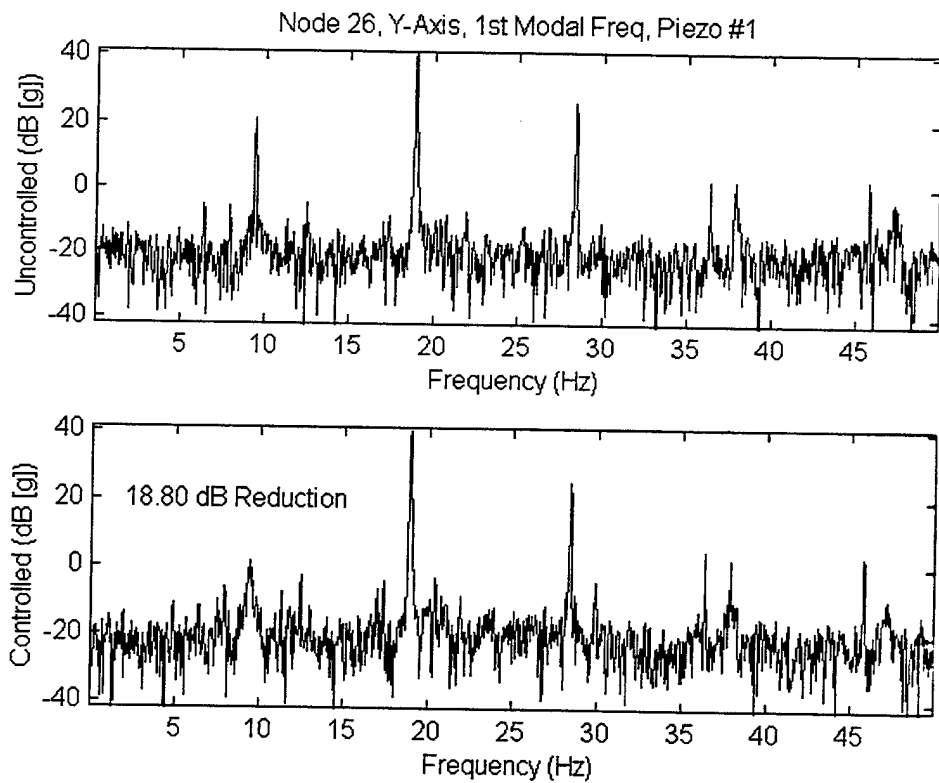
Figure 71. Exp. 5, Power Spectrum

150
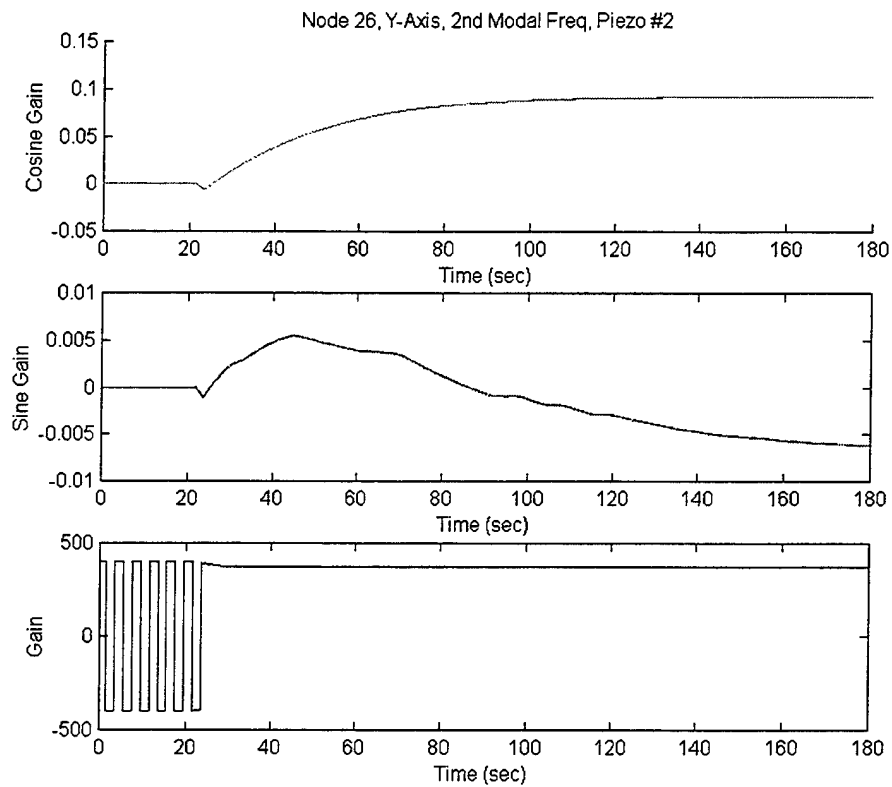
Figure 72. Exp. 6, Controller Gain Response
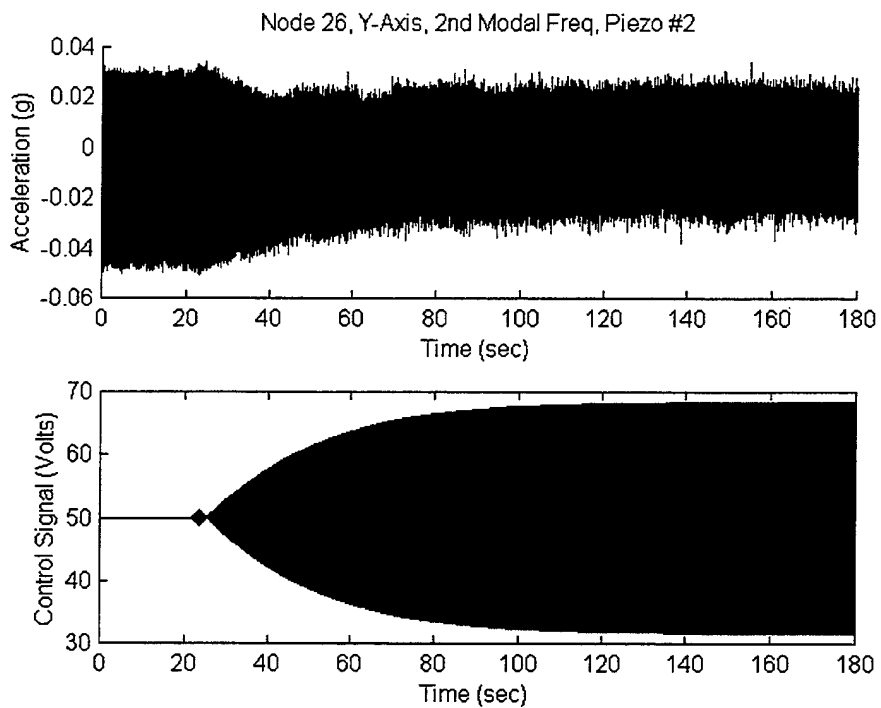
Figure 73. Exp. 6, System Response

151
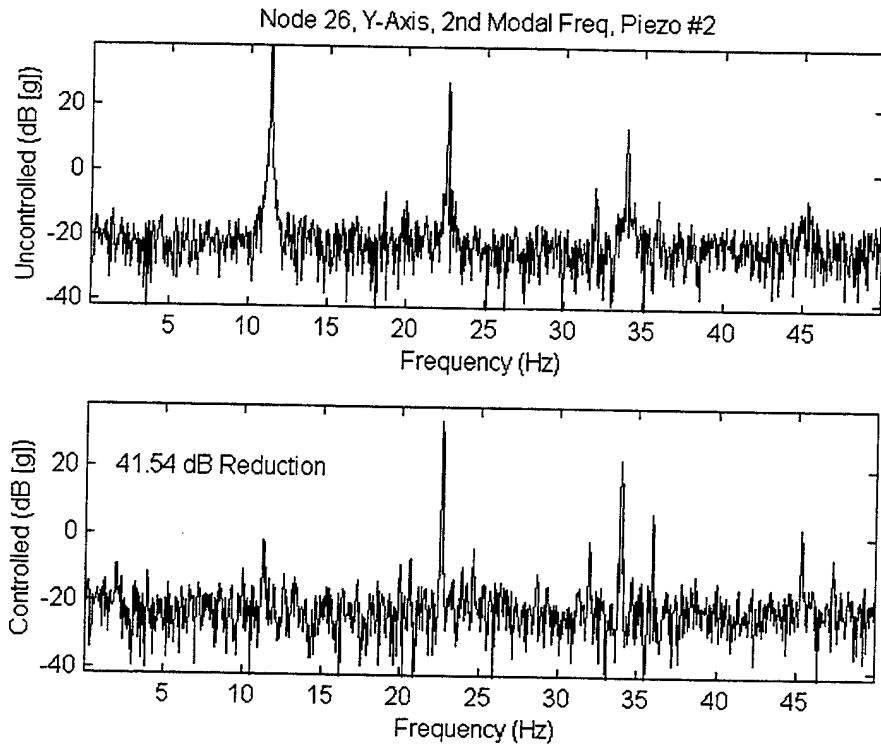
Figure 74. Exp. 6, Power Spectrum
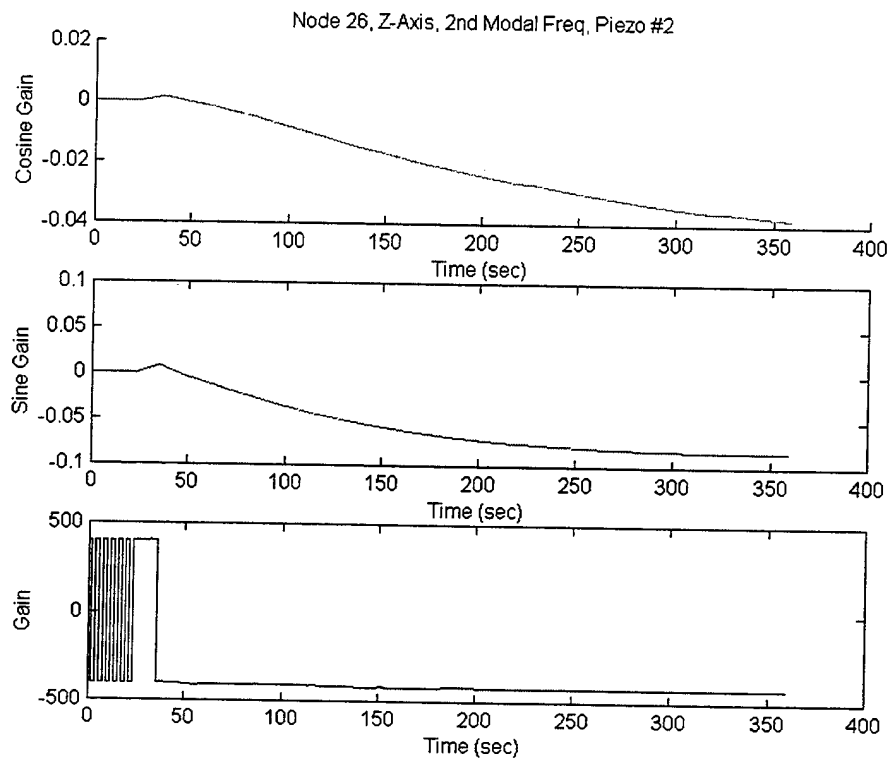
Figure 75. Exp. 7, Controller Gain Response
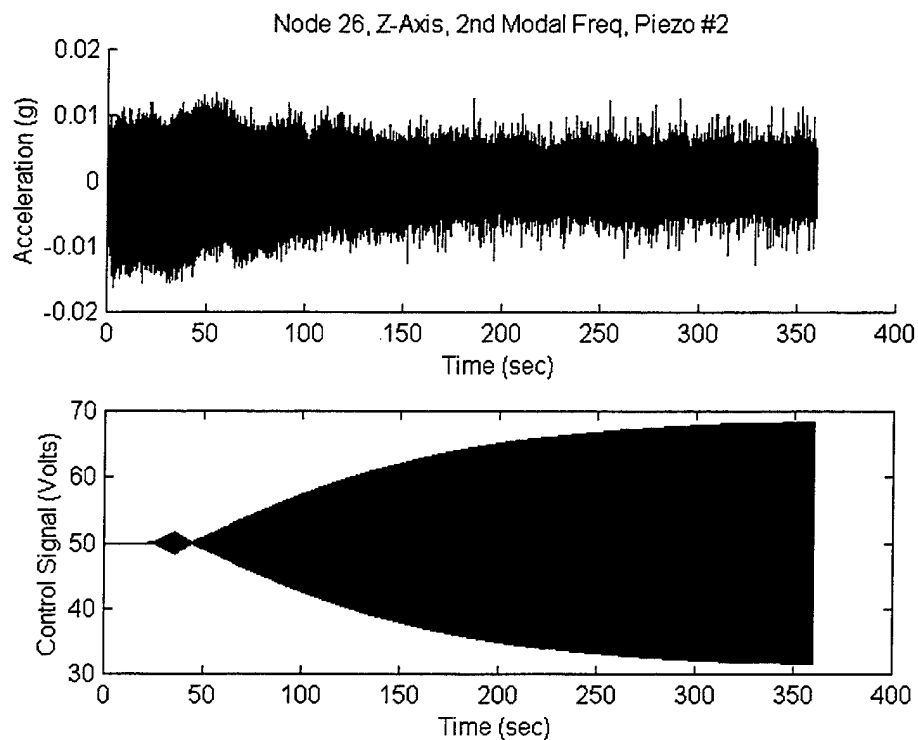
Figure 76. Exp. 7, System Response
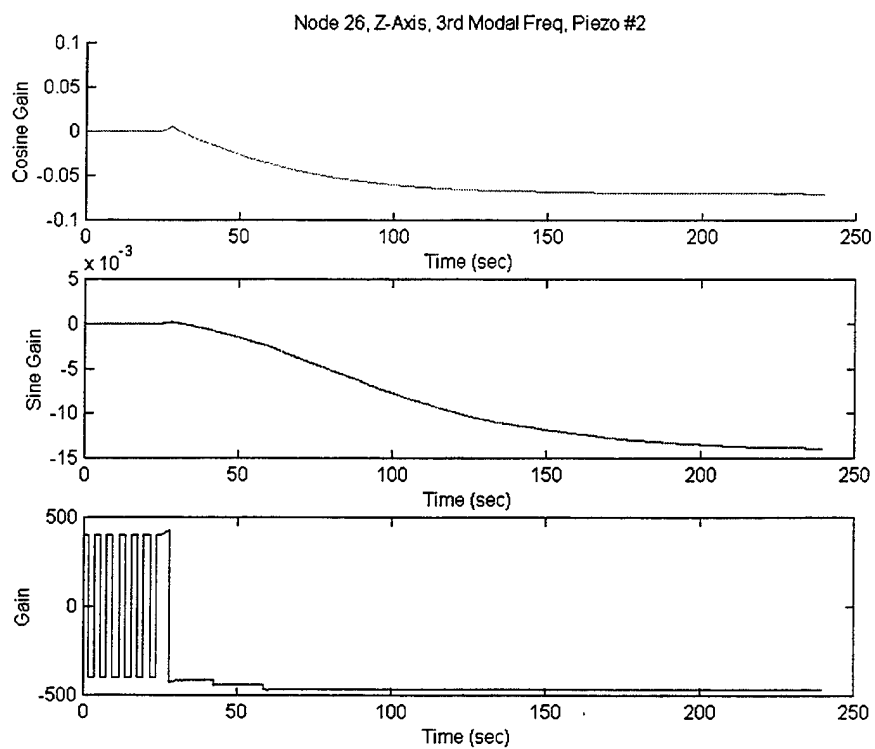
Figure 77. Exp. 8, Controller Gain Response

153
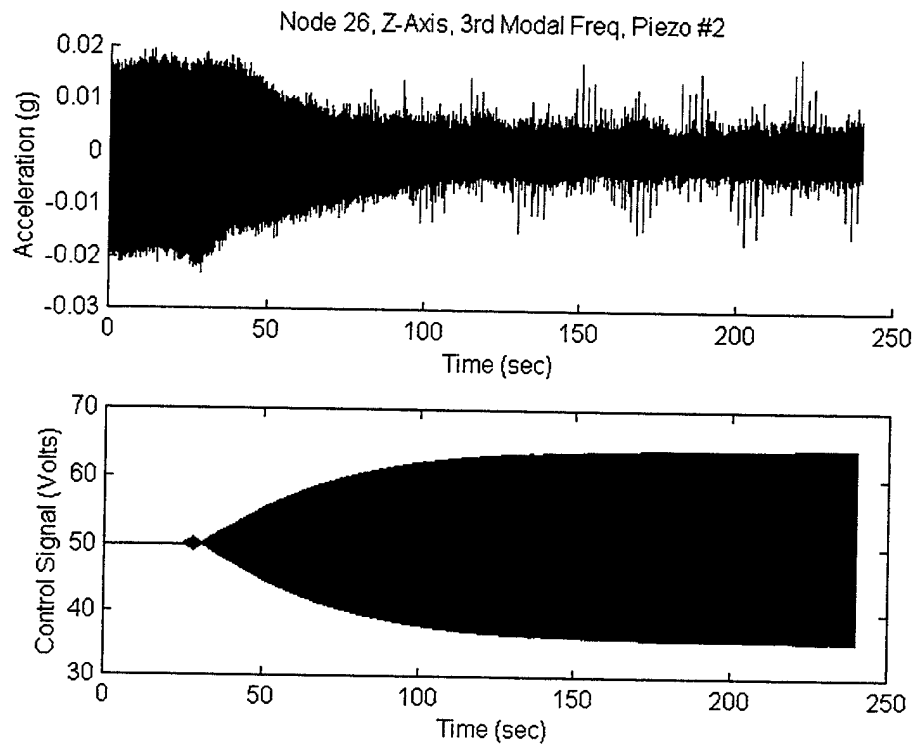
Figure 78. Exp. 8, System Response
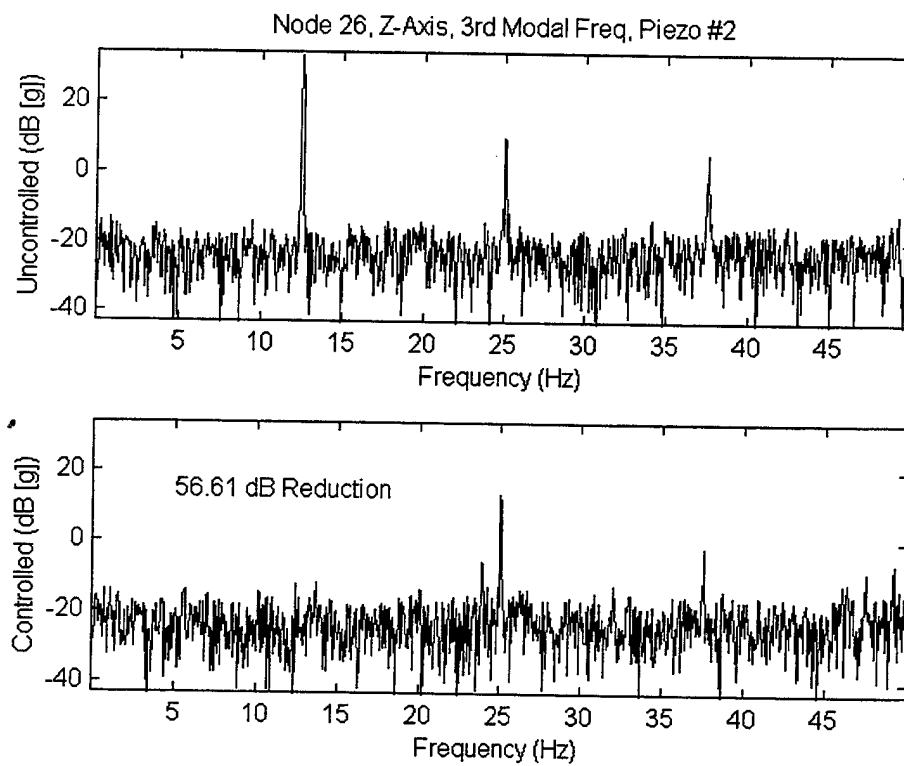
Figure 79. Exp. 6, Power Spectrum

154
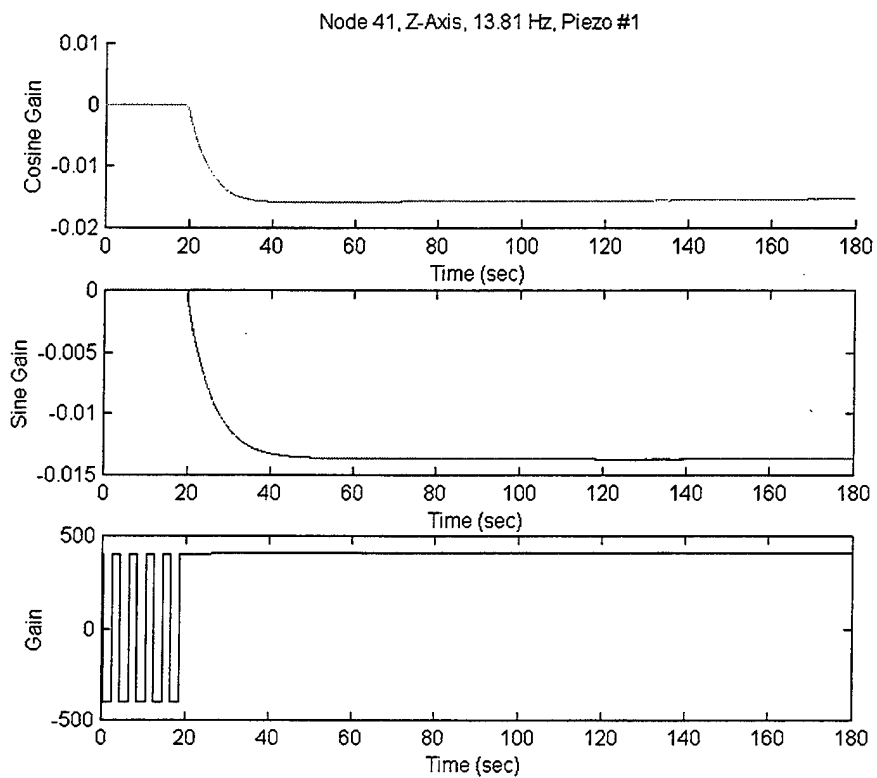
Figure 80. Exp. 9, Controller Gain Response
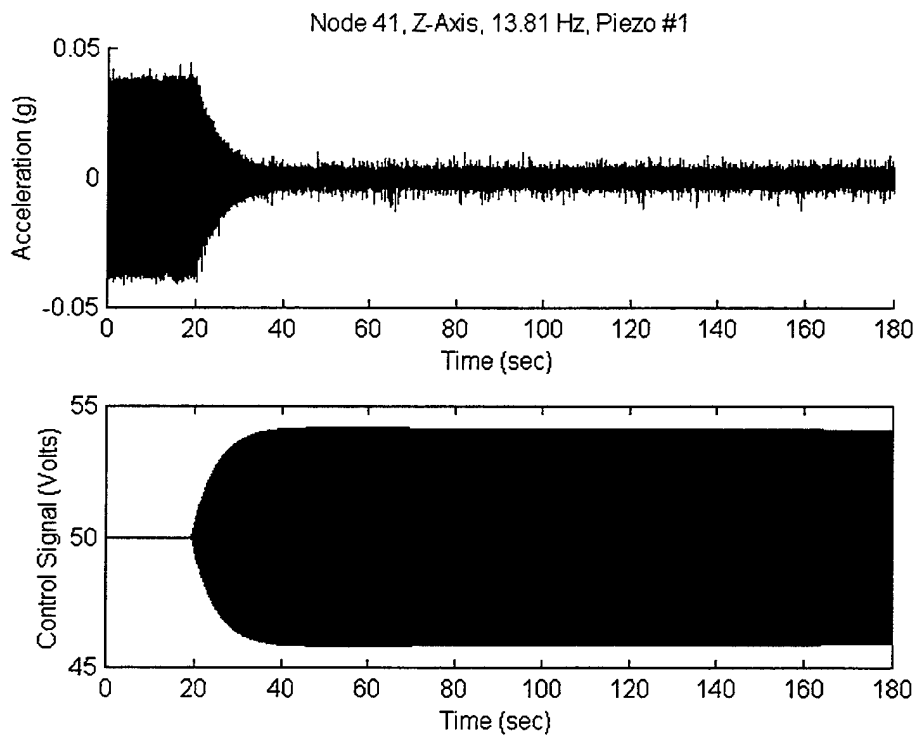
Figure 81. Exp. 9, System Response

155

THIS PAGE INTENTIONALLY LEFT BLANK

APPENDIX H. PROCESS1.M

```
%-----------------------------------------------------------------------%
% Plots the ControlDesk capture files from dSPACE Experimental runs    %
%        using the NPS Space Truss.                                     %
% Written by LT Timothy A. Barney                                       %
%                                                                       %
% Variable descriptions                                                 %
%    zCosine = Weighting value of the Cosine LMS                        %
%    zSine = Weighting value of the Sine LMS                            %
%    zGain = Adaptive Gain value                                        %
%    zCSoutput = Controler Output Signal to Piezo                       %
%    zNacel = Nodal Acceleration Being Controlled                       %
%-----------------------------------------------------------------------%


% DEMO #1
% Controlling the Y-axis of Node 18, with a 19 Hz disturbance, using
Piezo #2

clear all;
close all;

load demo1.mat
freq=19;                % Simulation Disturbance Frequency (Hz)
stop=180;               % Simulation Stop Time (sec)
dt=1/500;               % Downsampled from 1 kHz durring capture
sdt=1/freq/20;          % Time Step Used in Simualtion
stime=[sdt:sdt:stop];%  Simulation Time Vector
time=trace_x;           % Experimental Time Vector

zCosine=trace_y(4,:);    % Weighting value of the Cosine LMS
zSine=trace_y(5,:);      % Weighting value of the Sine LMS
zCSoutput=trace_y(1,:);  % Controler Output Signal to Piezo
zNacel=trace_y(2,:);     % Nodal Acceleration Being Controlled
zGain=trace_y(3,:);      % Loads Displacement at the Control Node

zNacel=zNacel./0.05;     % Converts Acceleration Signal into g's
zCSoutput=zCSoutput.*200;% Controler Output Signal to Piezo

%%%%%%%%%%%%%%%%%%%%%%%%%%%%%%%%%%%%%%%%%%%%%%%
% Plots the control siganl and the response. %
%%%%%%%%%%%%%%%%%%%%%%%%%%%%%%%%%%%%%%%%%%%%%%%

figure(1);
subplot(2,1,1)
hold on
plot(time,zNacel,'r')
title('Node 18, Y-Axis, 19 Hz, Piezo #2')
ylabel('Acceleration (g)')
xlabel('Time (sec)')
subplot(2,1,2)
plot(time,zCSoutput,'b')
xlabel('Time (sec)')
```

```
ylabel('Control Signal (Volts)')
hold off


%%%%%%%%%%%%%%%%%%%%%%%%%%%%%%%%%%%%%%%%%%%%
% Shows the convergence of the LMS weights. %
%%%%%%%%%%%%%%%%%%%%%%%%%%%%%%%%%%%%%%%%%%%%

figure(2);
subplot(3,1,1)
hold on
plot(time,zCosine,'g')
title('Node 18, Y-Axis, 19 Hz, Piezo #2')
ylabel('Cosine Gain')
xlabel('Time (sec)')
subplot(3,1,2)
plot(time,zSine,'m')
xlabel('Time (sec)')
ylabel('Sine Gain')
subplot(3,1,3)
plot(time,zGain,'b')
xlabel('Time (sec)')
ylabel('Gain')
hold off


%%%%%%%%%%%%%%%%%%%%%%%%%%%%%%%%%%%%%%%%%%%%%%%%%%%%%%%%%
% Determines Frequency Response Before and After Control %
%%%%%%%%%%%%%%%%%%%%%%%%%%%%%%%%%%%%%%%%%%%%%%%%%%%%%%%%%

t1=5*dt;
t2=16.8;
t3=(stop-t2)+6*dt;
r1=floor(t1/dt):floor(t2/dt);
r2=floor(t3/dt):length(zNacel);
v1=zNacel(r1);
v2=zNacel(r2);
f1=linspace(0,1/dt,length(r1));
f2=linspace(0,1/dt,length(r2));
before=fft(v1'.*hanning(length(v1)));
after=fft(v2'.*hanning(length(v2)));
av1=20*log10(abs(before));
av2=20*log10(abs(after));
rr1=find(f1<=50&f1>0);
rr2=find(f2<=50&f2>0);
strt=f1(rr1(1));
fnsh=f1(rr1(length(rr1)));
big=ceil(max(max(av1),max(av2)));
ltl=floor(mean(av1)-3*std(av1));


%%%%%%%%%%%%%%%%%%%%%%%%%%%%%%%%%%%%%%%%%%%%%%%%%%%%%
% Plots Frequency Response Before and After Control %
%%%%%%%%%%%%%%%%%%%%%%%%%%%%%%%%%%%%%%%%%%%%%%%%%%%%%

figure(3)
subplot(2,1,1)
plot(f1(rr1),av1(rr1))
```

```
axis([strt fnsh ltl big])
title('Node 18, Y-Axis, 19 Hz, Piezo #2')
ylabel('Uncontrolled (dB [g])')
xlabel('Frequency (Hz)')
subplot(2,1,2)
plot(f2(rr2),av2(rr2))
axis([strt fnsh ltl big])
ylabel('Controlled (dB [g])')
xlabel('Frequency (Hz)')
text(5,20,'47.38 dB Reduction at 19 Hz')

range=find(f1<=freq+1 & f1>=freq-1);
peak=av1(range);

figure(4)
plot(f1(range),av1(range),'r:',f2(range),av2(range),'k-')
axis([f1(range(1)) f1(range(length(range))) ltl big])
title('Node 18, Y-Axis, 19 Hz, Piezo #2')
ylabel('Power Spectrum (dB [g])')
xlabel('Frequency (Hz)')
text(18.2,30,'47.38 dB Reduction at 19 Hz')

%%%%%%%%%%%%%%%%%%%%%%%%%%%%%%%%%%%%%%%%%%%%%%%%%%%%%%%%%%%%%%%%
% Calculate the dB reduction at the peak undamped frequency %
%%%%%%%%%%%%%%%%%%%%%%%%%%%%%%%%%%%%%%%%%%%%%%%%%%%%%%%%%%%%%%%%

[m,i]=max(peak);
reduction=m-av2(range(i))
```

THIS PAGE INTENTIONALLY LEFT BLANK

APPENDIX I. RESULT COMPARISON
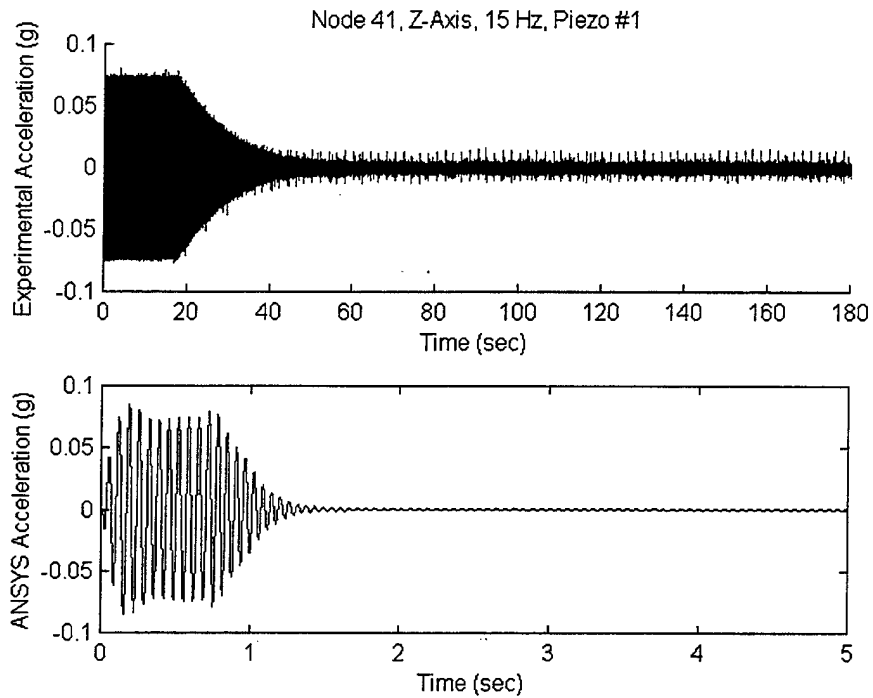
Figure 82. Case 2, Control Node Acceleration Comparison
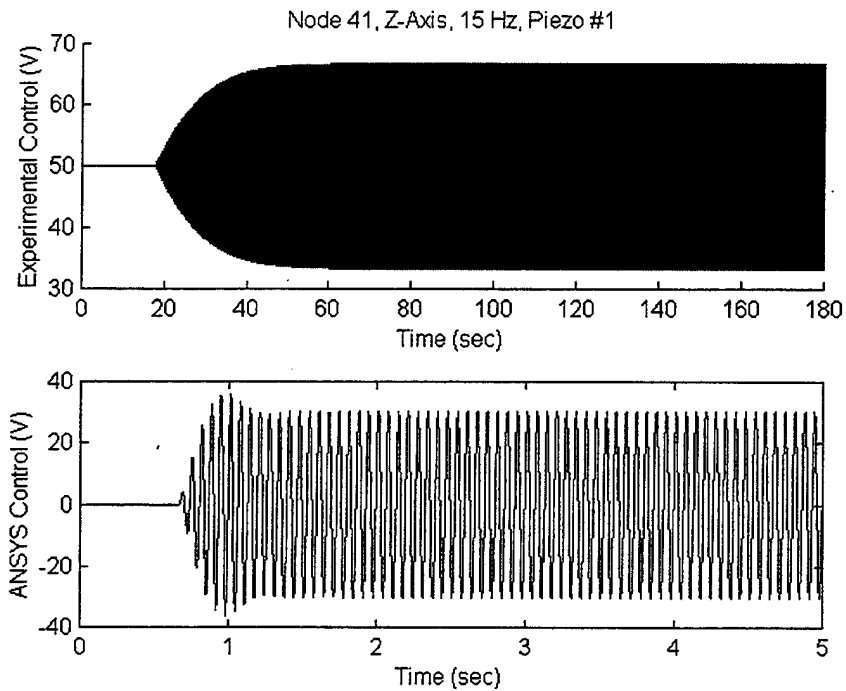
Figure 83. Case 2, Control Signal Comparison

161
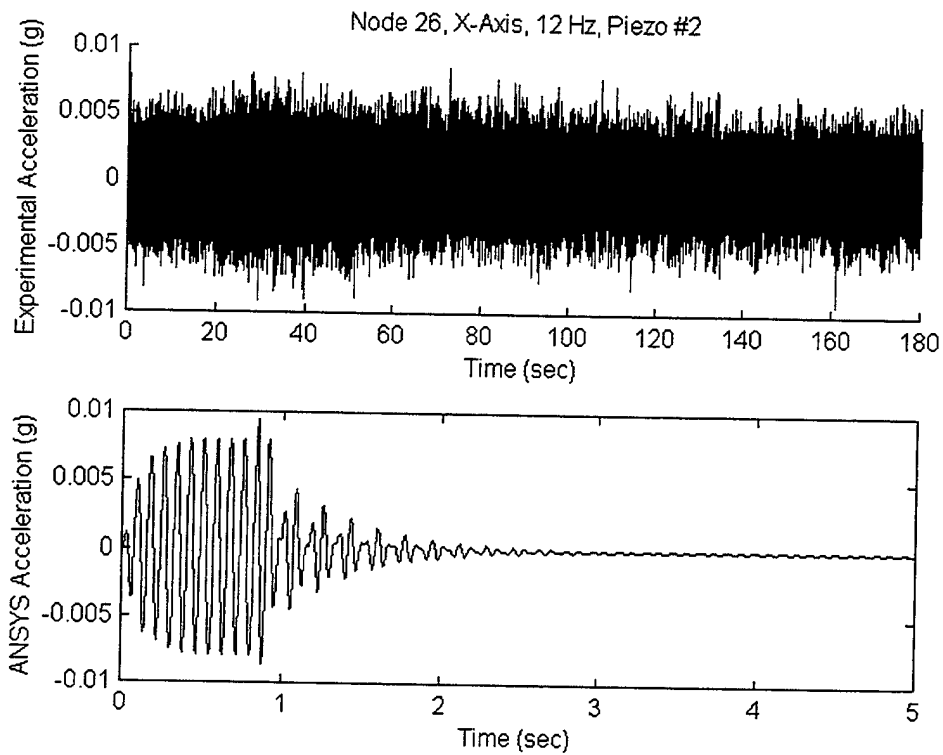
Figure 84. Case 3, Control Node Acceleration Comparison
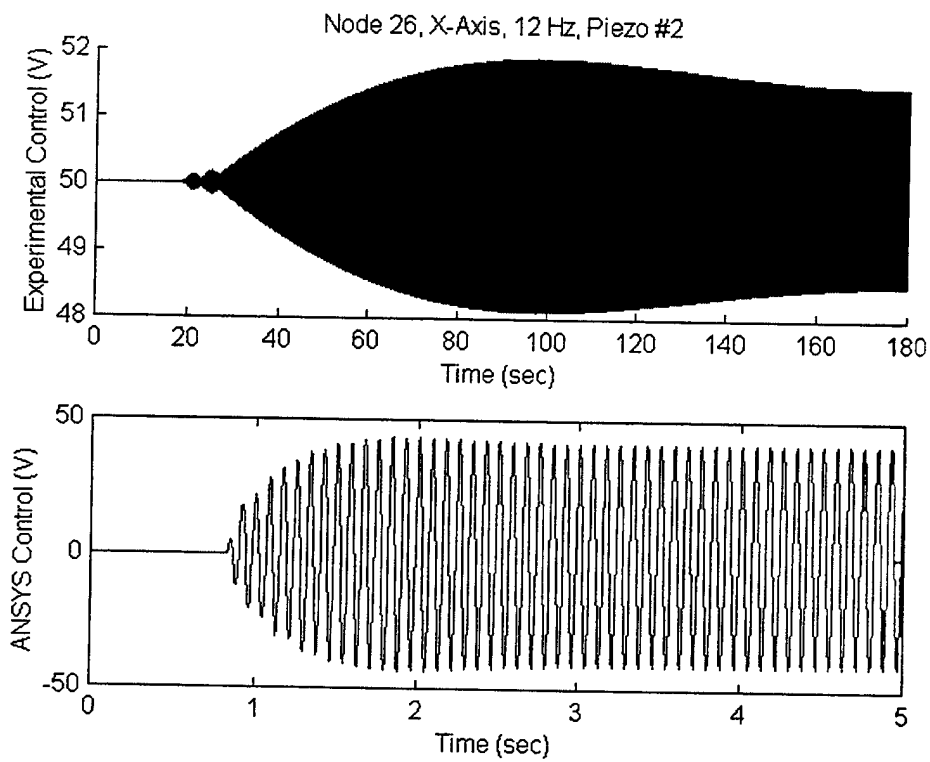
Figure 85. Case 3, Control Signal Comparison
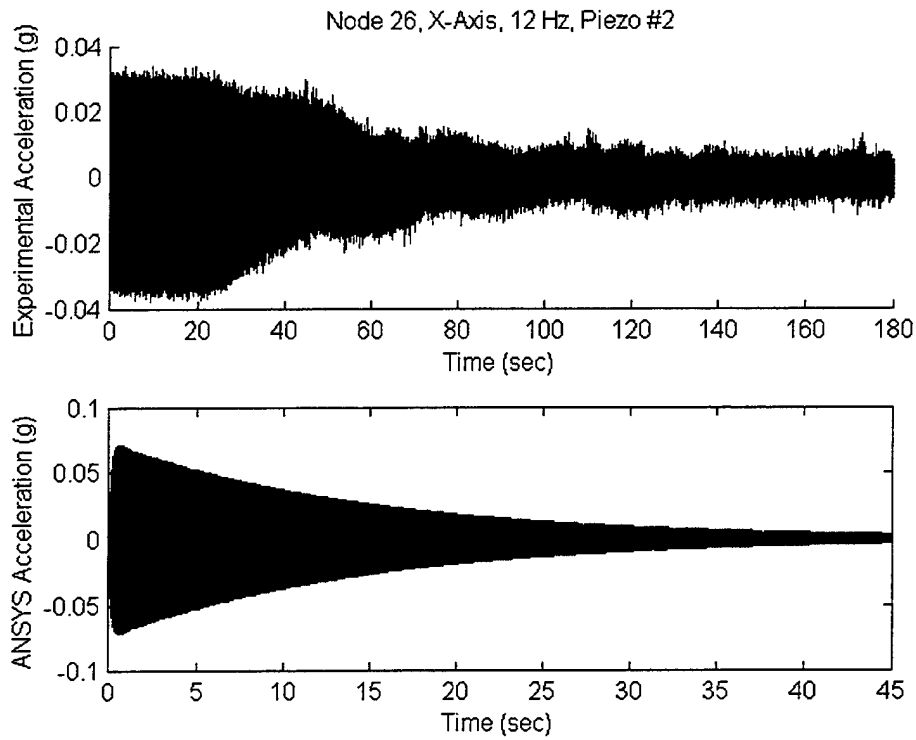
Figure 86. Case 4, Control Node Acceleration Comparison
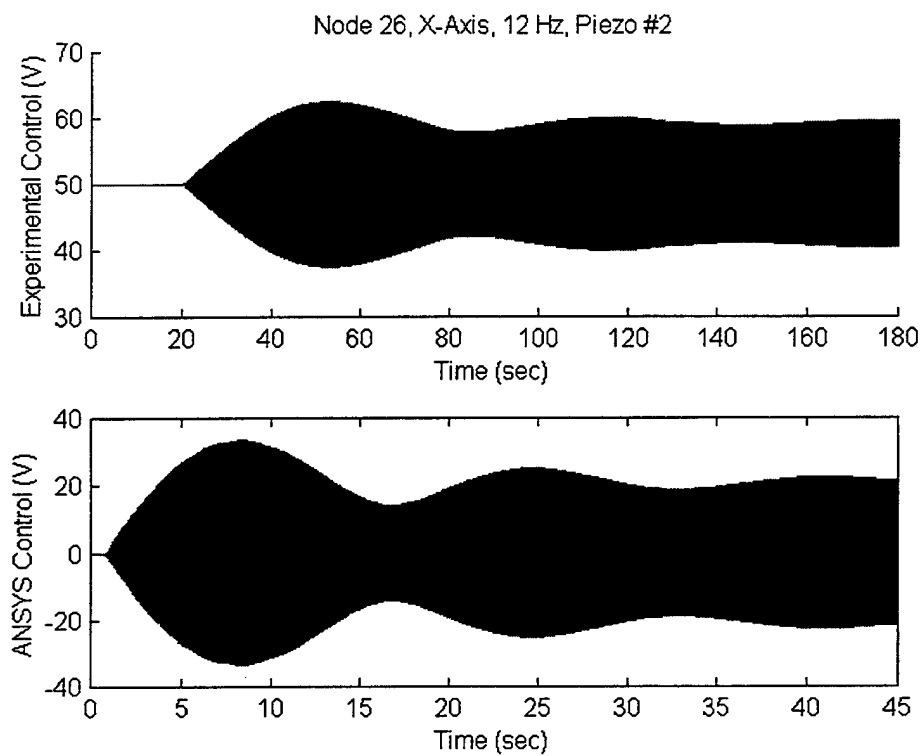
Figure 87. Case 4, Control Signal Comparison

163
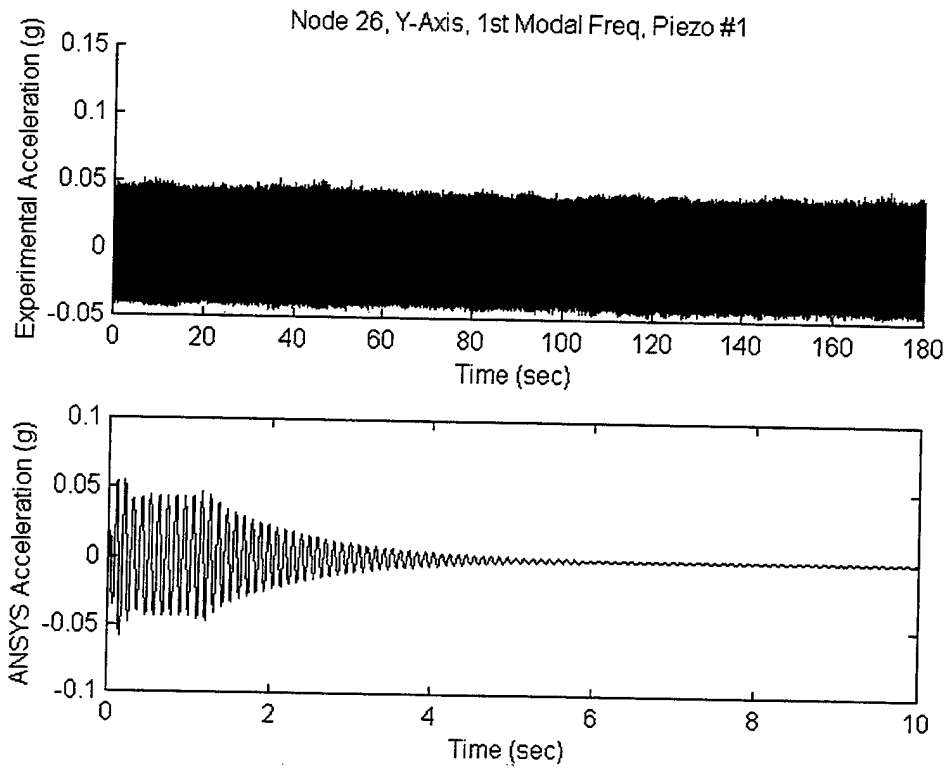
Figure 88. Case 5, Control Node Acceleration Comparison
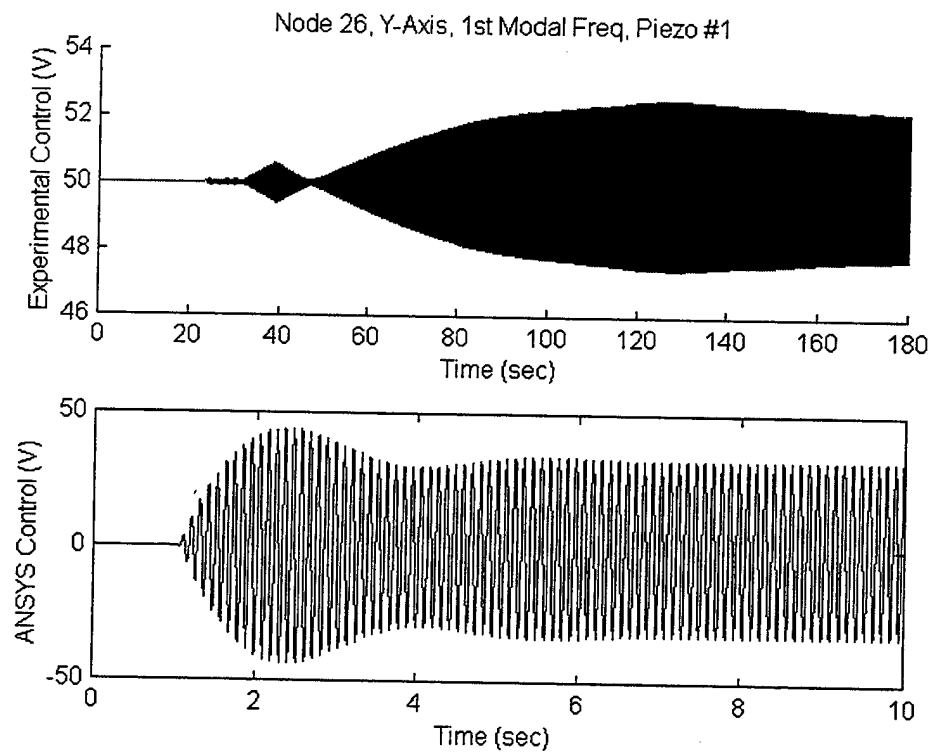
Figure 89. Case 5, Control Signal Comparison
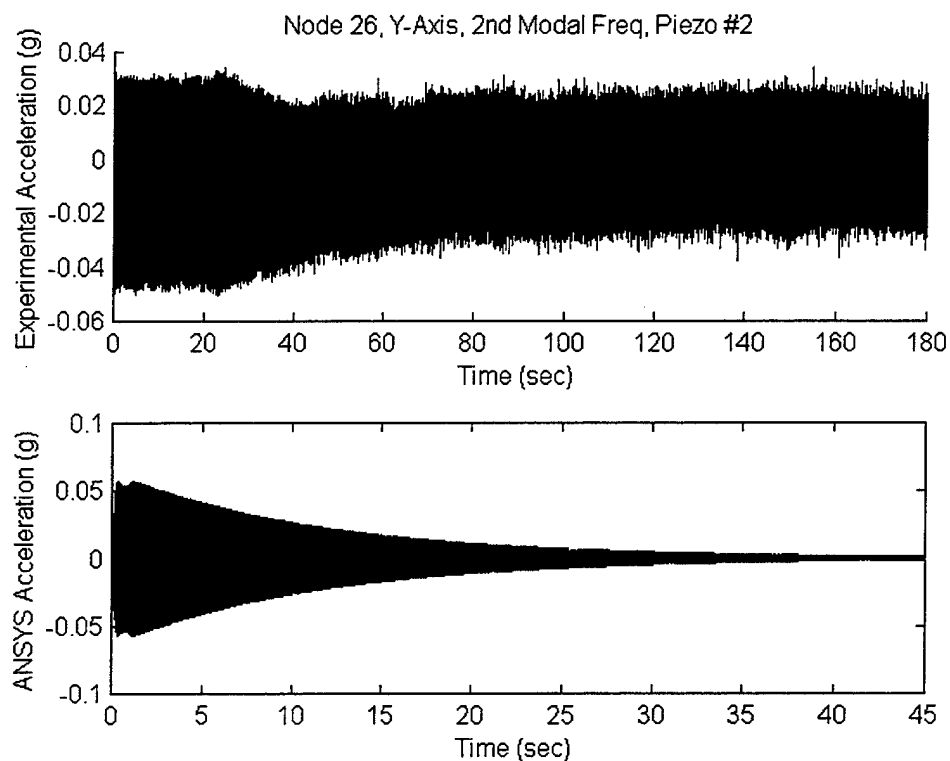
Figure 90. Case 6, Control Node Acceleration Comparison
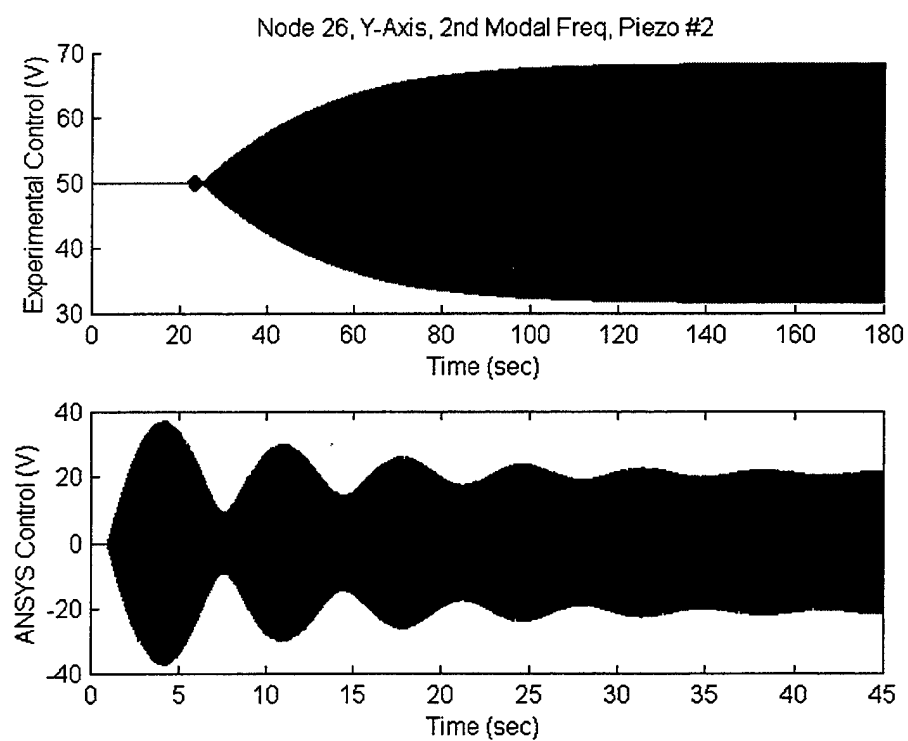
Figure 91. Case 6, Control Signal Comparison
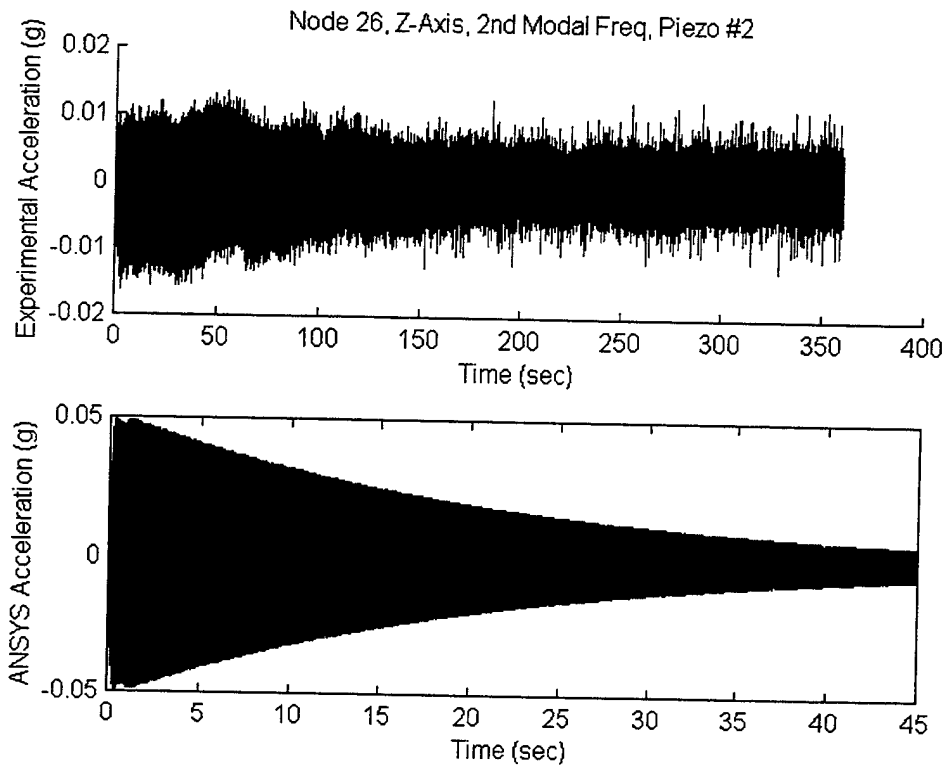
Figure 92. Case 7, Control Node Acceleration Comparison
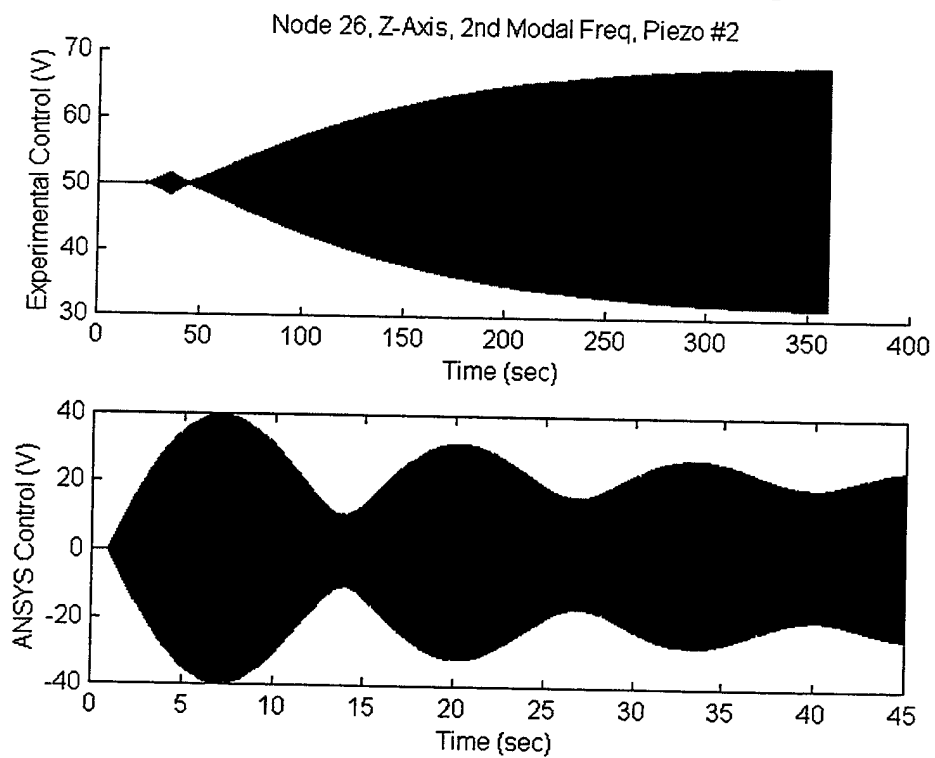
Figure 93. Case 7, Control Signal Comparison
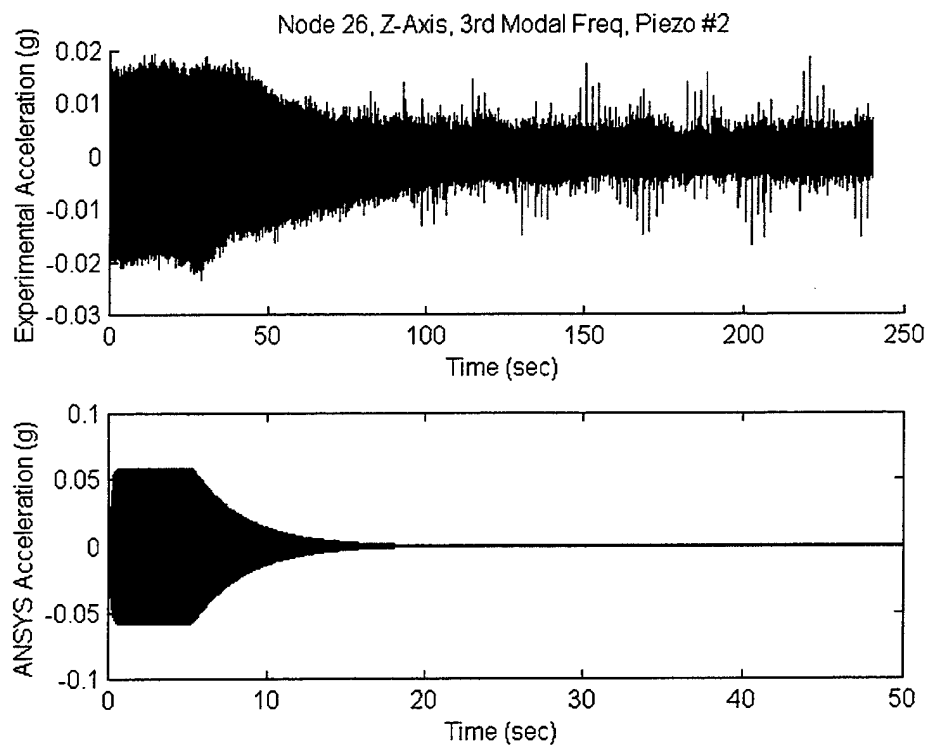
Figure 94. Case 8, Control Node Acceleration Comparison
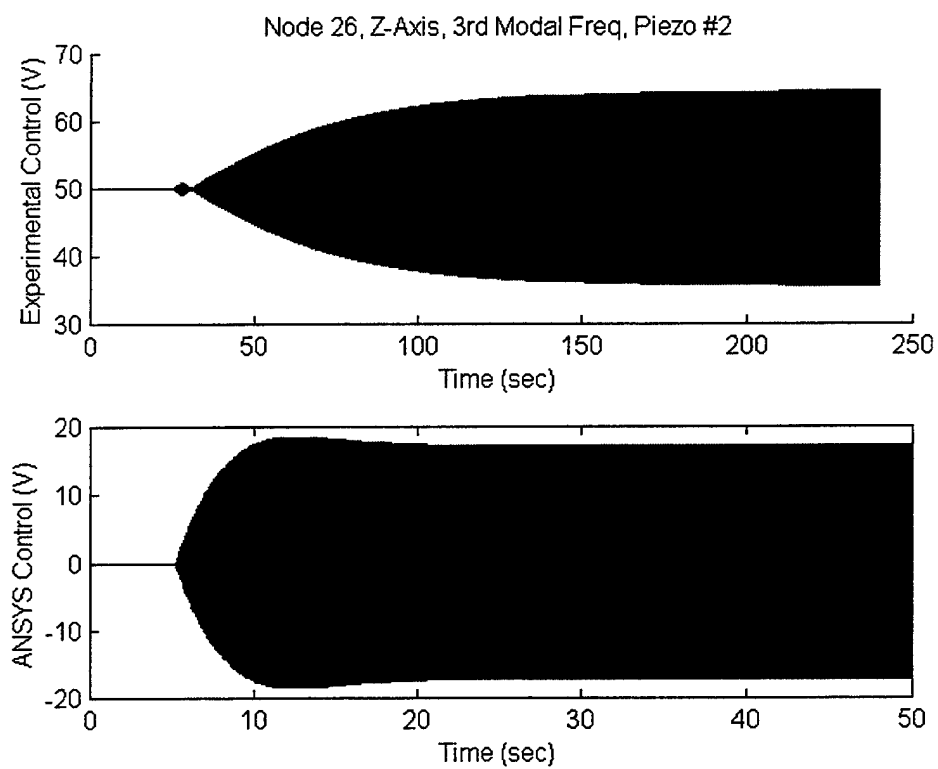
Figure 95. Case 8, Control Signal Comparison

167
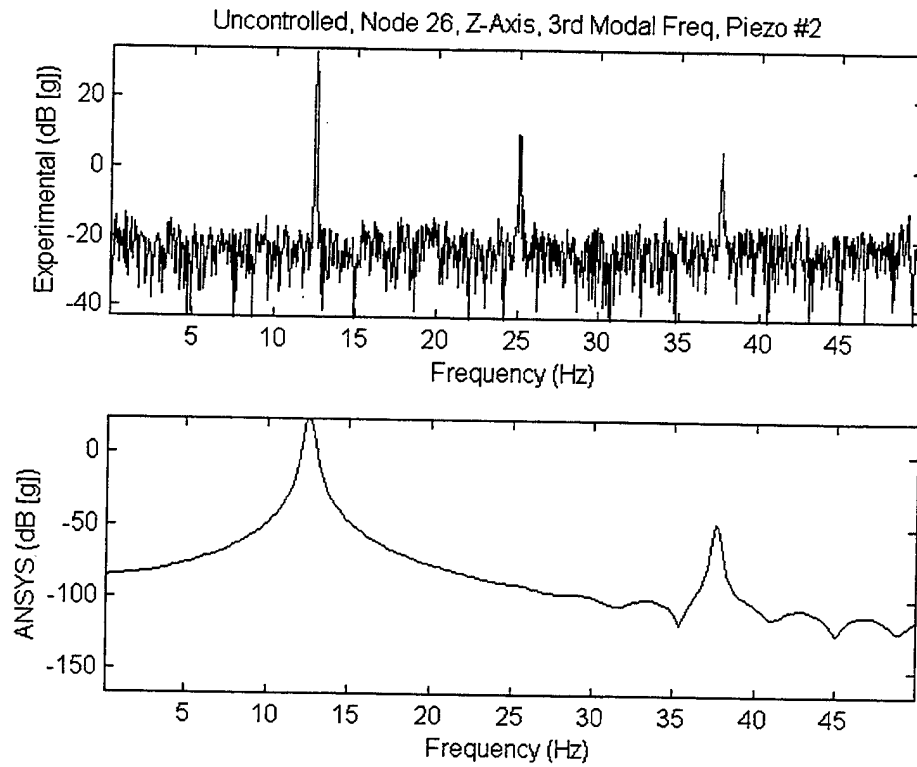
Figure 96. Case 8, No Control Power Spectrum Comparison
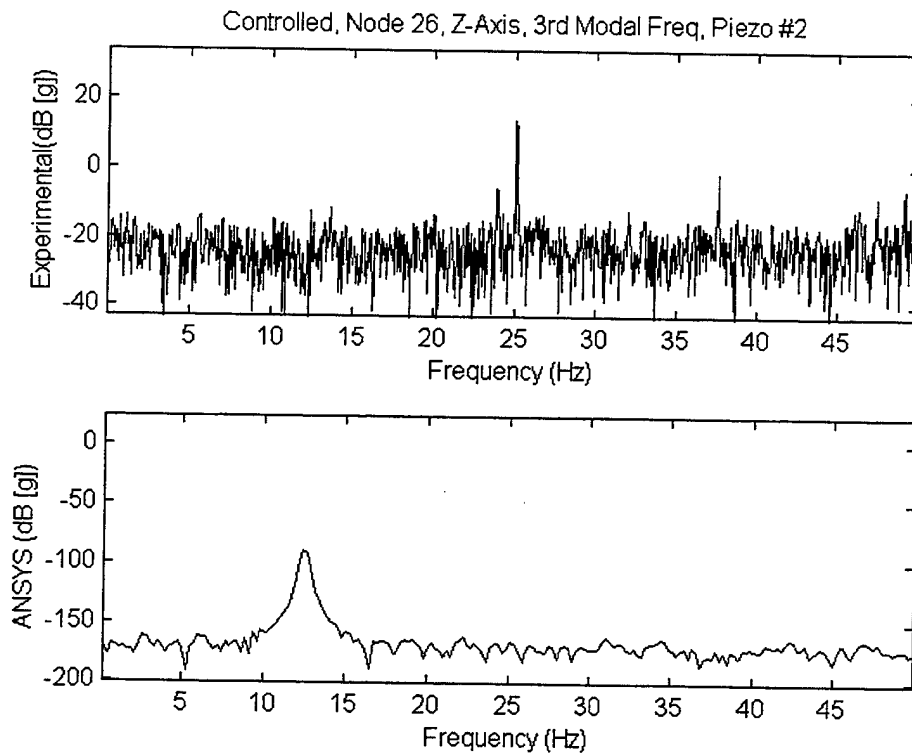
Figure 97. Case 8, Controlled Power Spectrum Comparison

APPENDIX J. OUTPUT.M

```
%-----------------------------------------------------------------%
% Plots the ANSYS output files generated by simulation runs        %
%        using a model of the NPS Space Truss.                     %
% Written by LT Timothy A. Barney                                  %
%                                                                  %
% Variable descriptions                                            %
%    zCosine = Weighting value of the Cosine LMS                   %
%    zSine = Weighting value of the Sine LMS                       %
%    zCSoutput = Controler Output Signal to Piezo                  %
%    zNacel = Nodal Acceleration Being Controlled                  %
%    zNdisp = Displacement at the Control Node                     %
%    zNvelo = Velocity at the Control Node                         %
%-----------------------------------------------------------------%


% DEMO #1
% Controlling the Y-axis of Node 18, with a 19 Hz disturbance, using
Piezo #2

clear all;
close all;

freq=19;               % Simulation Disturbance Frequency (Hz)
stop=5;                % Simulation Stop Time (sec)
dt=1/freq/20;          % Time Step Used in Simualtion
time=[dt:dt:stop];     % Time Vector

load zCosine.out;      % Loads Weighting value of the Cosine LMS
load zSine.out;        % Loads Weighting value of the Sine LMS
load zCSoutput.out;    % Loads Controler Output Signal to Piezo
load zNacel.out;       % Loads Nodal Acceleration Being Controlled
load zNdisp.out;       % Loads Displacement at the Control Node
load zNvelo.out;       % loads Velocity at the Control Node
zNacel=zNacel./9.8;    % Converts to g's

%%%%%%%%%%%%%%%%%%%%%%%%%%%%%%%%%%%%%%%%%%%%%%%%%%
% Plots the control siganl and the response. %
%%%%%%%%%%%%%%%%%%%%%%%%%%%%%%%%%%%%%%%%%%%%%%%%%%

figure(1);
subplot(2,1,1)
hold on
plot(time,zNacel,'r')
title('Node 18, Y-Axis, 19 Hz, Piezo #2')
ylabel('Acceleration (g)')
xlabel('Time (sec)')
subplot(2,1,2)
plot(time,zCSoutput,'b')
xlabel('Time (sec)')
ylabel('Control Signal (Volts)')
hold off
```

```
%%%%%%%%%%%%%%%%%%%%%%%%%%%%%%%%%%%%%%%%%%%%%%
% Shows the convergence of the LMS weights. %
%%%%%%%%%%%%%%%%%%%%%%%%%%%%%%%%%%%%%%%%%%%%%%

figure(2);
subplot(2,1,1)
hold on
plot(time,zCosine,'g')
title('Node 18, Y-Axis, 19 Hz, Piezo #2')
ylabel('Cosine Gain')
xlabel('Time (sec)')
subplot(2,1,2)
plot(time,zSine,'m')
xlabel('Time (sec)')
ylabel('Sine Gain')
hold off


%%%%%%%%%%%%%%%%%%%%%%%%%%%%%%%%%%%%%%%%%%%%%%%%%%%
% Shows the control node displacement and velocity. %
%%%%%%%%%%%%%%%%%%%%%%%%%%%%%%%%%%%%%%%%%%%%%%%%%%%

figure(3);
subplot(2,1,1)
hold on
plot(time,zNdisp,'k')
title('Node 18, Y-Axis, 19 Hz, Piezo #2')
ylabel('Displacement (m)')
xlabel('Time (sec)')
subplot(2,1,2)
plot(time,zNvelo,'c')
xlabel('Time (sec)')
ylabel('Velocity (m/s)')
hold off
```

170

APPENDIX K. COMPARE.M

```
%------------------------------------------------------------------%
% Plots the experimental and FEM results for comparison.          %
% Written by LT Timothy A. Barney                                 %
%                                                                 %
% Variable descriptions                                           %
%    eCSoutput = Experimental Controler Output Signal to Piezo    %
%    eNacel = Experimental Nodal Acceleration Being Controlled    %
%    zCSoutput = ANSYS Simulation Controler Output Signal to Piezo %
%    aNacel = ANSYS Simulation Nodal Acceleration Being Controlled %
%------------------------------------------------------------------%


% DEMO #1
% Controlling the Y-axis of Node 18, with a 19 Hz disturbance, using
Piezo #2

clear all;
close all;


%%%%%%%%%%%%%%%%%%%%%%%%%%%%%%%%%%%%%%
% Loads the Experimental Data %
%%%%%%%%%%%%%%%%%%%%%%%%%%%%%%%%%%%%%%

eval(['cd Experimental'])
load demo1.mat

freq=19;                % Disturbance Frequency (Hz)
stop=180;               % Experiment Stop Time (sec)
dt=1/500;               % Downsampled from 1 kHz during capture
time=trace_x;           % Experimental Time Vector

eCSoutput=trace_y(1,:);  % Controller Output Signal to Piezo
eNacel=trace_y(2,:);     % Nodal Acceleration Being Controlled

eNacel=eNacel./0.05;     % Converts Acceleration Signal into g's
eCSoutput=eCSoutput.*200;% Converts control signal to Voltage


%%%%%%%%%%%%%%%%%%%%%%%%%%%%%%%%
% Loads the ANSYS Data %
%%%%%%%%%%%%%%%%%%%%%%%%%%%%%%%%

eval(['cd ..'])
eval(['cd ANSYS'])
load zCSoutput.out;     % Loads Controller Output Signal to Piezo
load zNacel.out;        % Loads Nodal Acceleration Being Controlled

sstop=5;                % Simulation Stop Time (sec)
sdt=1/freq/20;          % Time Step Used in Simulation
stime=[sdt:sdt:sstop];% Simulation Time Vector

aNacel=zNacel./9.8;     % Converts to g's
```

171

```
%%%%%%%%%%%%%%%%%%%%%%%%%%%%
% Plots the Accelerations %
%%%%%%%%%%%%%%%%%%%%%%%%%%%%

figure(1);
subplot(2,1,1)
hold on
plot(time,eNacel,'r')
title('Node 18, Y-Axis, 19 Hz, Piezo #2')
ylabel('Experimental Acceleration (g)')
xlabel('Time (sec)')
subplot(2,1,2)
plot(stime,aNacel,'b')
xlabel('Time (sec)')
ylabel('ANSYS Acceleration (g)')
hold off


%%%%%%%%%%%%%%%%%%%%%%%%%%%%%%
% Plots the Control Signals %
%%%%%%%%%%%%%%%%%%%%%%%%%%%%%%

figure(2);
subplot(2,1,1)
hold on
plot(time,eCSoutput,'r')
title('Node 18, Y-Axis, 19 Hz, Piezo #2')
ylabel('Experimental Control (V)')
xlabel('Time (sec)')
subplot(2,1,2)
plot(stime,zCSoutput,'b')
xlabel('Time (sec)')
ylabel('ANSYS Control (V)')
hold off


%%%%%%%%%%%%%%%%%%%%%%%%%%%%%%%%%%%%%%%%%%%%%%%%%%%%%%%%%%%%%%%%%%%%
% Determines Frequency Response Before and After Control %
%%%%%%%%%%%%%%%%%%%%%%%%%%%%%%%%%%%%%%%%%%%%%%%%%%%%%%%%%%%%%%%%%%%%

et1=5*dt;
et2=16.8;
et3=(stop-et2)+6*dt;
st1=5*sdt;
st2=0.53;
st3=(sstop-st2)+6*sdt;

% Experimental FFT
er1=floor(et1/dt):floor(et2/dt);
er2=floor(et3/dt):length(eNacel);
ev1=eNacel(er1);
ev2=eNacel(er2);
ef1=linspace(0,1/dt,length(er1));
ef2=linspace(0,1/dt,length(er2));
ebefore=fft(ev1'.*hanning(length(ev1)));
eafter=fft(ev2'.*hanning(length(ev2)));
eav1=20*log10(abs(ebefore));
```

```
eav2=20*log10(abs(eafter));
err1=find(ef1<=50&ef1>0);
err2=find(ef2<=50&ef2>0);
estrt=ef1(err1(1));
efnsh=ef1(err1(length(err1)));
ebig=ceil(max(max(eav1),max(eav2)));
eltl=floor(mean(eav1)-3*std(eav1));

% ANSYS FFT
sr1=floor(st1/sdt):floor(st2/sdt);
sr2=floor(st3/sdt):length(aNacel);
sv1=aNacel(sr1);
sv2=aNacel(sr2);
sf1=linspace(0,1/sdt,length(sr1));
sf2=linspace(0,1/sdt,length(sr2));
sbefore=fft(sv1.*hanning(length(sv1)));
safter=fft(sv2.*hanning(length(sv2)));
sav1=20*log10(abs(sbefore));
sav2=20*log10(abs(safter));
srr1=find(sf1<=50&sf1>0);
srr2=find(sf2<=50&sf2>0);
sstrt=sf1(srr1(1));
sfnsh=sf1(srr1(length(srr1)));
sbig=ceil(max(max(sav1),max(sav2)));
slt1=floor(mean(sav1)-3*std(sav1));
slt2=floor(mean(sav2)-3*std(sav2));

%%%%%%%%%%%%%%%%%%%%%%%%%%%%%%%%%%%%%%%%%%%%%%%%%%%%%%
% Plots Frequency Response Before and After Control %
%%%%%%%%%%%%%%%%%%%%%%%%%%%%%%%%%%%%%%%%%%%%%%%%%%%%%%

% Before Control
figure(3)
subplot(2,1,1)
plot(ef1(err1),eav1(err1))
axis([estrt efnsh eltl ebig])
title('Uncontrolled, Node 18, Y-Axis, 19 Hz, Piezo #2')
ylabel('Experimental (dB [g])')
xlabel('Frequency (Hz)')
subplot(2,1,2)
plot(sf1(srr1),sav1(srr1))
axis([sstrt sfnsh slt1 sbig])
ylabel('ANSYS (dB [g])')
xlabel('Frequency (Hz)')

% After Control
figure(4)
subplot(2,1,1)
plot(ef2(err2),eav2(err2))
axis([estrt efnsh eltl ebig])
title('Controlled, Node 18, Y-Axis, 19 Hz, Piezo #2')
ylabel('Experimental (dB [g])')
xlabel('Frequency (Hz)')
subplot(2,1,2)
plot(sf2(srr2),sav2(srr2))
```

173

```
axis([sstrt sfnsh slt2 sbig])
ylabel('ANSYS (dB [g]))')
xlabel('Frequency (Hz)')

%%%%%%%%%%%%%%%%%%%%%%%%%%%%%%%%%%%%%%%%%%%%%%%%%%%%%%%%%%%%%%%%%
% Calculate the dB reduction at the peak undamped frequency %
%%%%%%%%%%%%%%%%%%%%%%%%%%%%%%%%%%%%%%%%%%%%%%%%%%%%%%%%%%%%%%%%%

[em,ei]=max(eav1);
ereduction=em-eav2(ei)

[sm,si]=max(sav1);
sreduction=sm-sav2(si)

eval(['cd ..'])
```

APPENDIX L. ANSYS RESULTS
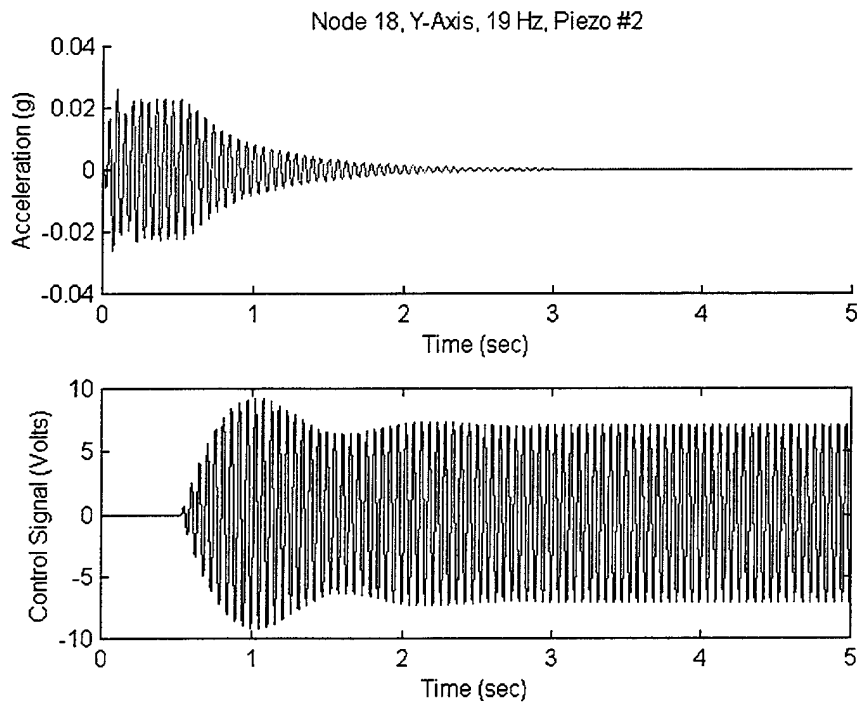
Figure 98. Simulation 1, System Response
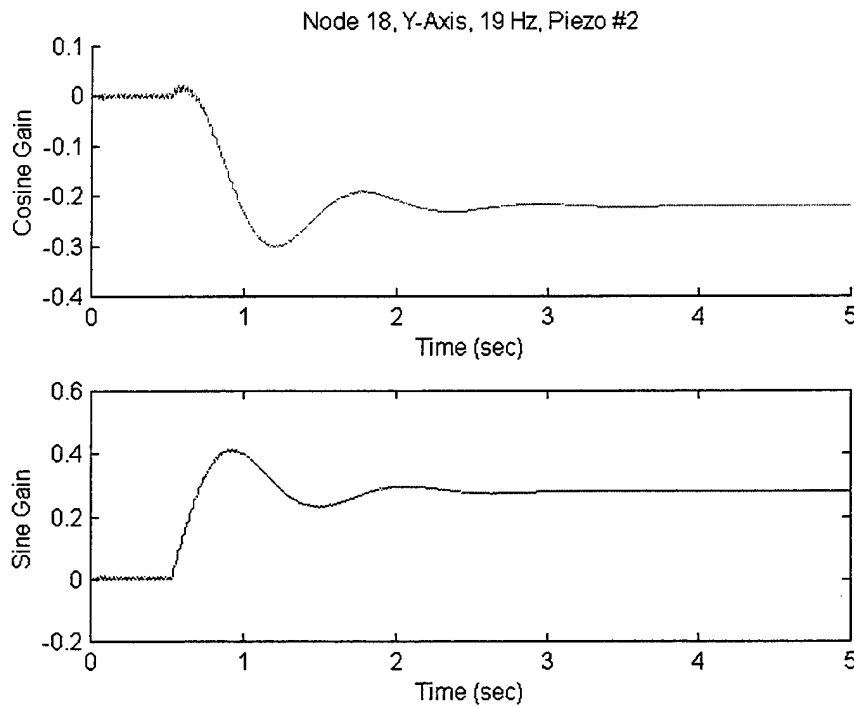
Figure 99. Simulation 1, Controller Gains
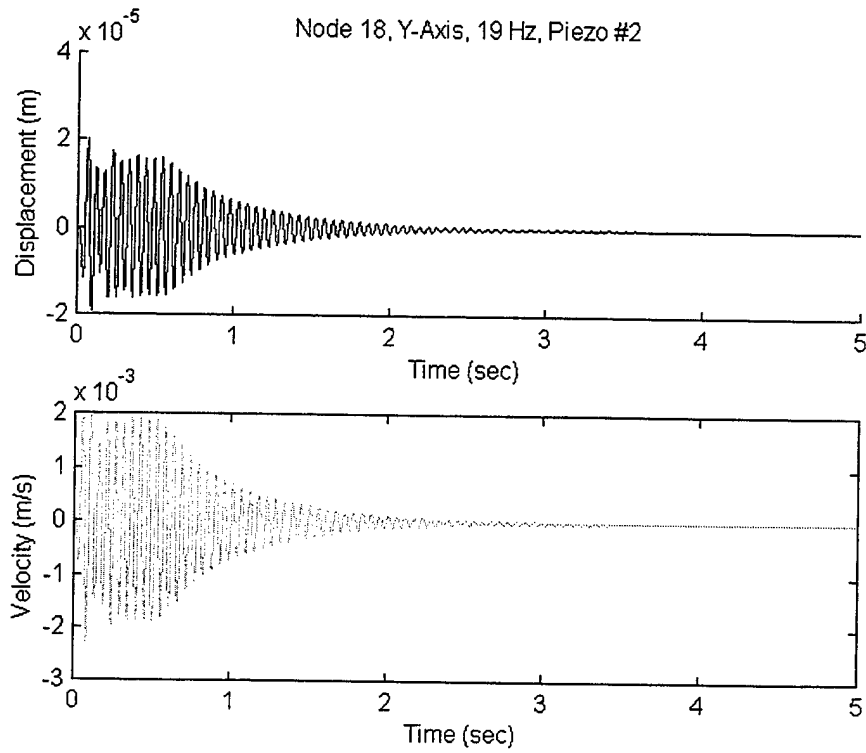
Figure 100. Simulation 1, Control Node Response
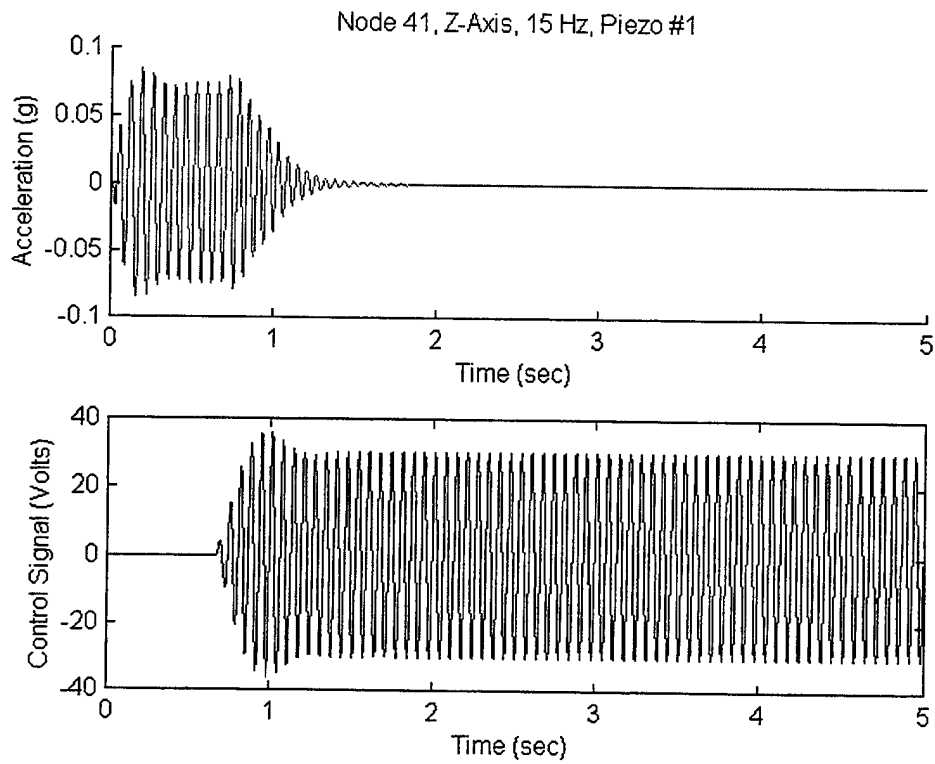
Figure 101. Simulation 2, System Response

176
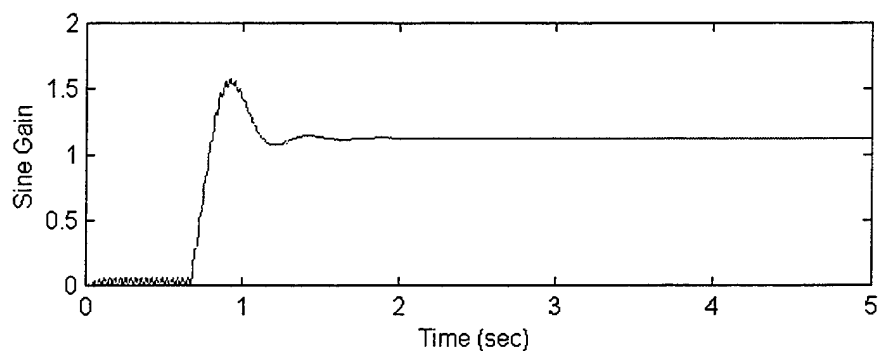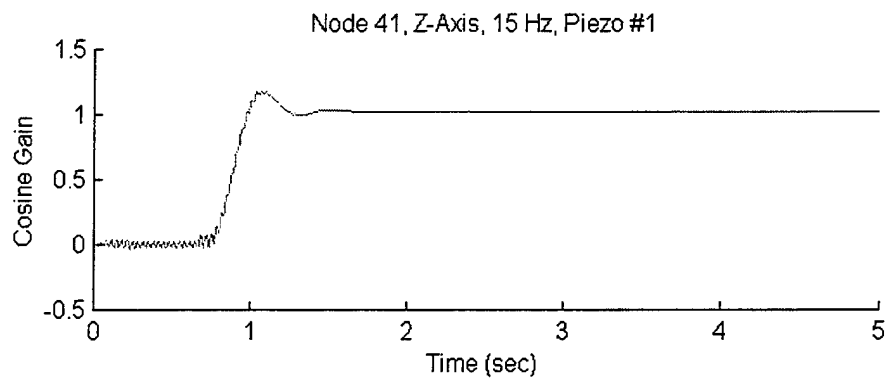
Figure 102. Simulation 2, Controller Gains
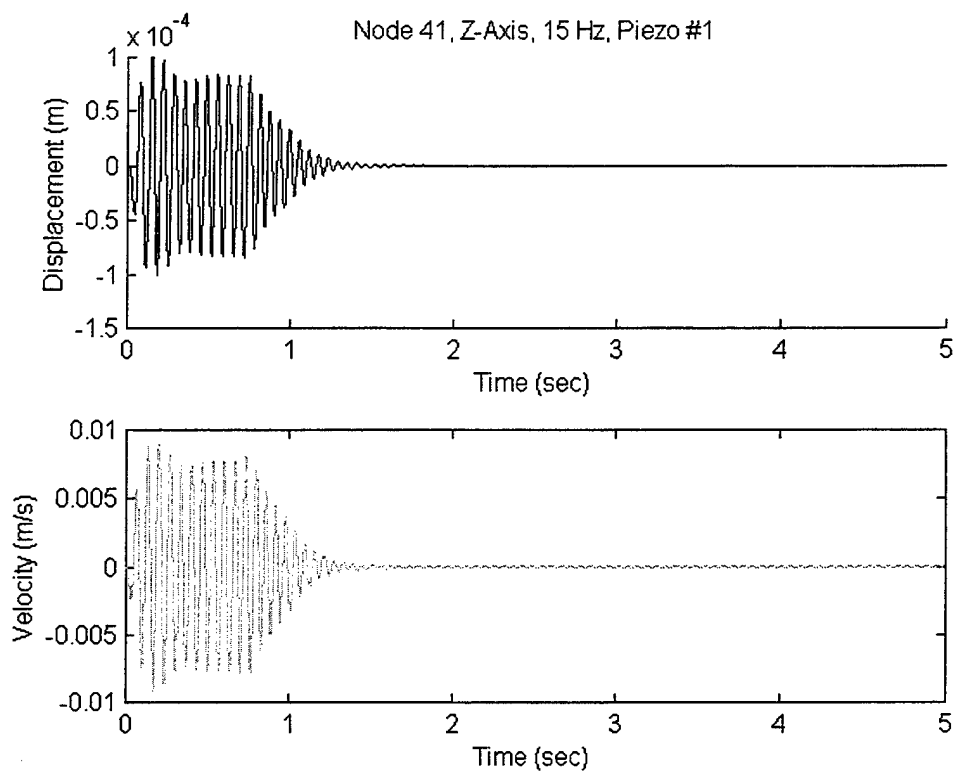
Figure 103. Simulation 2, Control Node Response
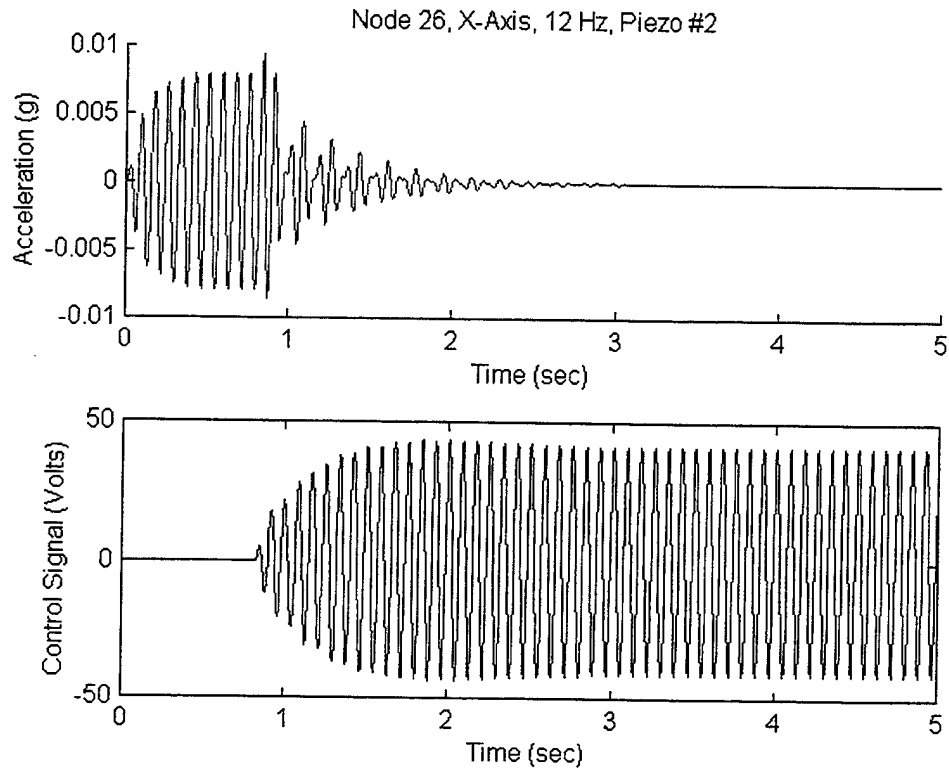
Figure 104. Simulation 3, System Response
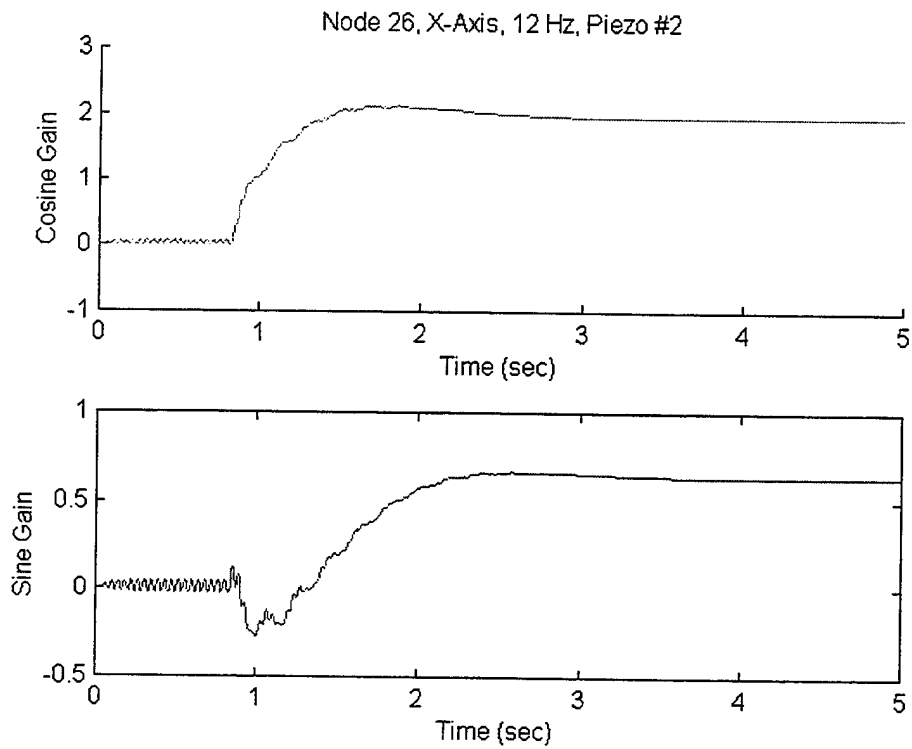
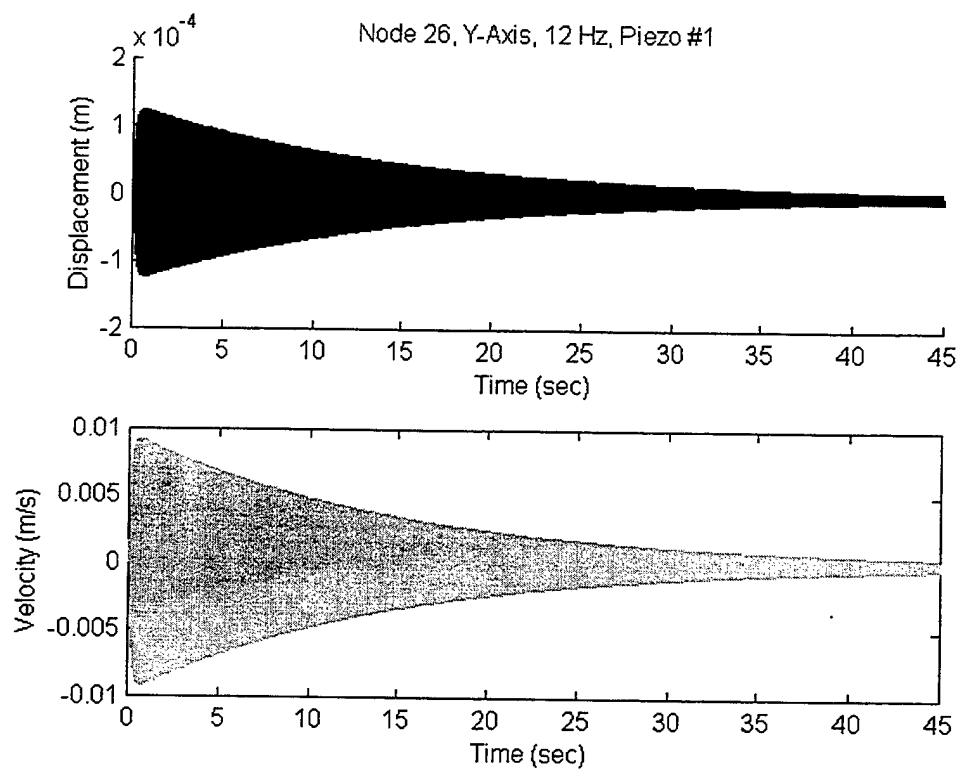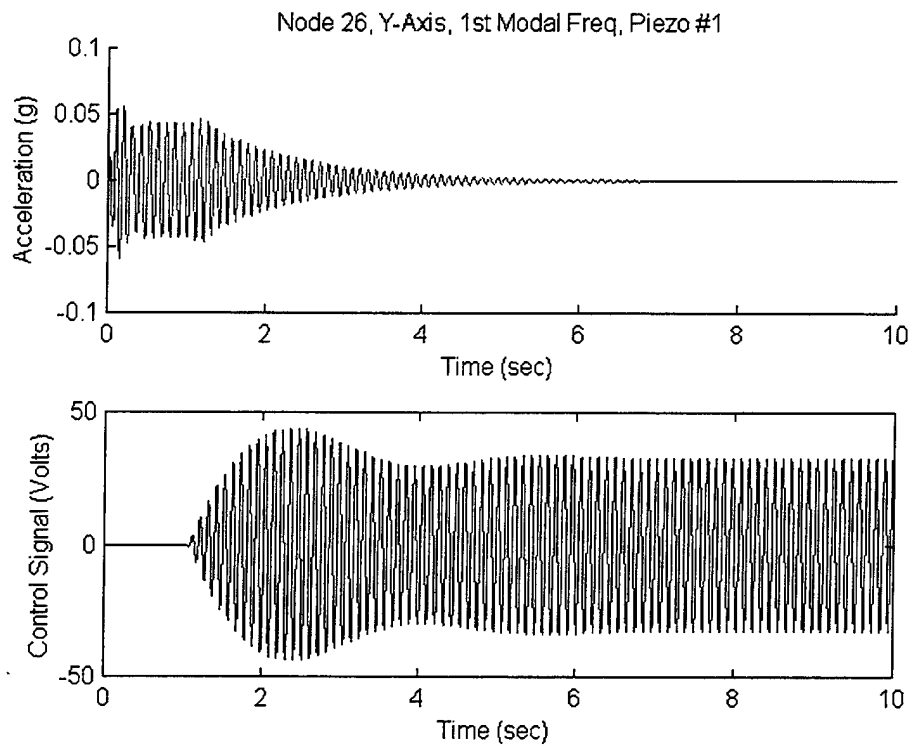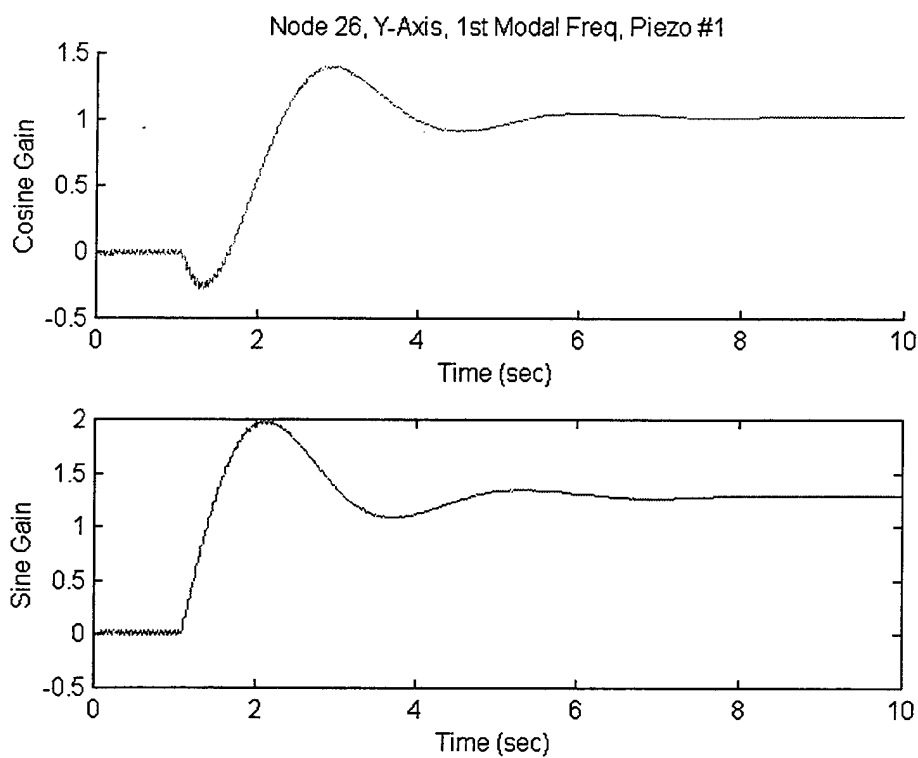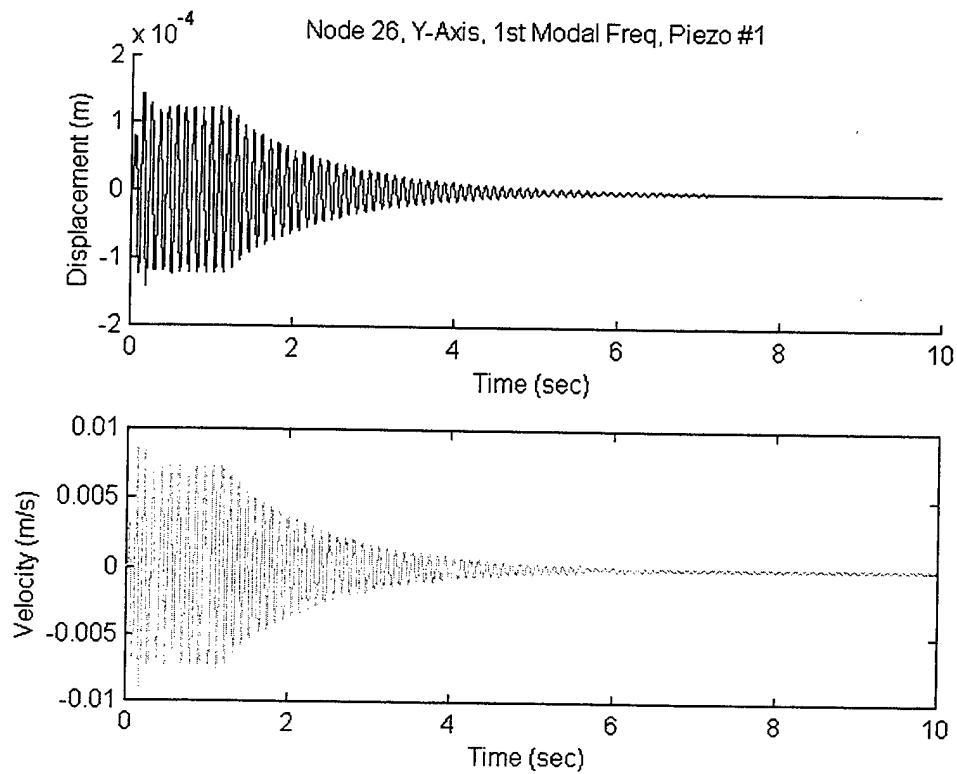Figure 105. Simulation 3, Controller Gains

178
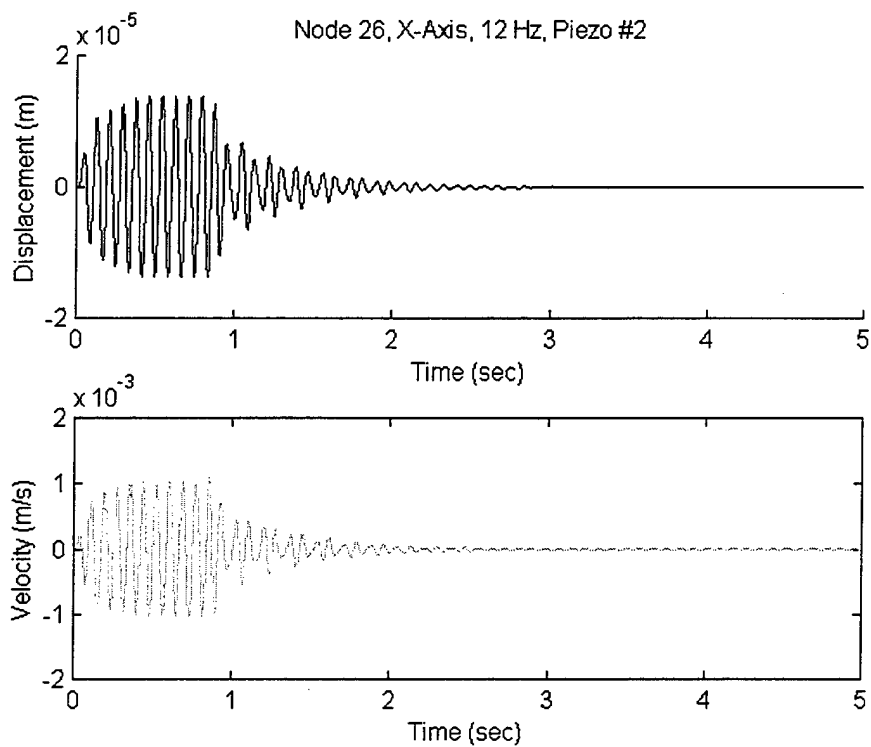
Figure 106. Simulation 3, Control Node Response
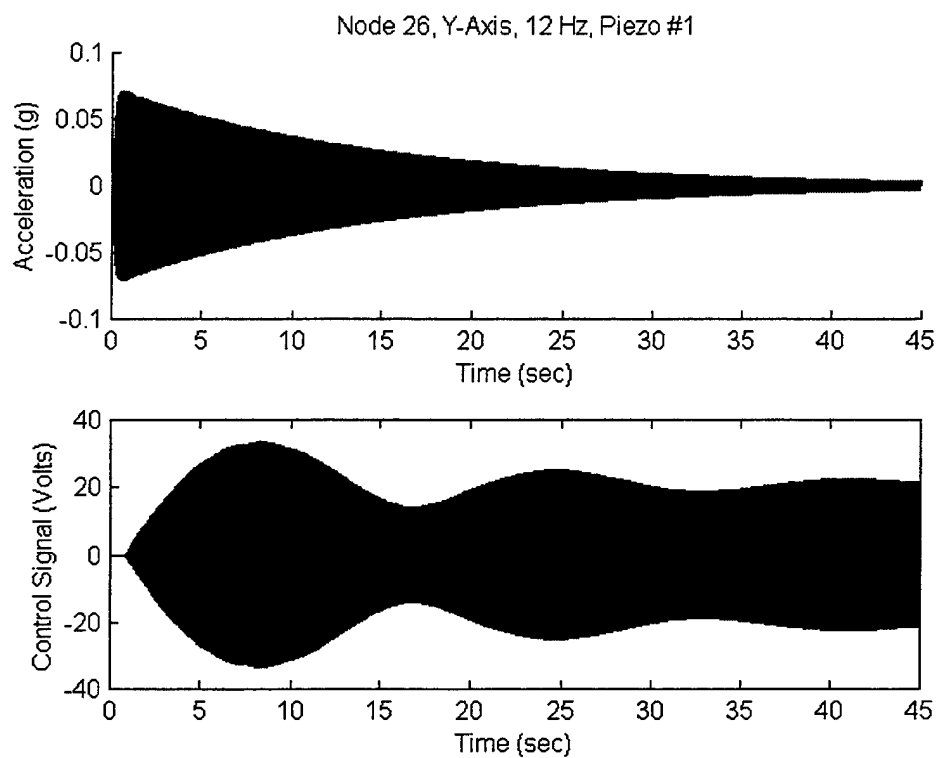
Figure 107. Simulation 4, System Response

179
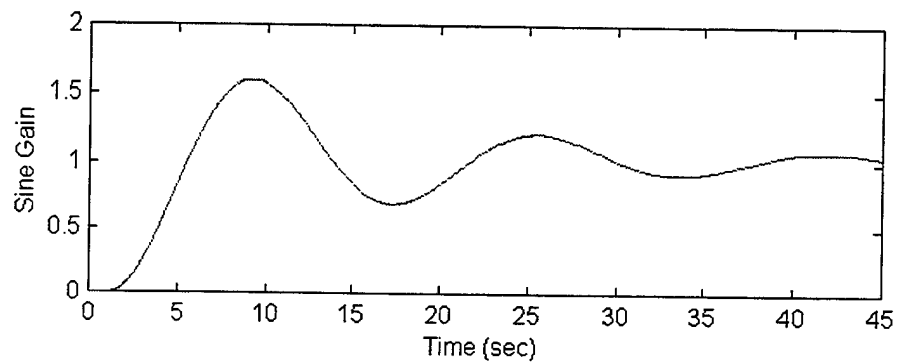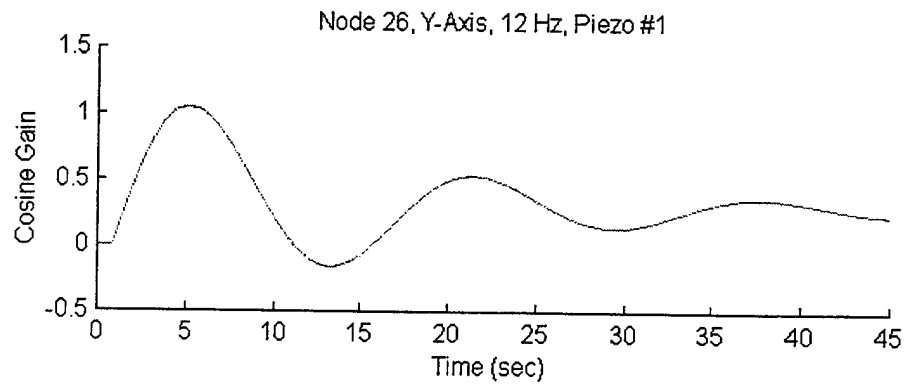
Figure 108. Simulation 4, Controller Gains

Figure 109. Simulation 4, Control Node Response

180

Node 26, Y-Axis, 1st Modal Freq, Piezo #1

Figure 110. Simulation 5, System Response

Node 26, Y-Axis, 1st Modal Freq, Piezo #1

Figure 111. Simulation 5, Controller Gains

181

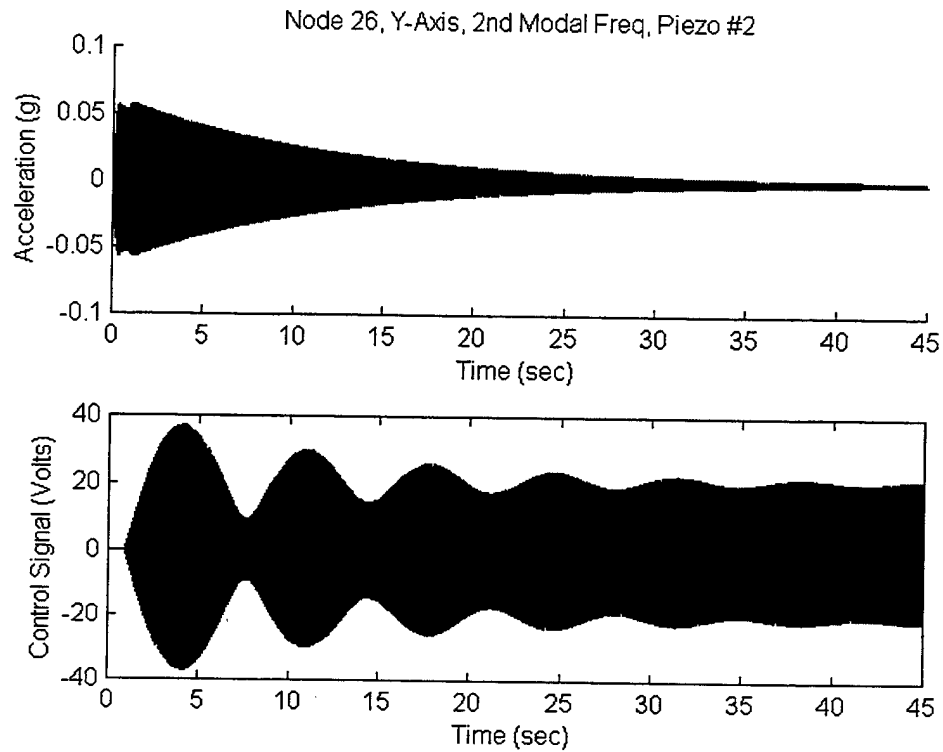Figure 112. Simulation 5, Control Node Response
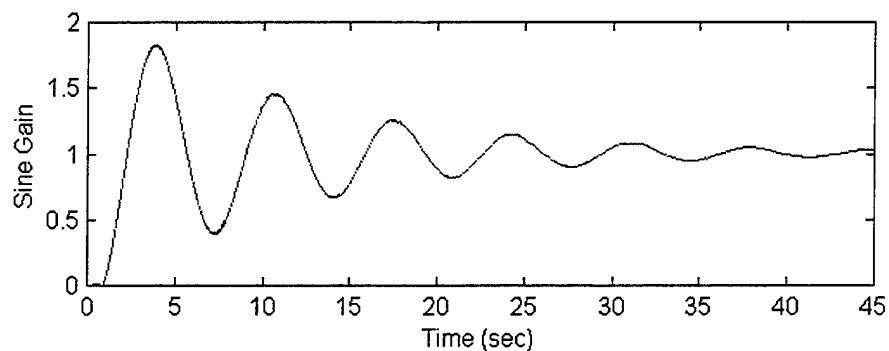

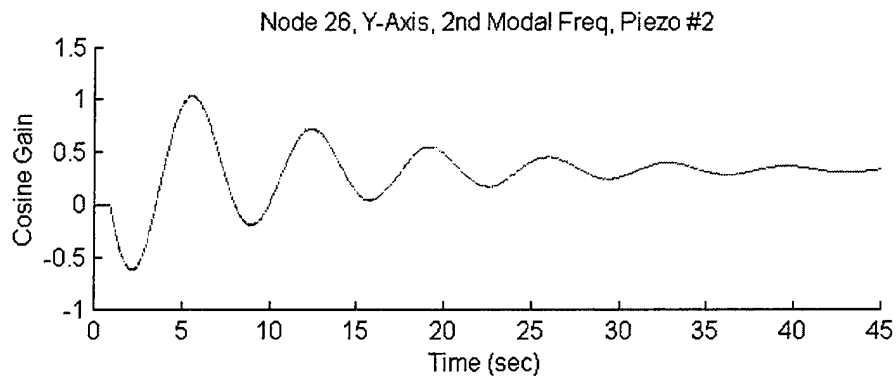Figure 113. Simulation 6, System Response

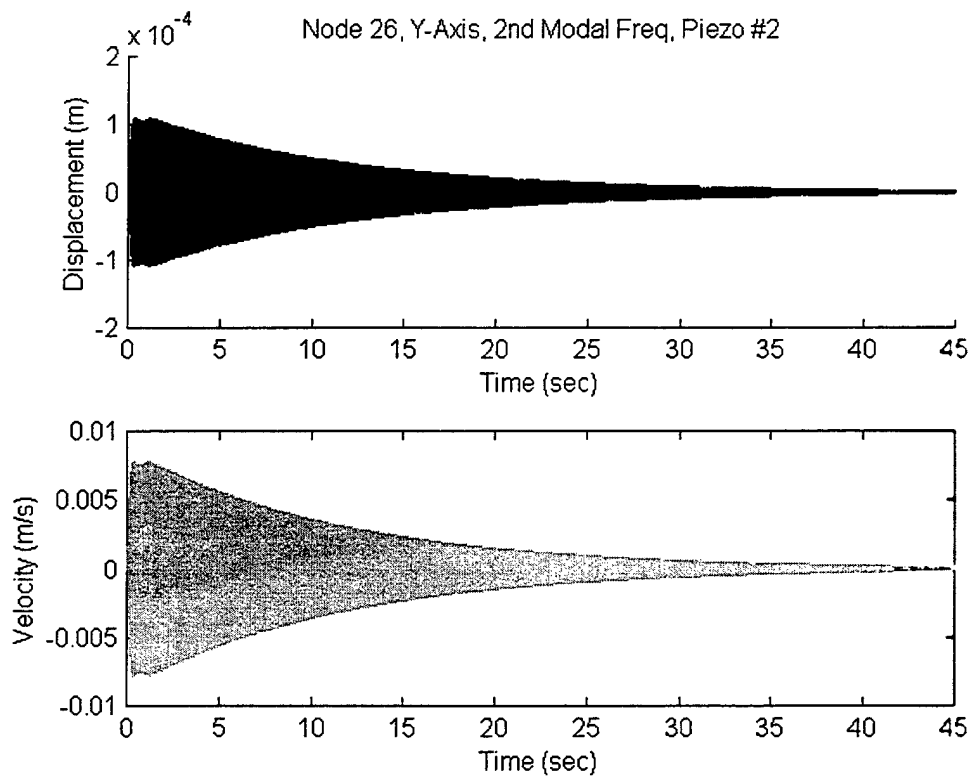Figure 114. Simulation 6, Controller Gains
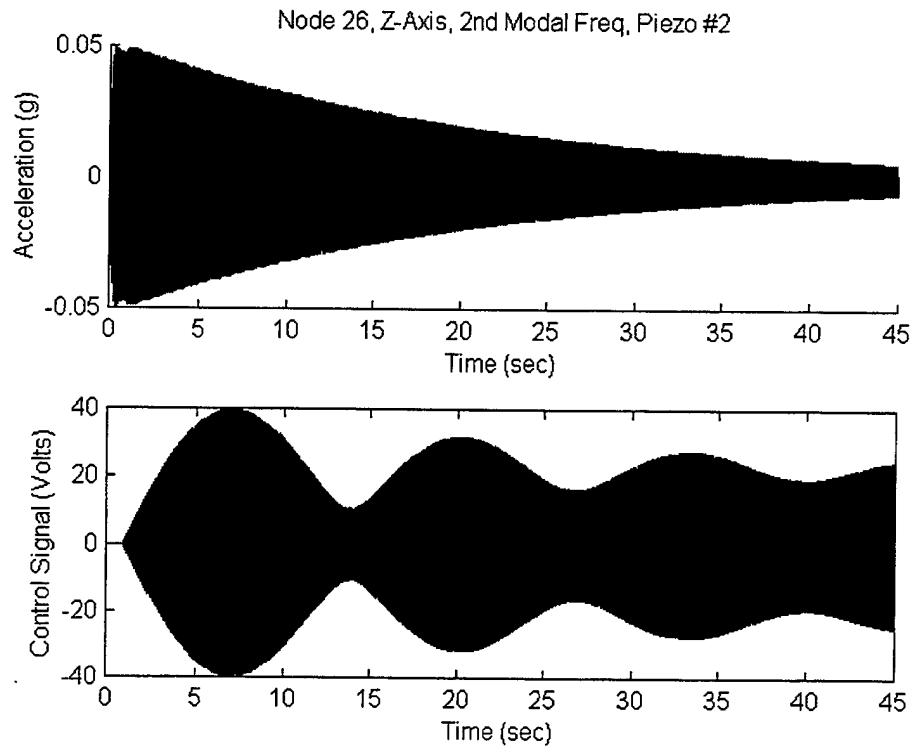

Figure 115. Simulation 6, Control Node Response
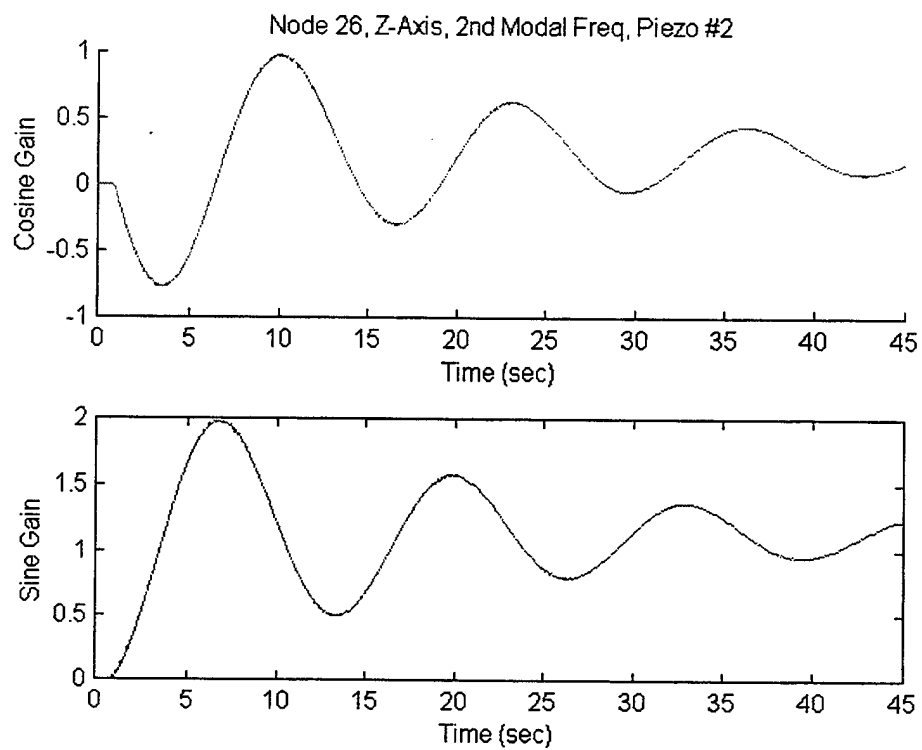
183

Figure 116. Simulation 7, System Response

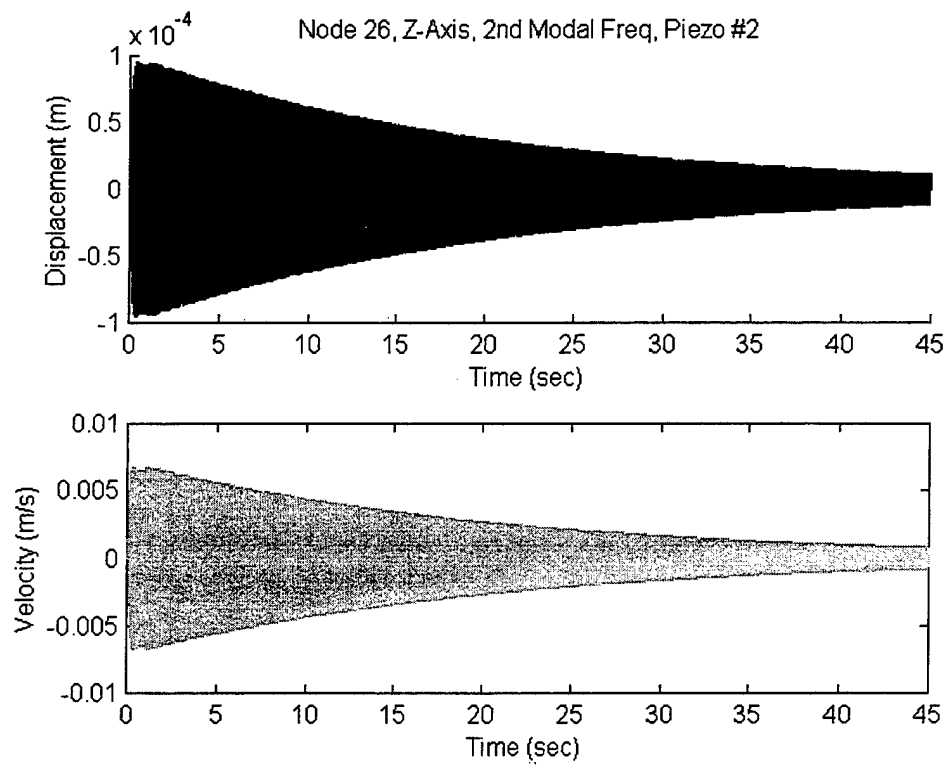Figure 117. Simulation 7, Controller Gains

184

Figure 118. Simulation 7, Control Node Response

THIS PAGE INTENTIONALLY LEFT BLANK

INITIAL DISTRIBUTION LIST

1. Defense Technical Information Center..2
   8725 John J. Kingman Rd., STE 0944
   Ft. Belvior, VA 22060-6218

2. Dudley Knox Library..2
   Naval Postgraduate School
   411 Dyer Rd.
   Monterey, CA 93943-5101

3. LT Timothy A. Barney, USN 1
   5399 Elm Forest Drive
   Virginia Beach, VA 23464

4. Professor Young S. Shin, Code ME/Sg...3
   Naval Postgraduate School
   699 Dyer Road Room 137
   Monterey, CA 93943-5106

5. Professor Brij N. Agrawal, Code AA/Ag..3
   Naval Postgraduate School
   699 Dyer Road Room 137
   Monterey, CA 93943-5106

6. Richard Barney, Associate Chief of the Instrument Technology Center..............1
   Code 550
   GSFC/NASA
   Greenbelt Road, MD 20771

7. Dr. Kajal Gupta, University Affairs Officer...2
   P.O. Box 273, MS D2701
   NASA Dryden Flight Research Center
   Edwards, CA 93523-0273

8. Sheldon Imaoka 1
   Collaborative Solutions, Inc.
   5962 La Place Court, Suite 100
   Carlsbad, CA 92008